

# Dynamics and Disorder at the Kosterlitz-Thouless Transition

by

Andrew D. Armour, B.Sc.

Thesis submitted to the University of Nottingham for  
the degree of Doctor of Philosophy, May 1999

---

# Contents

---

Abstract	iv
Acknowledgments	v
<b>1 Introduction</b>	<b>1</b>
<b>2 Critical Phenomena</b>	<b>5</b>
2.1 The Renormalization Group	6
2.2 Transitions in Two-Dimensions	12
<b>3 Superfluid Films</b>	<b>16</b>
3.1 Superfluidity in Two Dimensions	16
3.2 The Dielectric Picture	19
3.3 The Dynamic Theory of AHNS	22
3.4 Experiments on Superfluid Films	25
3.5 Minnhagen's Theory	28
3.6 Discussion	31
<b>4 Refined Dynamics</b>	<b>32</b>
4.1 Timm's Ansatz	33
4.2 Refined Theory	35
4.3 Comparison with Minnhagen	41
4.4 Comparison with Experiment	44
4.5 Discussion	50
<b>5 Roughening and Super-Roughening Transitions</b>	<b>52</b>
5.1 Formulation of a Continuous Model	53
5.2 Renormalization	55
5.3 Comparison with Experiment	61
5.4 Super-Roughening	64
<b>6 Roughening and Disorder</b>	<b>66</b>
6.1 Screw Dislocations	66
6.2 Renormalization with Disorder	68
6.3 Calculation of Correlation Functions	70
6.4 Dislocation Loops	74
6.5 The Strong Coupling Regime	76
6.6 Conclusions and Discussion	82
<b>7 New Dynamic Theory of Superfluid Films</b>	<b>84</b>
7.1 Comparison of Models	85
7.2 The Electric Field Analogue	86
7.3 Renormalization	88
7.4 Variations on the Theme	97
7.5 Conclusions and Discussion	99

---

<b>A Vortex-Vortex Interaction</b>	<b>101</b>
<b>B Calculation of <math>\Gamma(\mathbf{r}, t)</math></b>	<b>103</b>
<b>C Duality Transformation</b>	<b>105</b>
<b>D Layered Sine-Gordon Model</b>	<b>108</b>
References	110

---

## Abstract

---

This thesis describes theoretical investigations into the dynamics of superfluid films and the effects of disorder on the roughening transition of crystal surfaces. The dynamic theory of superfluid helium films, due to Ambegaokar et al., is refined to improve the precision of the predictions made. A detailed comparison is made between the predictions of the modified theory and the results from experiments on helium films and on superconducting systems. It is found that, despite the modifications in the theory, agreement with experiments on helium films remains only qualitative.

Consideration is then given to the effects on the roughening transition of disorder arising from screw dislocations. A crystal surface which is threaded by screw dislocation pairs may be in one of three different states depending on the temperature of the system and the way in which screw pairs are distributed. At high temperatures the interface is rough: it is not pinned to the lattice. At low temperatures the state of the interface depends on how the screw dislocations are distributed: when distributed as closely spaced pairs they lead to a faceted state with a single ground state energy; when distributed randomly they lead to a state of the interface which, though pinned to the underlying crystal lattice, has a degenerate ground state.

It is then shown that the dynamic sine-Gordon formulation of the roughening transition can be used, via a Hubbard-Stratonovich transformation, to model the dynamic behaviour of superfluid systems. This method provides a renormalization group framework within which the a.c. linear response can be studied. The ways in which the approach could be extended to study the effects of disorder and atomic layering are also discussed.

---

## Acknowledgments

---

It gives me great pleasure to be able to thank my supervisor Roger Bowley, for his constant encouragement and assistance over the last three years, and for showing me how Physics should be done. I would also like to acknowledge the financial support of the University of Nottingham, received in the form of a studentship. However, it was during the last three years that the Cystic Fibrosis, with which I was born, reached its clinical denouement and as a consequence there are a number of people not connected with Physics whom I would like to thank.

For the last twenty four years I have received care of the highest standard at the Nottingham City Hospital. Over the most serious period of my illness I was lucky enough to be cared for by Dr Knox, Dr Baldwin, Dr Teahon, Dr Rodgers and the CF team, which at that time included Sarah Wynn-Knight, Maria Marks, Fiona Haynes and Martin Newman.

My life was transformed, and my more pressing problems solved, in the Autumn of 1997 by a transplant operation carried out at Papworth hospital. I have to thank Mr Wallwork, Mr Dunning, Mr Friend, Dr McNeill and all the rest of the staff there for a change in quality of life far greater than I had ever imagined possible.

I would also like to thank my friends for their kindness throughout the times when I was sick. In particular, Jonathan, Jenny, Mike, Philip, Katy and Phil, who helped me far more than they realize.

Finally, I would like to thank my parents and brother, although they already know how much I appreciate their love and perseverance with what seemed to us all a lost cause. However, fundamentally this thesis came to be written because I was fortunate enough to benefit from the altruism of one whom I cannot thank. This work is dedicated to those of my friends with CF who were not as lucky.

---

## Chapter 1 Introduction

---

This thesis describes theoretical work on the dynamic properties of the superfluid transition in thin films of helium and the effect of disorder on the roughening transition of crystal surfaces. The two strands are closely connected because both of the transitions are continuous in nature and occur in effectively two-dimensional systems. Furthermore, these two phase transitions lie in the same universality class: that first described by Kosterlitz and Thouless [1, 2, 3].

The theory of continuous phase transitions represents one of the most successful developments in Physics of the last thirty years. Modern methods are based around the renormalization group and have been applied with great effect to a wide range of phase transitions. Indeed, it is beginning to be appreciated that the methods used to describe critical phenomena are also of great value in fields of study traditionally thought of as far from Physics. The renormalization group was initially developed to provide a framework in which the effects of thermal fluctuations on critical systems could be accounted for accurately. Previous methods, such as mean field theory, proved inaccurate for systems in three dimensions or less because they neglected the effects of fluctuations. In two dimensions fluctuations are even more important than in three and so a renormalization group approach becomes essential. The work presented here is both an extension and an adaptation of the various renormalization group methods that have been applied in the past, with mixed success, to superfluidity in thin films and to the roughening transition.

It was first realized that the theory of superfluidity in thin films must differ from that in bulk helium-four when Hohenberg, Mermin and Wagner showed that long range order was destroyed in two-dimensional systems with continuous symmetries [4, 5]. Their work left the scientific community with a puzzle: how could the superfluidity of helium films exist in the absence of long range order? The answer, which was both elegant and physically appealing, was provided by Kosterlitz and Thouless [1, 3], almost simultaneously with Berezinskii [6]. They focused attention on the behaviour of the topological defects of the system, the vortices, and showed that a lesser kind of order, known as quasi-long-range order, was sufficient to permit superfluidity. They described the superfluid system in terms of the unbinding of vortex/anti-vortex pairs, leading to a finite density of free vortices and hence the destruction of all order in the system.

Attempts to verify the theory proved frustrating as the principal experiments available had to be performed in the linear response regime and at finite frequency, leading to a strong broadening of the transition which could not be described accurately using the equilibrium Kosterlitz-Thouless theory. What was required was an extension of the theory to finite frequencies. Just such an extension was provided by the phenomenological theory of Am-

begaokar, Halperin, Nelson and Siggia (AHNS) [7, 8]. Qualitative agreement was obtained between the theory of AHNS and the results of torsional oscillator experiments and so the Kosterlitz-Thouless theory was accepted as the correct explanation of two-dimensional superfluidity.

Discrepancies between the actual predictions of Ambegaokar et al. and experiment were largely (but not completely) obscured by the large number of fitting parameters that were allowed; their work appears in the text books along with that of Kosterlitz and Thouless as *the* theory of superfluid films [9, 10, 11, 12]. This thesis contains a detailed description and critique of the theory of Ambegaokar et al.: excellent though their work was, it failed to provide anything more than qualitative agreement with experiment. Furthermore, recent experiments on superfluid systems have shown that there are two important physical effects which are not accounted for by the theory of AHNS. The first is a strong dependence on the degree and type of disorder that exists in the substrate; the second is a systematic variation in the dynamic response with the number of atomic layers in the films.

The work of Kosterlitz and Thouless did not provide a complete description of the eponymous class of transitions: the recursion relations they derived are valid under only a limited range of circumstances. However, several groups have subsequently derived groups of recursion relations to describe the critical behaviour which are more generally valid [13, 14, 15]. One such set, due to Timm [13], is used here as the basis of a more refined dynamic theory. This approach remains within the general framework of Ambegaokar et al., but leads to the prediction of a universal property which is readily compared with experiment, requiring at most one fitting parameter [16]. Nevertheless, even using the refined version of the dynamic theory the agreement with experiment remains qualitative.

The idea that the roughening of a crystal surface as the temperature is raised should be accompanied by a distinct phase transition, the roughening transition, was first suggested by Burton and Cabrera [17]. It is now widely accepted that the transition lies in the Kosterlitz-Thouless universality class and can be accurately described using renormalization group methods [18, 19, 20, 21, 22]. In particular, a renormalization group theory has been developed by Nozières and Gallet to describe the roughening transition in the linear response regime [19], the details of which have been confirmed by a series of experimental tests.

However, if the substrate on which a crystal is grown is strongly disordered then the crystal undergoes a different type of phase transition. This new transition is called the super-roughening transition and, in contrast to the roughening transition, is not of the Kosterlitz-Thouless type [23, 24]. Recent work has shown that the transition which a crystal surface undergoes, as the temperature is raised, is sensitive to the strength of the disorder in the underlying crystal lattice [25, 26]. If the lattice is disordered by screw dislocations then when they are distributed at random the surface undergoes a super-roughening transition, but if they are distributed as closely spaced pairs then the roughening transition remains, though the critical point is shifted slightly. In contrast, if the surface of a crystal is threaded by thermally generated dislocation loops then the roughening transition is

essentially the same as that for a perfect crystal.

The fact that a highly successful linear response theory for a transition in the Kosterlitz-Thouless universality class exists does not seem to be widely appreciated in the literature. However, because the roughening transition is in the same universality class as the superfluid transition in thin films, it may be possible to adapt the Nozières-Gallet theory to describe the dynamic response of superfluid films. A well known mathematical transformation can be used to ‘translate’ from the language of the roughening transition to that of superfluid films. A quantity analogous to the external driving field for films is identified in the context of the roughening transition so that when the Nozières-Gallet dynamic renormalization procedure is applied the response function of the superfluid system can be calculated accurately. An important advantage of this approach is that it is readily extended so that the effects of disorder and atomic layering on superfluid film systems can be investigated. It is hoped that these new methods will provide a more accurate description of the dynamic experiments on superfluid films.

Kosterlitz and Thouless were initially concerned with developing an understanding of superfluidity in thin films. However, they recognized that their work provides the appropriate description for the critical properties of a wide range of two-dimensional systems. The Kosterlitz-Thouless universality class is now known to include phase transitions in the following systems: superconducting sheets and wire networks [27, 28, 29]; the two-dimensional Coulomb gas model [14, 2]; the XY model of planar magnetism [2]; the roughening transition of crystal surfaces [30, 19]; the smectic-A to smectic-C transition in liquid crystal films [31]; the melting of two dimensional crystals (e.g. electrons on helium) [32, 33] and sand pile models displaying self-organized-criticality [34], though the list is not exhaustive.

Here attention is focused on just two of these systems: superfluidity in helium films and the roughening of crystal surfaces, but the hope is that the methods developed with these two systems in mind will be broadly applicable to many of the systems in the Kosterlitz-Thouless universality class. The motivation for studying the dynamics of superfluid films is straightforward: such a theory is an essential prerequisite for the interpretation of experimental results on films which were performed to test whether the Kosterlitz-Thouless approach is the correct description of superfluidity in thin films. Although such dynamic theories do already exist, they are unsatisfactory because they do not provide good quantitative agreement with experiment. The reason for investigating the effect of disorder on the roughening transition is rather different. Unlike the case with superfluid films, the dynamics of crystal surfaces close to the roughening transition is well understood [19]. However, it has been argued that the transition is destroyed by certain types of disorder [35, 36] and so the opportunity was taken to clear up what was in effect a dispute in the literature.

This work is organized as follows. Chapter 2 contains a description of the theoretical background to the thesis. It begins with a review of the basic ideas of the renormalization group theory, on which much of the following work is based. Next there is a discussion of the peculiar properties of two-dimensional phase transitions. Then the sine-Gordon and two-

dimensional Coulomb gas models, which are both used to describe systems in the Kosterlitz-Thouless universality class, are introduced. Finally, the original derivation of the Kosterlitz recursion relations is outlined using the language of the two-dimensional Coulomb gas.

Chapter 3 reviews the way in which Kosterlitz-Thouless theory can be applied to superfluid films. It begins with an explanation of how superfluid films can be modelled by the two-dimensional Coulomb gas model and goes on to describe in detail the dynamic theories of superfluid films due to AHNS and Minnhagen [14]. There is also a discussion of the results from early dynamical experiments on superfluid films with which the dynamical theories can be compared.

Chapter 4 describes the refined dynamical theory of superfluid films developed by Roger Bowley, Keith Benedict and myself [16]. It starts with an outline of how Timm obtained his generalized recursion relations, before going on to show how they can be used to improve on the theory of AHNS. The chapter concludes with detailed comparisons of the refined theory with Minnhagen's approach and the results of experiments carried out by the groups lead by John Reppy and John Saunders.

In the next two chapters the subject matter shifts to the roughening transition. Chapter 5 reviews the current theories of the roughening and super-roughening transitions, then chapter 6 describes recent investigations into the disordering effect of dislocations on crystal surfaces carried out by Roger Bowley, Philippe Nozières and myself [26, 37]. The modification in behaviour of a crystal surface caused by screw dislocations in the limit of weak coupling to the underlying lattice is considered in detail and then a qualitative description of the behaviour in the strong coupling limit is given.

Then in chapter 7, attention returns to the dynamics of superfluid films and the recent work I have been doing in collaboration with Roger Bowley. The way in which the dynamics might be analysed using the methods developed to study the roughening transition is described along with some preliminary results from renormalization group calculations. This is followed by outlines of how the method could be extended to model the effects of atomic layering and disorder in the substrate. The chapter concludes with a summary of the current position and a discussion of some interesting questions which have not yet been fully addressed. Finally there are several appendices which outline the mathematics required to derive some of the important results used in the text.

---

## Chapter 2 Critical Phenomena

---

This chapter introduces some of the basic ideas in the modern theory of critical phenomena. It starts with a description of the renormalization group method and then goes on to summarize the special properties of phase transitions in two-dimensions. Attention is focused on the Kosterlitz-Thouless transition which is the basis of the material described in later chapters.

Phase transitions have traditionally been divided into two groups: first order and continuous transitions. First order transitions are by far the most common and are characterized by a discontinuity in one or more of the derivatives of the free energy; in contrast, at continuous transitions there are only discontinuities in the second or higher order derivatives of the free energy. A first order transition is almost always accompanied by a latent heat; coexistence of phases can also occur and one phase may penetrate into another (e.g. superheating), particularly if nucleation is inhibited. In contrast, at a continuous phase transition the change is less dramatic: there is no latent heat, coexistence never occurs and superheating and supercooling are impossible. Instead, as a continuous transition is approached from below, the particular type of ordering which distinguishes the two phases becomes less and less pronounced until at the transition — at the critical point — it finally vanishes entirely. In quantitative terms this gradual disappearance of the ordering which distinguishes the two phases is usually modelled by an order parameter whose average value is finite below the transition and zero above it.

Another important feature of a continuous phase transition is the behaviour of the correlation length of the system: it diverges at the critical point. A correlation length can be thought of as the length scale on which the behaviour of the constituent parts of a system begin to differ markedly from the average values for the whole system and so is related to the length scale over which different parts of the system interact with each other. Hence, when the correlation length is divergent the interactions between different parts of the system are by no means short range — each part of the system is interacting with every other part. It is the coupling of so many degrees of freedom that make critical point phenomena so interesting. Since both the roughening and superfluid transitions are continuous, attention is concentrated on the theoretical framework which has been developed to describe this subset of phase transitions.

Traditionally the subject has been tackled by the formulation of a phenomenological model which is in reality a caricature of the physical system which it is supposed to represent. Of course the huge number of degrees of freedom makes an exact formulation in terms a complete description of all the particles involved out of the question — the hope is that the physics responsible for the change in behaviour at the transition can be encapsulated in the model. The first models of this type to be developed were for

magnetic systems and were written in terms of a discretised system of spins based on a lattice. In fact very similar methods can be used to describe a whole variety of systems when the spin variable is generalized to become the order parameter of the system — an approach known as Landau-Ginzburg theory. The models take the form of an expression for the energy of the system which is known as a Hamiltonian. However, it is the classical behaviour which is modelled since the fluctuations that occur on a macroscopic scale in systems close to criticality drown their quantum counterparts. The Hamiltonian is written using a set of coupling constants to represent the interactions of neighbouring spins on the lattice, next nearest neighbours and so on.

In very simple cases these models can be solved analytically for the partition function, though the solutions themselves are anything but trivial (the solution of the two-dimensional Ising model was a tour de force [38]), but in the vast majority of cases an approximate technique is resorted to. In the past mean field theory, low or high temperature expansions and transfer matrix methods were all popular choices [39]. Although it was found that the results obtained depended only very loosely on the details of any particular model (a property which could not be explained with these methods), the results obtained for the critical exponents by these diverse methods were only rarely in good agreement with experiment — as a cursory examination of any textbook on the subject that predates 1970 will show.

Progress towards a deeper understanding was made in 1966 when Kadanoff introduced the concept of block scaling [40]. However, what was required was a comprehensive framework of ideas for handling the models of critical systems and in particular their equilibrium fluctuations. Such a framework — known as the renormalization group — was proposed by Wilson in 1971 [41].

In this chapter only a broad outline of the philosophy of the renormalization group method is given as a large number of excellent reviews are available in the literature [42, 43, 44, 45, 46]. The modern theory of critical phenomena in two-dimensions is then considered. It represents a particular success of renormalization group theory because the strength of the typical fluctuations in two-dimensions is so large that mean field methods prove highly inaccurate. Next the Kosterlitz-Thouless transition is discussed. It is a prime example of a two-dimensional phase transition and is thought to describe both the superfluid transition in two dimensions and also the roughening transition of crystal surfaces.

## 2.1 The Renormalization Group

### 2.1.1 The Scaling Hypothesis

The divergence of the correlation length at criticality seems at first a serious complicating factor, implying as it does that all parts of the system are effectively coupled together. However, there is a powerful physical insight to be gained from the behaviour of the correlation length: it means that there is no longer any special length scale defined in the system, and so the system can be regarded as scale invariant. This way of looking at critical systems was first suggested by Kadanoff [40], who went on to show how

the critical properties of a system could be understood, to some extent, by rescaling. He considered a lattice based spin system which was divided into blocks and described by a set of spins with an associated set of coupling parameters. The spins of each block were averaged over, each being replaced by a single new spin, and so a new spin system could be obtained for which a new set of coupling parameters could be derived. Thus, in effect, a scale transformation was performed; by comparing the two systems it was possible to make inferences about the nature of the coupling parameters at the critical point, based on the assumption that the system was scale invariant at the transition.

The renormalization group method generalizes the idea of rescaling. There are three main steps in the procedure. Firstly, a small tranche of the degrees of freedom in the partition function are summed over (in real or momentum space), then the partially summed partition function is rewritten in the same form as the original one; finally the parameters in the old and new Hamiltonians are compared, leading to relations which describe how they change with scale.

In the case of a Hamiltonian,  $\mathcal{H}$ , describing the interactions of spins  $S_i$  on a given lattice via a set of coupling constants  $\{K_n\}$  (which contain subsumed within them the factor  $1/k_B T$ ), the renormalization procedure maps the original lattice onto another one with a rescaled linear dimension and spins  $S'_\alpha$  related to the original ones by some linear function,  $S'_\alpha = f(S_i)$  [44]. The probability of a given distribution of the spins,  $[S'_\alpha]$ , leads to the unique definition of a Hamiltonian for the rescaled system,  $\mathcal{H}'$ , which is related to the original Hamiltonian by the relation

$$e^{-\mathcal{H}'[S'_\alpha]} = \sum_{[S_i]} \prod_{\alpha} \delta(S'_\alpha - f(S_i)|_{i \in \alpha}) e^{-\mathcal{H}[S_i]}. \quad (2.1)$$

Thus given a configuration of the original spins  $[S_i]$ , there will be a unique configuration of the rescaled spins for which the delta function will be non-zero; hence

$$Z = \sum_{[S_i]} e^{-\mathcal{H}[S_i]} = \sum_{[S'_\alpha]} e^{-\mathcal{H}'[S'_\alpha]}. \quad (2.2)$$

The value of the partition function is preserved on rescaling.

However, the values of the couplings are changed: if the scaling relations for the coupling parameters in the Hamiltonian are written as differential equations then a flow surface can be determined in the parameter space and the associated fixed points of the system calculated. These points represent the special sets of values of the coupling parameters,  $\{K^*\}$ , which are unchanged by further applications of the renormalization group,  $R$ , and so are described by the relation

$$R[\{K^*\}] = \{K^*\}. \quad (2.3)$$

The parameters may flow towards, or away from, one or other fixed point as the renormalization group is successively applied; or they may follow a complex limit cycle in the parameter space. However, it is the fixed points which are of greatest interest as each one represents a critical point for the system.

It is now possible to see why complex real physical systems can be described to some effect using crude models and furthermore why such models, which differ in the number and size of the microscopic coupling parameters involved, often show the same critical behaviour. These properties, which are known collectively as universality, arise because the critical properties of a system are entirely determined by the characteristics of the fixed points that exist in the parameter space of the model. The starting point in parameter space and even its exact dimensionality do not dictate the critical behaviour that a model describes: it is instead the fixed points and the flow of the parameters nearby which determine the critical properties.

### 2.1.2 Scaling Variables

In order to investigate the behaviour of the parameters of a particular model close to a fixed point the simplest method is to linearise about that point. Consider again a Hamiltonian for a spin system containing a set,  $\{K_n\}$ , of constants which couple various spins [45]. If the constants are transformed to the set  $\{K'_n\}$  by application of the renormalization group and have the values  $\{K_n^*\}$  at the fixed point, then close to the fixed point,

$$K'_a - K_a^* = \sum_b T_{ab}(K_b - K_b^*) \quad (2.4)$$

where the matrix  $T$  has eigenvalues  $\lambda^i$ , and eigenvectors  $\phi^n$ , defined by:

$$\sum_a \phi_a^i T_{ab} = \lambda^i \phi_b^i. \quad (2.5)$$

One may then define the *scaling variables* of the system,  $u_i$ , as linear combinations of the deviations of the coupling constants from their fixed point values:  $u_i \equiv \sum_a \phi_a^i (K_a - K_a^*)$ . By definition then, the linearised renormalization flow equations for these quantities are multiplicative and take one of the following three forms:

$$\frac{du_i}{dl} = -a_1 u_i \quad (2.6)$$

$$\frac{du_j}{dl} = +a_2 u_j \quad (2.7)$$

$$\frac{du_k}{dl} = O(u_k^2), \quad (2.8)$$

where  $l$  is a renormalization parameter which defines the change in length scale when the renormalization group is applied and  $a_n$  is always a positive number. The naming of variables in renormalization group theory can be said to be non-intuitive. In eqn (2.6) the scaling variable  $u_i$  reduces steadily and will eventually vanish as scaling proceeds: operators which couple to scaling variables with flow equations like this are known as *irrelevant*, their exact behaviour does not affect the criticality of the system. The system will eventually flow to the critical point irrespective of the initial values of irrelevant scaling variables. Eqn (2.7) illustrates a *relevant* scaling variable:

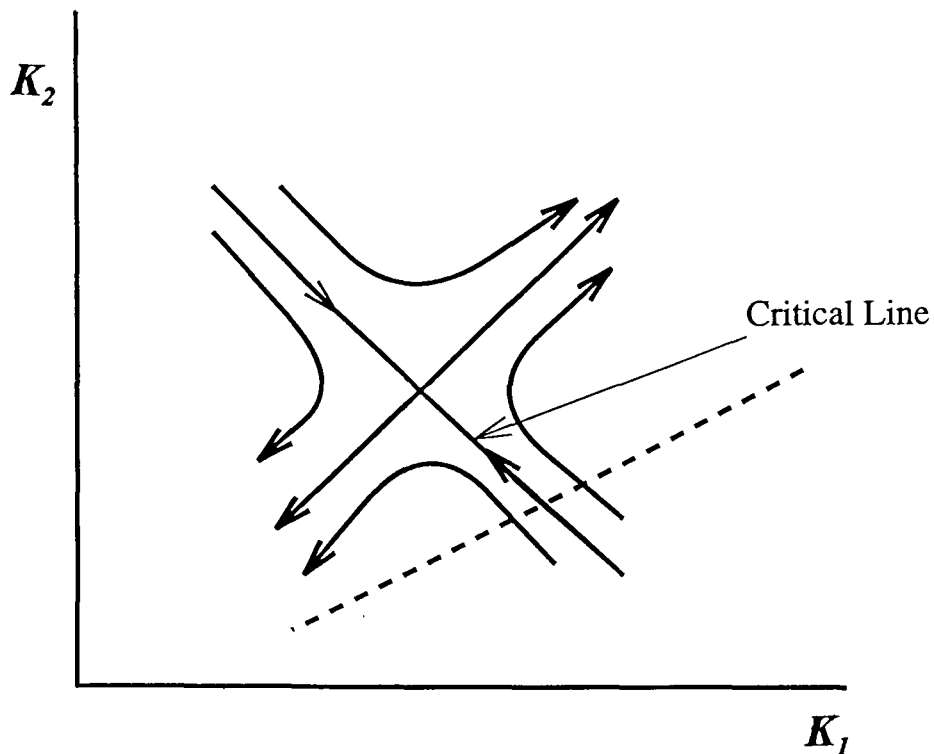


Figure 2.1 Critical surface and flow lines of a system described by two parameters  $K_1$  and  $K_2$ . The dotted line represents the trajectory in parameter space which is taken as one of the physical variables of the system is tuned (after [45]).

these variables increase close to the fixed point and their presence tells us that a phase transition will not occur unless such variables are initially zero. Heuristically one may think of relevant variables as analogous to those quantities which must be tuned in an experiment in order to reach a critical point. Finally eqn (2.8) illustrates the behaviour of a *marginal* scaling variable: to first order it remains the same as the fixed point is approached. The lowest order (non-zero) behaviour of marginal variables is frequently crucial in determining exactly when criticality occurs and the presence of such variables necessitates a higher order expansion about the fixed point.

In practice when renormalizing a model Hamiltonian for a system one must include all operators which are marginal and those which have the potential to become relevant when variable parameters reach certain values. However, under certain circumstances one may omit seemingly relevant operators without altering the physics of the system. Such ignorable operators are known as *redundant* and can be removed from a Hamiltonian by a shift in the coordinates of the parameters [45].

For a system described by  $n'$  parameters, of which say  $n$  are relevant close to a given fixed point, there will be a  $(n' - n)$ -dimensional hypersurface of points where the flow is attracted to the fixed point: this is the critical surface of the system. In practice when an experiment is tuned by adjusting physical

variables such as the temperature or magnetic field, a particular trajectory is taken through the parameter space whose exact form is determined by the dependence of the parameters,  $\{K_n\}$ , on the physical variables. A phase transition occurs when the trajectory dictated by the change in the physical variables intersects the critical surface. Figure 2.1, shows this process in detail for a system described by two parameters,  $K_1$  and  $K_2$ . The system can be analysed in terms of one relevant and one irrelevant scaling variable which are obtained from the parameters by an orthogonal transformation and lead to a critical surface which is simply a line. The dashed line represents the tuning of a single physical variable transformed into the parameter space — criticality occurs when it crosses the critical surface.

### 2.1.3 Landau-Ginzburg Theory

The description of the mechanics of the renormalization group given so far has been in terms of lattice based spin models which can be rescaled in a very straightforward way. However, there is a more general way of writing down the Hamiltonian of a system close to a phase transition which is also suitable for a renormalization group approach. This method, known as Landau-Ginzburg theory, is based around the order parameter of the system. It leads to a representation of the critical behaviour of condensed matter systems in terms of continuous classical fields to which the whole framework of functional integration and Feynman diagrams can be applied.

The first step in a Landau-Ginzburg theory is to identify the order parameter of the system — a step which in many cases proves non-trivial [47]. The low temperature phase almost always has a lower symmetry than the higher temperature phase and this is reflected in the nature of the order parameter which is uniform in the lowest energy state of the ordered phase. The order parameter need not be simply scalar; in fact except in the simplest cases it has two or more components, in particular the order parameter for superfluid helium was found to be a complex two-parameter field. Because it is the macroscopic fluctuations of the system which are of primary interest close to a phase transition, it is sufficient to define the order parameter as a classical field, that is as the continuous limit of a set of variables defined as the average of the parameter over cells which are large on an atomic scale. This method automatically introduces a minimum size for the fluctuations of the order parameter field, the size of the coarse graining cell, which is not defined exactly by the theory. The assumption is that close to a phase transition it is the long wavelength fluctuations which dominate the behaviour.

Having identified the order parameter of the system the next step is to write down a phenomenological Hamiltonian [48]. This is done in two parts: firstly there is a gradient term which reflects the preference the system has for a uniform order parameter field (this is the ‘free’ part of the Hamiltonian) and secondly a series of terms in powers of the order parameter, represented here by  $f[\phi(\mathbf{r})]$ , which are invariant under application of the symmetry group of the ordered phase

$$\mathcal{H} = \frac{K}{2} \int d^d \mathbf{r} (\nabla \phi(\mathbf{r}))^2 + \int d^d \mathbf{r} f[\phi(\mathbf{r})]. \quad (2.9)$$

The functional  $f[\phi(\mathbf{r})]$  models the coupling between the degrees of freedom in the system, whilst the gradient term describes the long wavelength fluctuations in the order parameter field.

The partition function can be written as a functional integral over the order parameter field weighted by the Boltzmann factor arising from the Hamiltonian:

$$\mathcal{Z} = \int \mathcal{D}\phi(\mathbf{r}) e^{-\mathcal{H}[\phi(\mathbf{r})]/k_B T}. \quad (2.10)$$

Renormalization proceeds by performing a partial integration, that is by summing over a thin tranche of the degrees of freedom in the system. This is often most conveniently done by writing the expression for the partition function in terms of momentum space and then integrating out a narrow section at the high momentum end. When the gradient operator is the most relevant the system is in its disordered phase: physically the ordering is destroyed by the long wavelength fluctuations (Goldstone modes). However, when the coupling term is the most relevant the system is in a more ordered state whose properties depend on the exact form of the coupling.

There is, however, a complication to this rather elegant scheme: the presence of defects or disorder in the order parameter field. Essentially a defect is a tear in the order parameter field. The most interesting cases are those tears which cannot be repaired by a continuous deformation of the field — the topological defects [47]. In order to understand the behaviour of a system at a continuous phase transition it is essential to identify the topological defects and decide whether they play a rôle in mediating the transition (as opposed to the Goldstone modes). If their behaviour is relevant then great care must be taken to include them explicitly in the phenomenological model. The Kosterlitz-Thouless transition in superfluid films is the best example of a defect mediated phase transition and the renormalization procedure described in this chapter explicitly includes the topological defects.

The Landau-Ginzburg model also has the advantage that it may be extended to model the dynamics of systems close to equilibrium. This is usually done by formulating a Langevin type equation in which the order parameter relaxes to equilibrium under the action of a generalized potential, arising from the phenomenological Hamiltonian, and the effects of random fluctuations due to the presence of a heat bath. The exact form of the equation of motion chosen depends on whether or not the order parameter is conserved and whether the dynamics are purely dissipative or contain reactive coupling between dynamical variables.

The simplest possible dynamical model is known as model A [49]. It is applicable to cases where there is no conservation law for the order parameter field. In this case the Langevin equation has the form

$$\eta \dot{\phi}(\mathbf{r}) = -\frac{\delta \mathcal{H}[\phi(\mathbf{r})]}{\delta \phi(\mathbf{r})} + R, \quad (2.11)$$

where  $R$  is a random noise term which has a Gaussian white spectrum,

$$\langle R(\mathbf{r}, t) R(\mathbf{r}', t') \rangle = 2D \delta(\mathbf{r} - \mathbf{r}') \delta(t - t') \quad (2.12)$$

and  $D$  is the diffusion constant. Models such as this may also be renormalized though the procedure is less well known than those involving partition functions in the form of functional integrals. The principle advantage of these so-called time dependent Landau-Ginzburg models is that they may be extended to explicitly include the effects of the external probing forces which are frequently used to study the behaviour of systems close to criticality.

Landau-Ginzburg theory has provided the basic framework and language which is used to analyse the behaviour of systems close to a phase transition. However, the Landau-Ginzburg method should be seen more as a broad outline rather than an explicit prescription for modelling critical behaviour. In particular, the approaches to the theory of the superfluid transition in thin films and the roughening transition of crystal surfaces described in this thesis both follow the spirit of the Landau-Ginzburg theory whilst differing somewhat in detail.

## 2.2 Transitions in Two-Dimensions

### 2.2.1 The Lower Critical Dimension

Two-dimensional systems display particularly interesting critical properties because the equilibrium fluctuations are much stronger than in three dimensions and yet they are not so overwhelming that the system is perpetually disordered as happens in most models with just one dimension. The case of a two-dimensional system with a continuous symmetry was considered by Mermin and Wagner. They proved that such systems cannot have a stable broken symmetry state at any finite temperature, which is equivalent to saying that there can be no long range order in such systems [5].

However the case of a two-dimensional system with a two component order parameter is a special case of Mermin and Wagner's theorem. It turns out that in this case the Landau-Ginzburg model leads to an order parameter correlation function which decays algebraically,

$$\langle \phi(0)\phi(\mathbf{r}) \rangle_{|\mathbf{r}| \rightarrow \infty} \sim |\mathbf{r}|^{-\eta},$$

where the parameter  $\eta$  depends on the temperature. Whilst a correlation function of this form undoubtedly precludes long range order, it does not have the form typical of disordered phases which is

$$\langle \phi(0)\phi(\mathbf{r}) \rangle_{|\mathbf{r}| \rightarrow \infty} \sim e^{-|\mathbf{r}|/\xi_+},$$

where  $\xi_+$  is the correlation length of the system. The curious state characterized by an algebraic decay of an order parameter field is known as quasi-long-range order. Since it cannot persist indefinitely as the temperature is raised, a phase transition must occur to the totally disordered state in which the order parameter field decays exponentially.

The exact nature of the transition was elucidated by Kosterlitz and Thouless who showed that the presence of a small but finite density of topological defects could lead to an algebraic decay in the order parameter field, whilst a proliferation of such objects destroyed all order [1, 2, 3]. In fact

the work of Kosterlitz and Thouless proved applicable to a diverse group of two-dimensional phase transition which share the property of a continuous symmetry in the  $O(2)$  group.

### 2.2.2 Kosterlitz-Thouless Theory

The essential properties of all the systems in the Kosterlitz-Thouless universality class can be described either in terms of a two-dimensional Coulomb gas model (an approach which emphasizes the importance of the topological defects) or as a sine-Gordon field theory. However, the two different approaches, though formally identical, actually involve rather different physical pictures.

The two-dimensional Coulomb gas model describes the behaviour of a neutral gas of classical charges confined to a two-dimensional world and is defined by the Hamiltonian:

$$\mathcal{H}_{CG} = - \sum_{\langle ij \rangle} q_i q_j \ln \left| \frac{\mathbf{r}_i - \mathbf{r}_j}{a} \right| + 2n\mu, \quad (2.13)$$

where  $q_i = \pm q$  and  $\mathbf{r}_i$  are the charge and position of the  $i$ th particle respectively;  $a$  is the particle radius;  $\mu$  the chemical potential;  $n$  the number of particles of each sign in the gas and the summation runs over all the pairings of the particles.

The two-dimensional Coulomb gas model is dual to another well known phenomenological model, the sine-Gordon model, even though the latter is formulated in terms of a field variable rather than discrete particles [9]. The Hamiltonian of the sine-Gordon model has the form

$$\frac{\mathcal{H}_{SG}}{k_B T} = \frac{1}{8\pi^2 K} \int d^2 \mathbf{r} (\nabla \phi(\mathbf{r}))^2 - \frac{2y}{a^2} \int d^2 \mathbf{r} \cos \phi(\mathbf{r}), \quad (2.14)$$

where  $y = \exp(-\mu/k_B T)$  and the Kosterlitz parameter  $K$  is defined by the relation  $\pi K = q^2/k_B T$ . The duality of the two systems means that the critical properties of all the systems which may be described by either model will be the same.

The two-dimensional Coulomb gas model is of interest because it undergoes a phase transition from an insulating state to a conducting plasma state. At low temperatures the charges form closely bound dipolar pairs; however, at the transition the charges spontaneously unbind and move independently of each other as in a conductor — they are said to be free. Kosterlitz and Thouless calculated the transition temperature heuristically by calculating the energy required to create free charges. The internal energy of an isolated charge of strength  $q$  and size  $a$ , is  $q^2 \ln(L/a)$ , where  $L$  is the linear dimension of the surface to which it is confined. Since the entropy of the particle is approximately  $k_B \ln(L/a)^2$ , the free energy is

$$F = \ln \left( \frac{L}{a} \right) (q^2 - 2k_B T). \quad (2.15)$$

In the simplest possible picture the transition to a conducting state occurs when the free energy of a single charge becomes less than zero, hence the transition temperature is  $T_{KT} = q^2/2k_B$ .

Kosterlitz applied the renormalization group to the two-dimensional Coulomb gas model and was thus able to give a far more detailed description of the transition [3]. Starting with a partition function of the form

$$Z = \sum_n \frac{1}{(n!)^2} \int_{D_{2n}} d^2\mathbf{r}_{2n} \dots \int_{D_2} d^2\mathbf{r}_2 \int_{D_1} d^2\mathbf{r}_1 \exp(-\mathcal{H}_{CG}/k_B T), \quad (2.16)$$

he used a calculational scheme based on that developed by Anderson and Yuval for the Kondo problem [50]. The regions of integration are actually quite complicated: the  $i$ th region,  $D_i$ , runs over all the possible positions in the plane of the  $i$ th topological defect. Thus  $D_1$  includes the whole plane,  $D_2$  includes all but a region of radius  $a$  around the position of the first defect,  $\mathbf{r}_1$ , and  $D_3$  excludes only the two regions around the first two defects, etc.

In order to make progress with the calculation, Kosterlitz made a number of assumptions about the system. Firstly he assumed that the fugacity,  $y$ , of the particles was small so that they could be considered as a dilute gas. Secondly he assumed that only particles of unit charge are present. Finally terms in the Hamiltonian that come from the interactions of charges of the same sign were ignored in the renormalization process as for small separations they make a negligible contribution to the partition function.

Renormalization then proceeds by carrying out a small part of the integrations and the core size is then rescaled to  $a + da$ . The effect is just to sum over contributions to the partition function from particles separated by distances between  $a$  and  $a + da$ . The final stage is to write the new expression for the partition function, obtained after the partial summation has been carried out, in the same form as the original one by introducing renormalized parameters. The differences between these renormalized parameters and their original counterparts then lead directly to the recursion relations of the system,

$$\frac{dy}{dl} = y(2 - \pi K) \quad (2.17)$$

$$\frac{dK^{-1}}{dl} = 4\pi^3 y^2, \quad (2.18)$$

where  $dl = da/a$ .

The structure of the critical surface can be understood more clearly if the reduced variable  $x = 1 - \pi K/2$  is introduced. Then the scaling variable can be eliminated and the resulting expression integrated to give the equation of the renormalization flow curves. Close to the fixed point at  $x = y = 0$ :

$$y^2 = \frac{1}{4\pi^2} (x^2 + C), \quad (2.19)$$

where  $C$  is a constant. Figure (2.2) shows the flow of the recursion relations. There are two lines of fixed points in the critical plane: for initial values of  $x$  less than zero and small values of  $y$ , the value of  $y$  always tends to zero as scaling proceeds, while for all other initial conditions  $y$  tends to infinity as scaling proceeds. The divergence of  $y$  signals a flow towards a trivial fixed point of the system at infinity, but the line of fixed points along the axis  $x < 0, y = 0$  in fact represents a *line* of well defined critical points.

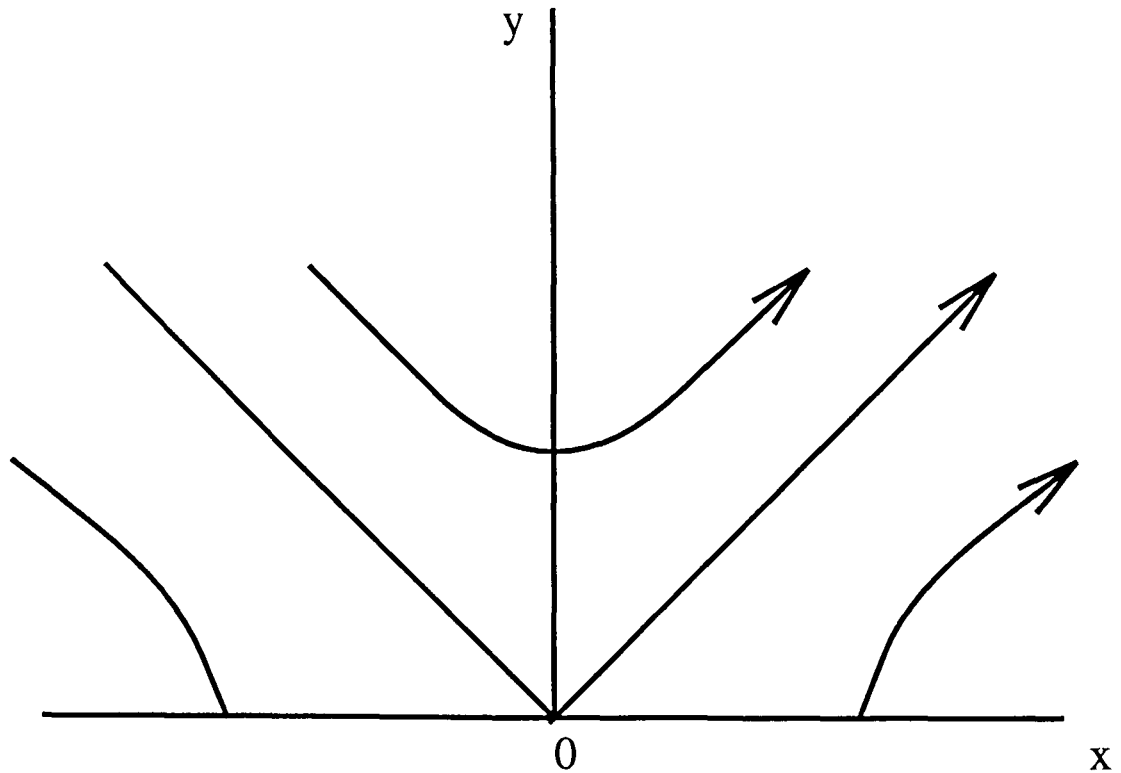


Figure 2.2 Renormalization flow of the Kosterlitz recursion relations close to the fixed point at  $x = y = 0$

The Kosterlitz-Thouless transition is marked by the separatrix of the basins of attraction of these fixed points. Since  $y$  is just the fugacity of a single charged particle, this implies (as expected) that there is a transition from a state where there are no free charges on large length scales to a state where they proliferate.

Kosterlitz also calculated the form of the correlation length,  $\xi_+$ , in the transition region. He found that it diverged faster than any power above the transition and was infinite for all temperatures below it,

$$\begin{aligned} \xi_+ &\sim \exp(bt^{-1/2}) \quad t > 0 \\ &= \infty \quad t < 0 \end{aligned} \tag{2.20}$$

where  $t = (T - T_{KT})/T$  and  $b$  is a constant which he found to have a value of approximately 1.5. This result is of course consistent with the idea derived from the renormalization flow that the low temperature phase is a line of critical points.

---

## Chapter 3 Superfluid Films

---

One of the most important achievements of the Kosterlitz-Thouless theory was the understanding it provided of superfluidity in thin films. Kosterlitz and Thouless recognized that the behaviour of superfluid films is controlled by the topological defects involved: in this case vortices. The presence of free vortices in a fluid film leads to the decay of superflow via the mechanism of phase slippage; but vortices of opposite sense exert an attraction on each other and where this is strong enough the film contains only closely bound vortex pairs which do not degrade the superflow. Thus Kosterlitz and Thouless postulated that the superfluid transition in films arose from the unbinding of vortex pairs. They wrote down a phenomenological Hamiltonian for the system solely in terms of the vortices, a Hamiltonian which is identical to that of a two-dimensional Coulomb gas.

This chapter contains a review of the Kosterlitz-Thouless transition as applied to superfluid films. It starts with a detailed exposition of how the superfluid transition in films may be described in terms of the behaviour of its topological defects. Then there is a derivation of the Kosterlitz recursion relations using the simplified ‘dielectric picture’, which as will be discussed, is of questionable validity despite its proliferation throughout the literature. This is followed by a detailed description of the linear response theory of Ambegaokar et al. (AHNS) [7, 8] and its application to the classic experiments on helium films performed by Bishop and Reppy [51]. Then a description of the alternative phenomenological linear response theory due to Minnhagen [14] is given. Finally there is a discussion of some of the problems with the theories. The majority of the material in this chapter has been obtained from the numerous excellent reviews of the field [14, 32, 33, 9, 43, 52].

### 3.1 Superfluidity in Two Dimensions

Superfluidity in bulk  $^4\text{He}$  is understood in terms of a Bose condensate. Crudely stated, a significant fraction of the atoms in the superfluid component condense into the ground state and become delocalised. The Bose condensate is described by annihilation and creation operators,  $\psi$  and  $\psi^*$ , and the order parameter is defined as the average value of the annihilation operator,  $\Psi(\mathbf{r}) = \langle \psi(\mathbf{r}) \rangle$ . This order parameter is a complex quantity, it lies in the  $O(2)$  symmetry group and is usually written explicitly in terms of a magnitude and phase

$$\Psi(\mathbf{r}) = |\Psi| e^{i\phi(\mathbf{r})}. \quad (3.1)$$

The properties of the superfluid depend crucially on the fact that there is phase coherence (i.e. long range order in the phase,  $\phi$ ), as well as uniformity in the magnitude of the order parameter [50]. The local superfluid velocity,

$\mathbf{v}_S$ , is given by the gradient of the phase at a point,

$$\mathbf{v}_S = \frac{\hbar}{m} \nabla \phi. \quad (3.2)$$

However, in two dimensions the Mermin-Wagner theorem predicts that long range order will be destroyed by phase fluctuations in the system for all finite temperatures because the phase displays a continuous symmetry. Therefore, until the work of Kosterlitz and Thouless in the early seventies, there was no convincing theoretical description for the superfluid behaviour of thin unsaturated helium films. Yet the superfluidity of helium films was known to occur as it had been observed experimentally as early as 1950 [53]. The validity of the Kosterlitz-Thouless approach was widely accepted after Ambegaokar et al. extended the theory to the finite frequency regime, which allowed direct comparison with a whole series of sophisticated experiments performed using superfluid films incorporated into torsional oscillators.

The key insight of Kosterlitz and Thouless was the realization that it was the statistical mechanics of the vortices that played the dominant rôle in mediating the transition. They started from a Landau-Ginzburg Hamiltonian for the system, which because of the underlying  $O(2)$  symmetry, has the form

$$\mathcal{H}[\Psi] = \int_{\Lambda} d^2\mathbf{r} \left( -\frac{\alpha}{2} |\Psi|^2 + \frac{\beta}{4} |\Psi|^4 + \frac{J}{2} |\nabla \Psi|^2 \right), \quad (3.3)$$

where  $\Psi$  is the order parameter of the system;  $\alpha$ ,  $\beta$  and  $J$  are functions of temperature, representing the fluctuations in the system on very short length scales which are averaged over in the process of coarse graining. The parameter which controls the extent of the coarse graining is the cut-off,  $\Lambda$ , which sets the minimum length scale in the problem.

The probability of the system being in an equilibrium state described by  $\Psi(\mathbf{r})$  is then simply

$$P_{eq}[\Psi(\mathbf{r})] \propto e^{-\mathcal{H}[\Psi]/k_B T}. \quad (3.4)$$

The simplest possible treatment of this system involves ignoring fluctuations in the magnitude of the order parameter: that is regarding  $|\Psi|$  as a constant. This approximation leads to a Hamiltonian of the form

$$\frac{\mathcal{H}}{k_B T} = \frac{1}{2} \int d^2\mathbf{r} K (\nabla \phi)^2, \quad (3.5)$$

where  $K = J|\Psi|^2/k_B T$ . The momentum density of a superfluid,  $\mathbf{g}_S$ , is defined by the relation [32]

$$\mathbf{g}_S = \frac{\delta \mathcal{H}}{\delta \mathbf{v}_S} \quad (3.6)$$

$$= \frac{m}{\hbar} J |\Psi|^2 \nabla \phi \quad (3.7)$$

so that if it is written in terms of a microscopic superfluid density,  $\mathbf{g}_S = \rho_S^0 \mathbf{v}_S$ , then this density is  $\rho_S^0/k_B T = (m/\hbar)^2 K$ .

A simple Hamiltonian like that defined in eqn (3.5) leads to a correlation function for the order parameter that decays algebraically as [32],

$$\langle \Psi^*(0) \Psi(r) \rangle \sim r^{-1/2\pi K}, \quad (3.8)$$

which, as described in chapter 2, is the signature of quasi-long-range order. However, that is as far as this model goes: it does not undergo a transition to another phase where the correlation function decays exponentially. What is described in this model is the behaviour of the long wavelength fluctuations in the phase (the Goldstone modes of the system). They destroy the long range order in the system at all finite temperatures, but they do not lead to a phase transition.

The next simplest model that can be formulated still ignores the effect of small fluctuations in the magnitude of the condensate wavefunction, but large fluctuations are included. Large fluctuations of the order parameter which cause it to vanish at discrete points are known as vortices. They have an important effect on the phase of the wavefunction in their immediate vicinity: the phase is undefined at the vortex core but away from the core the sum of the phases around any loop enclosing a vortex is quantised.

In order to include the effects of these large fluctuations in the magnitude of the wavefunction, the phase field is divided into two parts: a field entirely due to vortices,  $\varphi(\mathbf{r})$ , and a second vortex free field, which contains the phase fluctuations,  $\vartheta(\mathbf{r})$ :

$$\phi(\mathbf{r}) = \varphi(\mathbf{r}) + \vartheta(\mathbf{r}). \quad (3.9)$$

The two parts are distinguished by the values of the integrals of their gradients around closed paths. For the vortex field

$$\oint_C \nabla\varphi \cdot d\mathbf{r} = 2\pi n, \quad (3.10)$$

for some path  $C$ , surrounding a number of vortices where  $n$  is an integer equal to the algebraic sum of the winding numbers of the vortices enclosed by the contour. In contrast, the corresponding integral for the vortex free part is

$$\oint_R \nabla\vartheta \cdot d\mathbf{r} = 0, \quad (3.11)$$

for *all* paths  $R$ . The vortex field contains all the singularities in the order parameter field, by construction, and so must be treated carefully. The vortex free field, on the other hand, is smoothly varying. In addition, the vortex field is the minimum energy configuration which contains a given distribution of vortices — this is possible because the minimum energy configuration differs from all neighbouring configurations by a continuous transformation which can of course be included in the vortex free part.

Thus if vortices are explicitly allowed for in the Hamiltonian (eqn 3.5), it takes a modified form which may be separated into two parts due to vortices and phase fluctuations respectively,

$$\frac{\mathcal{H}}{k_B T} = \frac{1}{2} \int d^2\mathbf{r} K (\nabla\varphi + \nabla\vartheta)^2 \quad (3.12)$$

$$= \frac{1}{2} \int d^2\mathbf{r} K (\nabla\varphi)^2 + \frac{1}{2} \int d^2\mathbf{r} K (\nabla\vartheta)^2 \quad (3.13)$$

$$= \frac{\mathcal{H}_V}{k_B T} + \frac{\mathcal{H}_P}{k_B T}. \quad (3.14)$$

The cross term vanishes because of the constraint on  $\nabla\vartheta$ , eqn (3.11) [54]. Thus the vortex contribution can be totally decoupled from the spin wave contribution, which as has been discussed, is essentially uninteresting and does not lead to a phase transition. This leaves the vortices which may be treated as discrete, localized, entities with an interaction potential and a chemical potential which is simply the core energy,  $E_C$ , of a vortex. As is demonstrated in appendix A, the inter-vortex potential is logarithmic and so the contribution to the Hamiltonian from vortex excitations with a core radius of  $a$  may be written as

$$\frac{\mathcal{H}_V}{k_B T} = 2\pi^2 K \int \int_{|\mathbf{r}-\mathbf{r}'|>a} d^2\mathbf{r} d^2\mathbf{r}' n_v(\mathbf{r}) G(\mathbf{r}-\mathbf{r}') n_v(\mathbf{r}') + \frac{E_C}{k_B T} \int d^2\mathbf{r} |n_v(\mathbf{r})| \quad (3.15)$$

where  $n_v(\mathbf{r})$  is the position density of vortices of unit strength at  $\mathbf{r}$  and  $G(\mathbf{r}-\mathbf{r}')$  the Green's function for the interaction, which takes the form

$$G(r) = -\frac{\ln(r/a)}{2\pi}. \quad (3.16)$$

The core energies have to be added on separately because they represent the energy associated with the points where the magnitude of the condensate wavefunction drops to zero and so the phase is undefined.

Kosterlitz and Thouless predicted that at low temperatures the vortices in a superfluid film are all present as closely bound pairs and that the superfluid transition is caused by the unbinding of these pairs — leading to the presence of free vortices which cause phase slippage, rapidly destroying the superflow. Because the inter-vortex potential is logarithmic it is identical to the Coulomb interaction between charges when they are confined to two dimensions: if the identification  $q^2/k_B T \Leftrightarrow K$  is made, then the Hamiltonian above (eqn 3.15) is equivalent to that of the two-dimensional Coulomb gas given in chapter 2. This means that the phase transition in superfluid films is entirely analogous to the conductor/insulator transition in the two-dimensional Coulomb gas and indeed it is usually very convenient to use the language of electrostatics to describe the more exotic superfluid system.

### 3.2 The Dielectric Picture

A simple way of deriving the Kosterlitz recursion relations is to use an iterative mean field theory method, first derived by Kosterlitz and Thouless [1], which exploits the electrostatic analogy. This approach, known as the dielectric picture, is considerably simpler than the renormalization group method outlined in the previous chapter — both conceptually and in terms of mathematical content. Though this alternative picture was first considered by Kosterlitz and Thouless, it was Young who showed that it leads to the Kosterlitz recursion relations [55]. The dielectric model is probably the most common form in which the Kosterlitz-Thouless transition is described in the literature. However, despite the simplicity and consequent attractiveness of this model there is a serious drawback to this approach, as hopefully will become clear.

This derivation makes use of the analogy between vortices in helium films and charges in the neutral two-dimensional Coulomb gas model since it is

easier to work in the language of electrostatics: the implications for the helium system of the results obtained can then be deduced. The starting point is the expression for the energy of a pair of isolated charges,  $\pm q$ , which are separated by a distance  $r$  in a two-dimensional world,

$$U_0(r) = 2q^2 \ln \left( \frac{r}{a} \right) + 2E_C, \quad (3.17)$$

where  $a$  is the core radius of the charge and  $E_c$  the chemical potential, the charges are analogous to vortices with the magnitudes of the charges corresponding to the winding numbers of the vortices. In the two-dimensional Coulomb gas this pair-energy is modified by the presence of intervening pairs of smaller separation. The effect of these smaller dipoles can be taken into account by introducing a dielectric constant into the potential; the dielectric constant is defined with respect to an electric susceptibility, which itself depends on the density of pairs of a given size and their polarizability. Thus the static dielectric constant,  $\tilde{\epsilon}$ , may be defined by the relation

$$\tilde{\epsilon}(r) = 1 + 4\pi\chi(r) \quad (3.18)$$

$$= 1 + 4\pi \int_{a < |r'| < r} d^2\mathbf{r}' \Gamma(r') \alpha(r') \quad (3.19)$$

where  $\Gamma(r')$  and  $\alpha(r')$  are the number density and polarizability of charge pairs of separation  $r'$  respectively. Crucially the integration runs from  $a$  to  $r$ : small pairs polarize larger pairs but not the other way around. This assumption, known as the one-sided polarization approximation, is usually justified by observing that pairs with separation  $r' \gg r$  do not screen the test pair [55]. However, the effect of pairs of separation  $r' \simeq r$  is not represented accurately by eqn (3.19) [56].

The polarizability is obtained by considering a single dipole of moment  $qr = p_0$ , in the presence of a weak external field  $E_m$  — such as that which might be induced by pairs of larger separation. The average dipole moment in the direction of the field is  $\langle p_0 \cos \theta \rangle$ , the average being taken over all orientations weighted with the Boltzmann factor for the interaction energy  $-p_0 E_m \cos \theta$ ,

$$\langle p_0 \cos \theta \rangle = \frac{\int_0^{2\pi} d\theta p_0 \cos \theta e^{p_0 E_m \cos \theta / k_B T}}{\int_0^{2\pi} d\theta e^{p_0 E_m \cos \theta / k_B T}} \quad (3.20)$$

$$\simeq \frac{p_0^2 E_m}{2k_B T}, \quad (3.21)$$

since the field  $E_m$  is weak. Thus the polarizability is given by

$$\alpha(r) = \frac{\langle p_0 \cos \theta \rangle}{E_m} = \frac{q^2 r^2}{2k_B T}. \quad (3.22)$$

The interaction between two charges (eqn 3.17) can therefore be modified to take into account the effect of smaller pairs, thus

$$U_0(r) = 2q^2 \int_a^r \frac{dr'}{r' \tilde{\epsilon}(r')} + 2E_C. \quad (3.23)$$

In equilibrium the number density of pairs is given by

$$\Gamma(r) = \frac{1}{a^4} e^{-U_0(r)/k_B T} \quad (3.24)$$

$$= \frac{y_0^2}{a^4} \exp\left(\frac{-2q^2}{k_B T} \int_a^r \frac{dr'}{r' \tilde{\epsilon}(r')}\right), \quad (3.25)$$

where the bare fugacity of a vortex is  $y_0 = \exp(-E_C/k_B T)$ , so that by substituting this into the original expression for the dielectric constant (eqn 3.19) a self consistent equation can be obtained,

$$\tilde{\epsilon}(r) = 1 + 4\pi \int_{a < |r'| < r} d^2 \mathbf{r}' \frac{y_0^2 q^2 r'^2}{2k_B T a^4} \exp\left(\frac{-2q^2}{k_B T} \int_a^{r'} \frac{dr''}{r'' \tilde{\epsilon}(r'')}\right). \quad (3.26)$$

The Kosterlitz recursion relations then follow directly from this result, all that remains is to define the Kosterlitz parameter  $K$  in terms of the dielectric function. This is readily achieved as the unrenormalized value of the parameter is given by

$$\pi K(a) = \frac{q^2}{k_B T}, \quad (3.27)$$

hence

$$K(r) = \frac{K(a)}{\tilde{\epsilon}(r)}, \quad (3.28)$$

so the equation for the dielectric constant (eqn 3.26) reads:

$$K(r)^{-1} = K(a)^{-1} + 4\pi^3 \int_a^r dr' \frac{r'^3}{a^4} y_0^2 \exp\left(-2\pi \int_a^{r'} \frac{dr''}{r''} K(r'')\right). \quad (3.29)$$

If the standard scaling parameter,  $l = \ln(r/a)$ , is then introduced the equation for  $K$  becomes

$$K(l)^{-1} = K(0)^{-1} + 4\pi^3 \int_0^l dl' e^{4l'} y_0^2 \exp\left(-2\pi \int_0^{l'} dl'' K(l'')\right), \quad (3.30)$$

so that, if the renormalized fugacity is defined as

$$y(l) = y_0 e^{2l} \exp\left(-\pi \int_0^l dl' K(l')\right), \quad (3.31)$$

then

$$K(l)^{-1} = K(0)^{-1} + 4\pi^3 \int_0^l dl' y(l')^2 \quad (3.32)$$

and the Kosterlitz recursion relations follow:

$$\frac{dK^{-1}}{dl} = 4\pi^3 y^2 \quad (3.33)$$

$$\frac{dy}{dl} = (2 - \pi K) y. \quad (3.34)$$

This method of derivation is essentially a mean field theory, and as a consequence it is sensible to treat the results obtained with some caution. In

particular, the derivation involves the one-sided polarization approximation which is difficult to justify. Actually this dielectric model is just one of a range of similar models, each based on slightly differing assumptions, that lead to widely differing results [56]. This becomes clear from the equation for  $K$  which is obtained if the one-sided polarization assumption is not made,

$$K(\infty)^{-1} = K(0)^{-1} + 4\pi^3 \int_0^\infty dl' e^{4l'} y_0^2 \exp\left(-2\pi \int_0^{l'} dl'' K(l'')\right), \quad (3.35)$$

as it becomes apparent that the function  $K(r)$  is no longer defined.

The connection between the Kosterlitz recursion relations and the superfluid transition becomes clear when the charges of the Coulomb gas analogy are 'translated' into the language of liquid helium:

$$q^2 \Leftrightarrow \frac{\pi \hbar^2 \rho_S^0}{m^2}.$$

The macroscopic superfluid density is obtained from the renormalized Kosterlitz parameter,  $\rho_S = (m/\hbar)^2 K(\infty) k_B T$  and so can be related to the microscopic density via the dielectric function

$$\frac{\rho_S^0}{\rho_S} = \tilde{\epsilon}(\infty). \quad (3.36)$$

Hence according to the recursion relations, the macroscopic superfluid density tends to a universal value as the transition is approached from below [57],

$$\lim_{T \rightarrow T_{KT}^-} \rho_S = \frac{2k_B T m^2}{\pi \hbar^2}. \quad (3.37)$$

At the transition and at all higher temperatures the macroscopic superfluid density vanishes: the film becomes a normal fluid.

### 3.3 The Dynamic Theory of AHNS

The linear response of superfluid films to an oscillating substrate was initially considered by Ambegaokar, Halperin, Nelson and Siggia (AHNS) [7, 8]. Their theory proved to be in excellent qualitative agreement with experiments. However, quantitative agreement was rather more difficult to achieve.

When the substrate is set in motion it is assumed to couple perfectly to the normal component of the film (the film is assumed to be 'thin' in the sense that its depth is taken to be much less than the viscous penetration depth of the normal fluid), the vortices in turn are subject to the Magnus force due to the differences in velocity of the normal and superfluid components. This extra force can be seen as a modification of the intra-pair vortex potential,  $U(\mathbf{r}, t)$ , from the static form,  $U_0(\mathbf{r})$ , so that

$$U(\mathbf{r}, t) = U_0(\mathbf{r}) - \frac{2\pi \hbar \rho_s^0}{m} \mathbf{r} \cdot (\mathbf{k} \times (\mathbf{v}_n - \mathbf{u}_s)), \quad (3.38)$$

where  $\mathbf{v}_n$  is the local velocity of the normal component and  $\mathbf{u}_s$  the spatially averaged superfluid velocity. The easiest way of describing the dynamics of

superfluid films, again because of the resultant simplification in the notation, is to exploit the analogy with the two-dimensional Coulomb gas. The motion of the normal component is equivalent to an external electric field being applied across the Coulomb gas

$$q\mathbf{E}_{ext} \Leftrightarrow 2\pi \frac{\rho_s^0 \hbar}{m} \mathbf{k} \times \mathbf{v}_n. \quad (3.39)$$

However, the macroscopic field actually experienced by any pair of charges,  $\mathbf{E}$ , will be modified from the value of the external field by the average dipole moment of all the other pairs in the system, this of course just corresponds to the term in  $\mathbf{u}_s$  in eqn (3.38), thus

$$q\mathbf{E} \Leftrightarrow 2\pi \frac{\rho_s^0 \hbar}{m} \mathbf{k} \times (\mathbf{v}_n - \mathbf{u}_s). \quad (3.40)$$

Hence in the language of the Coulomb gas the charge dipole potential becomes

$$U(\mathbf{r}, t) = U_0(\mathbf{r}) - q\mathbf{E}(t) \cdot \mathbf{r}. \quad (3.41)$$

A dynamic dielectric function is then defined as the ratio of the macroscopic field,  $\mathbf{E}$ , to the magnitude of the external field:

$$\varepsilon(\omega) = \frac{\mathbf{E}_{ext}(t)}{\mathbf{E}(t)}. \quad (3.42)$$

The dielectric function is a complex quantity: the imaginary part arises from the component of the macroscopic field which is  $90^\circ$  out of phase with the external field.

It turns out that the dynamic dielectric function can be measured experimentally, as is discussed later on in this chapter, so it emerges as the key quantity to be calculated in the theory. In terms of the two-fluid model, the dielectric function simply relates the velocities of the superfluid and normal components

$$\mathbf{u}_S(\omega) = \left(1 - \varepsilon^{-1}(\omega)\right) \mathbf{v}_n(\omega).$$

AHNS model the motion of the  $i$ th dipole using a Langevin equation for the dipole length,  $\mathbf{r}_i$ :

$$\frac{d\mathbf{r}_i}{dt} = -\frac{2D}{k_B T} \nabla U(\mathbf{r}_i, t) + \boldsymbol{\eta}(t), \quad (3.43)$$

where  $D$  is the diffusion constant for the charges and  $\boldsymbol{\eta}$  a noise term, with Gaussian white spectrum

$$\langle \eta_i^\alpha(t) \eta_j^\beta(t') \rangle = 4D \delta_{ij} \delta_{\alpha\beta} \delta(t - t'). \quad (3.44)$$

An equivalent way of describing the dynamics [58] is to formulate a Fokker-Planck equation for the number density of pairs  $\Gamma(\mathbf{r}, t)$ ,

$$\frac{\partial \Gamma(\mathbf{r}, t)}{\partial t} = \frac{2D}{k_B T} \nabla \cdot (\Gamma(\mathbf{r}, t) \nabla U(\mathbf{r}, t) + k_B T \nabla \Gamma(\mathbf{r}, t)), \quad (3.45)$$

with the effective potential

$$U(\mathbf{r}, t) = U_0(\mathbf{r}) - qE(t)r \cos \theta. \quad (3.46)$$

When there is no external field applied the distribution evolves to an equilibrium value obtained by simply equating the time derivative to zero,

$$\Gamma_0(\mathbf{r}) = \frac{e^{-U_0(\mathbf{r})/k_B T}}{a^4} = \frac{y_0^2}{a^4} e^{-2\pi \int_0^l dl' K(l')}. \quad (3.47)$$

In the linear response regime, where the external field is sufficiently weak,  $\Gamma_0(\mathbf{r})$  provides the starting point for the calculation of the full time dependent distribution function. The electric field is taken to be a simple harmonic function of time  $\mathbf{E}_{ext}(t) = \mathbf{E}_{ext} e^{-i\omega t}$  and, as described in appendix B, up to linear order the dynamic distribution function may be written as

$$\Gamma(\mathbf{r}, t) = \Gamma_0(r) \left( 1 + \frac{qrE}{k_B T} g(r) \cos \theta e^{-i\omega t} + \dots \right), \quad (3.48)$$

where  $E$  is magnitude of the local field and the function  $g(r)$  is obtained by substituting this expression back into the Fokker-Planck equation. The linear differential equation for  $g(r)$  then has the form

$$\frac{i\omega r^2}{2D} g + r^2 \frac{d^2 g}{dr^2} + (3 - rV') r \frac{dg}{dr} - rV' g = -rV', \quad (3.49)$$

where  $V(r) = U_0/k_B T$ . AHNS use the function

$$g(r, \omega) \simeq \frac{14Dr^{-2}}{(14Dr^{-2} - i\omega)}, \quad (3.50)$$

which is an approximation to the exact solution when  $rV'$  in eqn (3.49) is replaced by 4, its value at the transition [58].

The average dipole moment of the charge pairs can now be calculated, so that the external and local fields can be related

$$\mathbf{E} = \mathbf{E}_{ext} - 4\pi \int d^2\mathbf{r} \, qr\Gamma(\mathbf{r}, t). \quad (3.51)$$

Substituting the linearised dynamic distribution function (eqn 3.48) into this equation and picking out the component along the direction of the external field and varying as  $e^{-i\omega t}$ , leads to an expression for the dynamic dielectric function:

$$\varepsilon(\omega) = 1 + \frac{4\pi q^2}{k_B T} \int d^2\mathbf{r} \, r^2 \cos^2 \theta g(r) \Gamma_0(r). \quad (3.52)$$

In the static limit ( $\omega \rightarrow 0$ ) the dynamic dielectric function reduces to the static value,

$$\lim_{\omega \rightarrow 0} \varepsilon(\omega) = \tilde{\varepsilon}(\infty)$$

and so the association of the dielectric function to the ratio of microscopic to macroscopic superfluid densities is generalized to

$$\varepsilon(\omega) = \frac{\rho_S^0}{\rho_S(\omega)}. \quad (3.53)$$

The analysis is complicated by the fact that in the dynamic regime the transition is broadened to include temperatures above the transition temperature.

According to the Kosterlitz recursion relations, above the transition temperature the fugacity diverges on long length scales and in consequence so does the pair distribution function. Hence the expression for the dielectric function (eqn 3.52) becomes invalid on long length scales. AHNS resolved this difficulty by making a sharp distinction between ‘bound’ and ‘free’ vortices. They claimed that it made no sense to describe vortices separated by large distances as bound, so they imposed a cut-off on the integral in eqn (3.52), at  $r = \xi_+$ , corresponding to the largest pair size considered bound:

$$\varepsilon_b(\omega) = 1 + \frac{4\pi^2 q^2}{k_B T} \int_a^{\xi_+} dr r^3 g(r) \Gamma_0(r). \quad (3.54)$$

This rather complicated expression can, after some algebraic manipulation, be rewritten in the simplified form

$$\varepsilon_b(\omega) = 1 + \int_a^{\xi_+} dr g(r) \frac{d\tilde{\varepsilon}}{dr}, \quad (3.55)$$

without further approximation.

They then added a contribution from the remaining free vortices, the density of which is chosen to agree with experiment via a fitting parameter  $F$ ,

$$n_f = \frac{F}{\xi_+^2}. \quad (3.56)$$

This leads to agreement with the static Kosterlitz-Thouless theory at the transition temperature for a value  $F = 1/2\pi$ . The free vortices are then simply assumed to diffuse in the macroscopic field leading, in the plasma analogy, to a conductivity of the form

$$\sigma = \frac{n_f q^2 D}{k_B T}.$$

This gives an extra contribution to the dielectric function, the free vortex contribution, which is

$$\varepsilon_f = i \frac{4\pi\sigma}{\omega}. \quad (3.57)$$

The total dielectric function for the system is simply the sum of the ‘free’ and ‘bound’ contributions:

$$\varepsilon(\omega) = \varepsilon_b(\xi_+, \omega) + \varepsilon_f(\xi_+, \omega). \quad (3.58)$$

### 3.4 Experiments on Superfluid Films

As mentioned above, the most successful experiments performed on films of helium were all performed at finite frequency. The most common experiments involved incorporating a helium film into a driven torsional oscillator, though the propagation of third sound through a film has also been measured.

The hydrodynamic propagation of third sound is of course a dynamic process and so can be analysed using the theory of AHNS and the results compared with those obtained from experiment [59, 33]. However, these studies give

far less information about the behaviour of the system close to the transition than torsional oscillator experiments and much less data is available for them, therefore they will not be considered in any detail here.

Torsional oscillator experiments on helium films were first performed by Reppy's group at Cornell in the late 1970s [51]. The basic method is to coat a substrate with a thin film of helium and then attach it to a torsional rod, either as a series of discs, or as originally described by Bishop and Reppy, in the form of a rectangular piece of substrate coated with a film which is tightly wound around itself (a geometry known as a 'jelly roll'). As the torsional oscillator is driven back and forth the normal component of the film locks to the substrate and so moves back and forth, but the superfluid component does not couple and so remains stationary.

The moment of inertia of a torsional oscillator which contains an area  $A$  coated with superfluid, of density  $\rho_S$ , is given by the expression

$$I(T, \omega) = R^2 (M + A(\rho - \rho_S)) \quad (3.59)$$

where  $R$  and  $M$  are the radius and mass of the oscillator system and  $\rho$  the density of helium. Because the moment of inertia depends on the superfluid density, changes in this density lead to a change in the period of the oscillator. Also as the normal component moves back and forth with respect to the superfluid component a Magnus force is exerted on the vortices, this leads to phase slippage and hence dissipation if the vortices are not tightly bound in pairs, so that the inverse  $Q$ -factor of the oscillator depends on the free vortex density.

Viewing the experiment as a simple harmonic oscillator [51, 60], with mass  $M$ , spring constant  $k$  and an internal dissipation  $\gamma$ , in the absence of any superfluid it has an equation of motion of the form

$$\left(-\omega^2 (M + A\rho) + i\omega\gamma + k\right) x = 0, \quad (3.60)$$

where  $x(t) = xe^{-i\omega t}$  is the displacement of the oscillator. In the presence of a finite macroscopic superfluid density, which is of course complex, this becomes

$$\left(-\omega^2 \left(M + A\rho - \rho_S^0 \operatorname{Re}(\varepsilon^{-1})\right) + i\omega \left(\gamma + \omega A\rho_S^0 \operatorname{Im}(\varepsilon^{-1})\right) + k\right) x = 0 \quad (3.61)$$

so that, in the limit of weak damping, the period is

$$P = 2\pi \left( \frac{M + A\rho - \rho_S^0 \operatorname{Re}(\varepsilon^{-1})}{k} \right)^{1/2} \quad (3.62)$$

If  $P_0$  is the period in the absence of any superfluid component, then the period shift is given by

$$\frac{2\Delta P}{P} = \frac{(P^2 - P_0^2)}{P_0^2} = \frac{A\rho_S^0}{M} \operatorname{Re}(\varepsilon^{-1}(\omega)). \quad (3.63)$$

The imaginary part of the superfluid density leads to a contribution to the dissipation so that if  $Q_0$  denotes the  $Q$ -factor in the absence of superfluid,

$$\Delta Q^{-1} = Q^{-1} - Q_0^{-1} = \frac{A\rho_S^0}{M} \text{Im} \left( -\varepsilon^{-1}(\omega) \right). \quad (3.64)$$

There is a further complication which prevents a direct application of these relations to the results of the experiments. It is found experimentally that the superfluid component does not remain entirely stationary during the experiment, a sizeable portion becomes mechanically entrained by imperfections in the substrate and oscillates back and forth. This effect is crudely accounted for by modifying the value of  $A/M$  by a factor  $(1 - \chi)$ , where  $\chi$  is the proportion of the superfluid component entrained by the substrate.

The value of  $\chi$  may be determined experimentally by the following procedure. As the cell is filled with helium the value of the period increases steadily until the film is thick enough to undergo a superfluid transition whereupon the period drops abruptly; then as more helium is added the period begins to increase again, but at a much slower rate than before. If it is assumed that the film is entirely superfluid then this increase in period with increasing helium density can be used to determine the proportion of the superfluid which is entrained [60]. The explanation usually given for this behaviour is a vague one which essentially attributes it to disorder in the substrate — in the case of the experiment using the ‘jelly roll’ configuration of the substrate it has been associated with a pinching together of different layers in the roll. It has been suggested that the  $\chi$ -factor arises from some geometrical feature of the system and this is supported by the fact that there seems to be no variation in its value with film thickness [60]. The theory of AHNS can only be applied to the experimental data after this effect has been taken into account and so within the context of their approach  $\chi$  is an empirical number for which there is no theoretical explanation.

Since the late 1970s, a fit to the theory of AHNS has formed an essential part of almost every experimental paper on the dynamics of two-dimensional superfluid and superconducting systems. The first and most detailed account of the actual fitting procedure is contained in an appendix, written by Teitel and Ambegaokar, to the classic paper of Bishop and Reppy [51].

Their fitting procedure was rather complex, involving as it did 6 separate fitting parameters. Values of the transition temperature,  $T_{KT}$ , the dynamic length scale,  $\sqrt{D/\omega}$ , the magnitude of the free vortex density  $F$ , the mass sensitivity of the oscillator  $\rho_S^0 A/M$  and a parameter  $b$  which describes the trajectories of the recursion relations, were all chosen to obtain the best fit to the experimental results.

The comparison of AHNS’s theory with experiment which originally appeared in Bishop and Reppy’s paper is reproduced in figure (3.1). The left hand side of the dissipation peak drops to an anomalously high value — something which has not usually been seen in subsequent experiments — and this was accounted for by Teitel and Ambegaokar simply by the introduction of a sixth fitting parameter which gave an additional contribution to the imaginary part of the dielectric function. It is worth noting that whilst the fit is good in most places, it certainly fails at the dissipation peak.

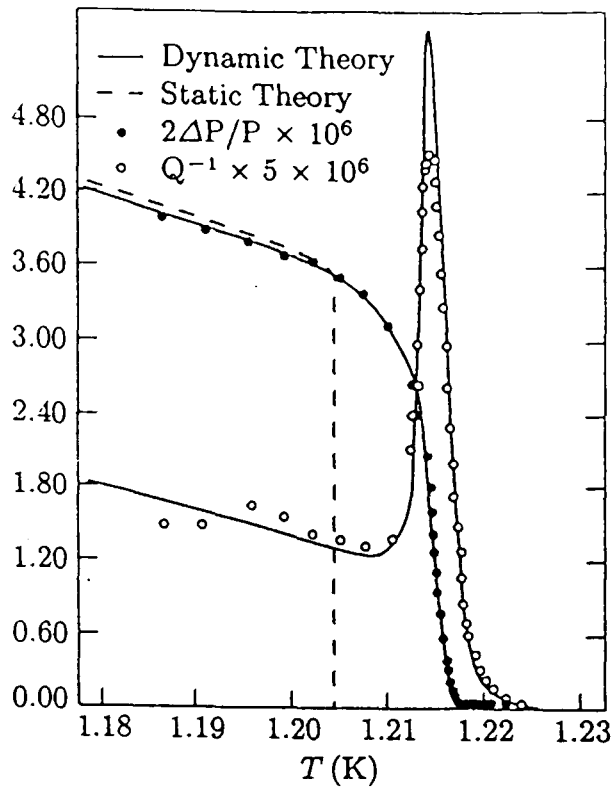


Figure 3.1  $2\Delta P/P$  and  $\Delta Q^{-1}$  measured by Bishop and Reppy [51], compared with the dynamic theory of AHNS and the prediction of the static theory (from [9]).

AHNS's theory has been compared with the results of more recent experiments on superfluid systems using a Mylar substrate [60, 61]. However, it has been found to provide a reasonable fit for only part of the data, despite the use of 5 or 6 fitting parameters. This is because there are considerable quantitative differences between experiments with different thicknesses of film.

### 3.5 Minnhagen's Theory

An alternative phenomenological theory of the dynamics of superfluid films and other two-dimensional superconducting systems is due to Minnhagen [14]. Although similar to the AHNS framework in its general approach and structure, Minnhagen's theory differs in several important ways. A detailed comparison of the predictions of Minnhagen's dynamic theory with the results of experiments on superconducting wire networks and the theory of AHNS was performed by Wallin [62].

The behaviour of vortices below the unbinding temperature is readily modelled using the logarithmic interaction potential: the difficulty arises, as was seen with the AHNS theory, in accounting correctly for the behaviour of the vortices above the transition temperature. Minnhagen also introduces the concept of free vortices, but does so in a carefully controlled way. There are three key quantities in the static version of his theory: the static dielectric constant  $\tilde{\epsilon}$  the screening length  $\lambda$  and the interaction cutoff  $\lambda_c$ . The two quantities  $\tilde{\epsilon}$  and  $\lambda$  represent the effects of bound and free vortices respectively on the bare vortex-vortex interaction whilst the length  $\lambda_c$  is the

maximum possible length for the interaction.

In Minnhagen's theory the limiting forms for the interaction potential between vortices are given by:

$$U(r) \propto \begin{cases} e^{-r/\lambda_c}/\sqrt{r} & \lambda_c \ll r \\ -\ln(r/\lambda_c) & a \leq r \ll \lambda_c \end{cases}. \quad (3.65)$$

The screening length,  $\lambda$ , is infinite below the transition temperature and finite above it: in the region of the transition, as  $T \rightarrow T_{KT}^+$ , it has the form

$$\lambda^{-2} = C_1 e^{(-C_2/\sqrt{T/T_{KT}-1})} \quad (3.66)$$

where  $C_1$  and  $C_2$  are constants and  $T_{KT}$  is the transition temperature. In this formulation the ratio of the bare to renormalized Kosterlitz parameters is calculated using the Fourier transforms of the bare and screened interaction potentials; it takes the form

$$\frac{K(\infty)}{K(0)} = \tilde{\epsilon}^{-1} \left. \frac{k^2 + \lambda_c^{-2}}{k^2 + \lambda^{-2}} \right|_{k=0}. \quad (3.67)$$

In formulating the dynamics, Minnhagen proceeds in a similar way to AHNS, that is by using a Langevin type equation of motion. The charges respond to an effective force made up of a component due to vortex-vortex interactions and another due to an external, time varying, electric field. In the linear response description the dynamic dielectric function relates the external field,  $\mathbf{E}^0$ , to the effective field felt by the charges

$$\mathbf{E}^{eff}(t) = \mathbf{E}^0 \text{Re} \left[ \epsilon^{-1}(\omega) e^{-i\omega t} \right]. \quad (3.68)$$

The key question is how eqn (3.67) is modified by the dynamics. Minnhagen assumes that the only major effect of the dynamics is to introduce a new length scale, the diffusion length  $\lambda_\omega = \sqrt{D/\omega}$ , into the problem. Pairs separated by distances less than the diffusion length respond adiabatically to the field, whilst pairs of larger separation do not have time to relax and their contributions to the renormalized quantities average out to zero. Thus the real part of the response function is given by

$$\text{Re} \left[ \epsilon^{-1}(\omega) \right] = \tilde{\epsilon}^{-1} \left. \frac{k^2 + \lambda_c^{-2}}{k^2 + \lambda^{-2}} \right|_{k=\lambda_\omega^{-1}} \quad (3.69)$$

$$= \tilde{\epsilon}^{-1} \frac{1+C}{1+Y} \quad (3.70)$$

where  $C = (\lambda_\omega/\lambda_c)^2$  and  $Y = (\lambda_\omega/\lambda)^2$ . The imaginary part is then obtained using the Kramers-Kronig relation [62],

$$\text{Im} \left[ \epsilon^{-1}(\omega) \right] = \tilde{\epsilon}^{-1} \frac{2}{\pi} \frac{Y-C}{1-Y^2} \ln Y. \quad (3.71)$$

Wallin compared the approach of Minnhagen to experiment. He points out that one of the problems in making a direct comparison between the theory

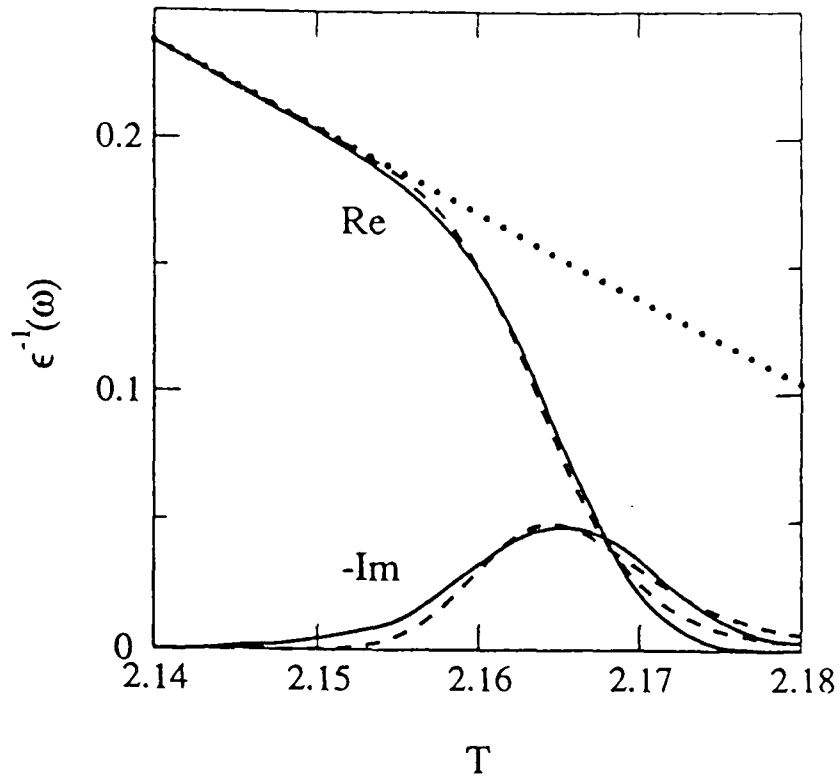


Figure 3.2 Comparison of the theoretical curves for the real and imaginary parts of  $\epsilon(\omega)^{-1}$  obtained by Wallin and the data of Jeanneret et al. (from [62]). The straight dotted line was used to obtain  $\tilde{\epsilon}^{-1}$  as a function of temperature from the data.

and experiments arises because the temperature dependence of the static dielectric constant,  $\tilde{\epsilon}$ , is not determined by the model. However, this problem can be bypassed if the ratio of the imaginary to real parts of the dynamic dielectric function is considered. For an ideal system in which the cut-off length,  $\lambda_c$ , is effectively infinite, a value for the ratio at the peak in the dissipation (known simply as the peak ratio) of  $2/\pi$  is obtained. Furthermore, Wallin points out that the effects of disorder in a system may be modelled in this framework by introducing a finite value for  $\lambda_c$  to represent the distance between inhomogeneities. This leads to a smooth decrease in the peak ratio to a value of about 0.2 when  $C = 5$ .

Wallin also compared the temperature dependence of the real and imaginary parts of  $\epsilon^{-1}(\omega)$  with a set of experimental data from a superconducting wire network, performed by Jeanneret et al. [27], which has a peak ratio of almost exactly  $2/\pi$ . Jeanneret et al. measured the complex a.c. conductance of networks of superconducting wires whose real and imaginary parts correspond to the quantities  $\text{Im}(-\epsilon^{-1}(\omega))$  and  $\text{Re}(\epsilon^{-1}(\omega))$  respectively. Wallin found that a good fit of both real and imaginary parts could be obtained if the value of the parameter  $\tilde{\epsilon}^{-1}$  was inferred from the straight line defined by the value of  $\text{Re}(\epsilon^{-1}(\omega))$  in the low temperature limit (see figure 3.2). The values of  $C_1$ ,  $C_2$  and  $T_{KT}$  required to calculate  $\lambda$  from eqn (3.66) were also obtained from the data.

### 3.6 Discussion

The qualitative agreement between the theory of AHNS and the results of torsional oscillator experiments has never been disputed; the theory has been successful in providing a phenomenological understanding of the dynamic behaviour of superfluid films. Their work appears widely in textbooks with the experimental results of Bishop and Reppy and the dielectric picture of Kosterlitz and Thouless. However, the dynamic theory has a number of weaknesses.

The most serious problem with the theory is the lack of precision in the predictions it makes: with up to six fitting parameters a whole range of curves could be obtained, without any reason why one should fit experiment better than the rest. The magnitude of the free vortex contribution and the crossover between the ‘bound’ and ‘free’ regimes in particular are obtained in an ad-hoc manner. Furthermore, despite the six parameter fit, the theory still does not fit at the dissipation peak and there is no obvious reason why it should fail in this region.

There are also some rather more subtle difficulties which only become apparent on a closer analysis of the experimental results. Most importantly there is nothing in the theory to account for the need to introduce the  $\chi$ -factor; more precisely it does not provide a natural way in which the disorder in the substrate can be described. The position was summed up by Reppy in a paper published in 1996, ‘quantitative agreement between the imaginary part of  $\rho_S$  and the predictions of the dynamic KT theory model has never been fully established for Mylar’ [63].

Minnhagen’s theory rests on a similar phenomenological basis to that of AHNS, but is rather more precise in the predictions it makes. It also has the advantage that it allows, to some degree, for the possible effects of substrate disorder. However, the prediction that the peak ratio should be  $2/\pi$  or less, although somewhat vague, is readily compared with experiment and proves to be inconsistent with much of the recent data available for superfluid films on Mylar for which the ratio varies from 0.3 to more than 2 [60, 61]. In addition, the need to obtain the value of the static dielectric function from the data is a serious drawback.

---

## Chapter 4 Refined Dynamics

---

This chapter contains a description of how the theoretical picture of the dynamics of superfluid films developed by AHNS can be refined. The purpose of such a refinement is to help determine whether the lack of quantitative agreement between the theory of AHNS and the results of torsional oscillator experiments is due to imprecisions in the theory or because it fails to capture some of the essential physics of superfluid films.

One of the most serious problems with the approach of AHNS is the need to add in the contribution of free vortices by hand. This is required because in the dynamic regime the transition is broadened and it is necessary to work in the region above the transition temperature where the use of Kosterlitz's recursion relations leads to a divergence of the fugacity on long length scales. One way of avoiding this problem is to derive recursion relations which are accurate to higher order in the fugacity. If such modified relations lead to a finite value of the fugacity under all conditions then in principle there would be no need to introduce an artificial cut-off on the integration over bound pairs and the additional free vortex term would not be needed.

Recursion relations accurate to next higher order in the fugacity have been worked out for the Kosterlitz-Thouless transition by several groups. There is general agreement about the order and sign of the next term in the fugacity recursion relation, but unfortunately estimates of its coefficient vary considerably. Most notable amongst the various calculations are those of Amit et al. [15], who used field theoretic methods to renormalize the sine-Gordon model; those of Minnhagen [14], and those of Timm who provides a very appealing geometrical argument to support his derivation [13]. Timm's form of the higher order recursion relations is particularly attractive because they have a very simple form which leads to a well defined high temperature fixed point at which the fugacity is finite. Minnhagen's higher order recursion relations are not considered here in any detail because his language is so different from that used by Kosterlitz and Timm.

This chapter describes how Timm's ideas can be used along with other refinements to improve the theory of AHNS, before going on to discuss how effective the resulting predictions are in describing the results of recent experiments. The first section contains a summary of how Timm obtained his recursion relations; this is followed by a description of how they may be used to calculate the dynamic response more accurately; next there is a comparison between the predictions of the refined theory and those of Minnhagen's dynamical theory; then there is a detailed comparison with the results of recent torsional oscillator experiments performed using Mylar and Grafoil substrates; finally there is a discussion of the successes and failures of the refined theory.

#### 4.1 Timm's Ansatz

The derivation of the generalized recursion relations by Timm is appealing in its simplicity. Although his argument is intrinsically interesting [13], there is no evidence, *a priori*, to suggest that the coefficients he obtains are more likely to be correct than any of the other derivations in the literature. However, in refining the dynamic theory it is the existence of a well defined high temperature fixed point, at which the fugacity is finite, which is of crucial importance. Timm's recursion relations, unlike those of Amit et al., satisfy this condition and so have been chosen to form the basis of the refined dynamic theory.

Timm sought to generalize the Kosterlitz-Thouless theory in two ways: first by correcting for the presence of overlapping dipolar pairs which must occur at higher vortex densities; second, by using a dielectric approximation for the polarization of the vortex system. The higher order term in the recursion relation for the fugacity arises from the inclusion of a geometric correction factor in the calculation which accounts for the presence of overlapping pairs. If  $\Gamma_0(r)d^2\mathbf{r}$  is the number of pairs per unit area with separations between  $r$  and  $r + dr$ , then the total pair density is just

$$N = \int_a^\infty d^2\mathbf{r}\Gamma_0(r). \quad (4.1)$$

As described in the previous chapter, in the AHNS picture the static pair distribution function is given by

$$\Gamma_0(r) = \frac{y_0^2}{a^4} e^{-2\pi \int_0^r dl' K(l')}. \quad (4.2)$$

Hence above the transition, when  $K(l)$  is renormalized to zero,  $\int dl' K(l')$  tends to a finite value as  $l \rightarrow \infty$  and so the total number density of pairs,  $N$ , is divergent. This result cannot be valid as the energy cost of a vortex pair is always at least  $2E_c$ , which is of course finite.

The apparent contradiction can be avoided by taking more care over the way in which vortices are assigned to pairs. To define the pairs uniquely, it is essential that they are formed in such a way that the total intra-pair separation is the minimum possible at each stage. Timm's ansatz is to introduce a factor into the pair distribution function to represent the probability that the pairings have been assigned correctly. Of course the gas of vortices is a many body system in which each vortex will interact with every other vortex, but Timm treats the assignment of vortices to pairs as a bookkeeping device. As long as the gas of vortices is neutral (in the sense that the algebraic sum of winding numbers is zero) it is possible to assign each of the vortices to a pair and so describe the interactions between vortices solely in terms of the interactions between pairs. Below the transition the pairings have physical significance since the vortices are bound together; in contrast, above the transition the pairings are purely a calculational device, but are valid so long as they are performed self consistently.

Consider adding a pair of separation  $r$  to a system containing pairs of separation up to but not including  $r$ . The probability that the vortex of the

pair being added *does not* lie within a distance  $r'$  of an anti-vortex already present, which belongs to a pair of separation  $r'$ , is just

$$1 - \Gamma_0(r')d^2\mathbf{r}'\pi r'^2.$$

Hence the probability that the vortex is not placed too close to *any* pre-existing anti-vortex is

$$\prod_{r' < r} (1 - \Gamma_0(r')d^2\mathbf{r}'\pi r'^2) = \exp\left(-\pi \int_a^r d^2\mathbf{r}'r'^2\Gamma_0(r')\right). \quad (4.3)$$

An identical factor is obtained from consideration of the placement of the anti-vortex, thus the pair distribution function may be written in the self consistent form

$$\Gamma_0(r) = \frac{y_0^2}{a^4} \exp\left(-2\pi \int_0^l dl' K(l') - 4\pi^2 \int_0^l dl' e^{4l'} a^4 \Gamma_0(l')\right). \quad (4.4)$$

Then since  $y^2(r) = r^4\Gamma_0(r)$ , a new self consistent relation for the fugacity is obtained

$$y^2(l) = y_0^2 \exp\left(4l - 2\pi \int_0^l dl' K(l') - 4\pi^2 \int_0^l dl' y^2(l')\right). \quad (4.5)$$

A new recursion relation for the fugacity follows immediately,

$$\frac{dy^2(l)}{dl} = y^2(l)(4 - 2\pi K) - 4\pi^2 y^4(l). \quad (4.6)$$

The second part of Timm's work concentrates on a possible way in which the recursion relation for  $K(l)$  can be generalized. He makes the observation that the standard dielectric picture (as discussed in the previous chapter) treats the dipoles as a continuous medium and so fails to include the effects due to the local field around any given charge. Timm suggests that this can be done using the Clausius-Mossotti type formula valid in two dimensions,

$$\tilde{\epsilon} = \frac{1 + \tilde{\epsilon}_a}{3 - \tilde{\epsilon}_a}, \quad (4.7)$$

where  $\tilde{\epsilon}_a$  is the dielectric constant calculated previously, ignoring local field effects.

Using Timm's method, the new fourth-order recursion relation for  $K(l)$  takes the form

$$\frac{dK}{dl} = -4\pi^3 y^2 K^2 \left(2 - \frac{K}{K(0)}\right). \quad (4.8)$$

The generalized recursion relations obtained by Timm lead to a flow diagram which is significantly modified from the usual Kosterlitz-Thouless form (see figure 4.1). There are two important new features in the diagram: firstly, for temperatures above the transition there is a fixed point which lies at  $(K(\infty) = 0, y(\infty) = 1/\pi)$ , so the fugacity remains bounded under all circumstances; secondly, because of the presence of the parameter  $K(0)$  the flow lines from different sets of initial conditions can cross. It is also worth

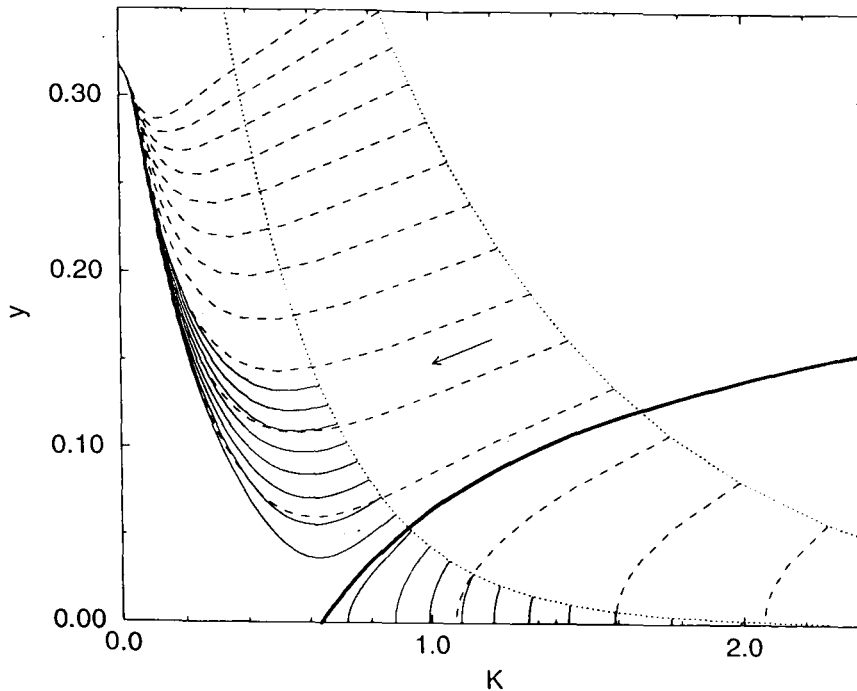


Figure 4.1 Plot of Timm's recursion relations (from [13]).

noting that the line of fixed points which correspond to the low temperature phase remain essentially unchanged.

Timm goes on to demonstrate that his recursion relations lead to exactly the same form of scaling for the correlation length,  $\xi_+$ , as in the standard Kosterlitz-Thouless theory. However, now the total vortex number remains finite, even above the transition temperature and so, as Timm points out, the regions above and below the transition may be treated on an equal footing.

## 4.2 Refined Theory

The idea of the refined theory is to calculate the dynamic response using the general approach of AHNS, but using Timm's recursion relations instead of those obtained by Kosterlitz. Because the total vortex number remains finite, an expression for the bound vortex contribution to the dynamic dielectric function can be derived which remains valid, even for temperatures above the transition, so that an arbitrary 'free' vortex contribution is no longer required. However, it is clear that even using Timm's generalized recursion relations involves a considerable approximation, they are after all only accurate to fourth order in the fugacity. The hope is that the approximations made using this method will be less arbitrary than those involved in adding in a 'free' vortex term.

In order to work out the dynamics of the system using the new recursion relations the starting point is Timm's expression for the static pair distribution function [16]. If the equilibrium pair distribution, given by eqn (4.4) above, is assumed to arise from an effective potential in a Boltzmann factor

then this potential must have the form

$$\frac{U_0^{eff}}{k_B T} = 2\pi \int_0^l dl' K(l') + 4\pi^2 \int_0^l dl' y^2(l') + \frac{2E_c}{k_B T}. \quad (4.9)$$

To obtain the correct static limit, a Fokker-Planck equation is again used to obtain the dynamic pair distribution function,

$$\frac{\partial \Gamma(\mathbf{r}, t)}{\partial t} = \frac{2D}{k_B T} \nabla \cdot \left[ \Gamma(\mathbf{r}, t) \nabla U^{eff}(\mathbf{r}, t) + k_B T \nabla \Gamma(\mathbf{r}, t) \right], \quad (4.10)$$

with

$$U^{eff}(\mathbf{r}, t) = U_0^{eff}(r) - qEr \cos \theta e^{-i\omega t}. \quad (4.11)$$

The extra term in the potential leads to an additional radial probability current term in the Fokker-Planck equation. Physically this extra current term is due to the rearrangement of pairs: over time the positions of the charges change so that the pairings will need to change continually in order to remain consistent.

As before, a solution up to just linear order is required and so a substitution of a trial function of the form

$$\Gamma(\mathbf{r}, t) = \Gamma_0(r) \left( 1 + \frac{qrE}{k_B T} g(r) \cos \theta e^{-i\omega t} + \dots \right), \quad (4.12)$$

is made into the Fokker-Planck equation. This again leads to a differential equation for the function  $g(r)$ ,

$$\frac{i\omega r^2}{2D} g + r^2 \frac{d^2 g}{dr^2} + (3 - rV') r \frac{dg}{dr} - rV' g = -rV', \quad (4.13)$$

but this time the potential term has the modified form

$$rV' = r \frac{d}{dr} \left( \frac{U_0^{eff}}{k_B T} \right) = 2\pi \left( K(l) + 2\pi y^2(l) \right) = 2\pi \kappa(l). \quad (4.14)$$

It is now straightforward to recalculate the dynamic dielectric constant: first Timm's recursion relations are used to get  $K(l)$  and  $y(l)$ , starting from a convenient set of initial conditions; eqn (4.14) is then used to obtain the function  $g(r)$ ; finally, the dynamic dielectric function comes from the relation used by AHNS to calculate the bound pair response

$$\varepsilon(\omega) = 1 + \int_a^\infty dr g(r) \frac{d\tilde{\epsilon}}{dr}. \quad (4.15)$$

Crucially though, there is no longer a term from 'free' vortices to be added in: the integral runs to infinity, including all the vortices.

#### 4.2.1 Numerical Method

Obtaining the function  $g(r)$  from eqn (4.13) is essentially a standard two point boundary value problem. However, the presence of the  $\kappa(l)$  term complicates matters: to obtain it accurately it is necessary to integrate Timm's recursion relations up to the length scale  $l$  and values for  $K(0)$  and  $y(0)$  have

to be chosen. In practice a small initial value of the fugacity is chosen as the recursion relations still represent a very limited expansion in powers of this quantity, whilst the value of  $K(0)$  is carefully varied in order to sweep through the transition.

The equation for  $g(r)$  is readily rewritten in terms of  $\kappa(l)$  and the scaling parameter  $l$ ,

$$\frac{i\omega a^2 e^{2l}}{2D}g + \frac{d^2g}{dl^2} + (2 - 2\pi\kappa(l))\frac{dg}{dl} - 2\pi\kappa(l)g = -2\pi\kappa(l). \quad (4.16)$$

The simplest way of obtaining a numerical solution to this equation is to split it into two coupled, first order, differential equations of the form

$$\frac{dg}{dl} = f \quad (4.17)$$

$$\frac{df}{dl} = -(2 - 2\pi\kappa(l))f + 2\pi\kappa(l)g - \frac{i\omega a^2 e^{2l}}{2D}g - 2\pi\kappa(l). \quad (4.18)$$

The boundary condition at  $l = 0$  is  $g(0) = 1$ , obtained using the static limit. The far boundary is set at a value  $l = l_f$ , and the boundary condition there is obtained from the asymptotic solution of eqn (4.16) for large  $l$ ,

$$g(l_f) \simeq i \frac{4\pi\kappa(l_f) D e^{-2l_f}}{\omega a^2}. \quad (4.19)$$

The value of  $l_f$  is chosen to be sufficiently large that the value of  $g(l_f)$  is negligible, this condition is achieved using

$$l_f = \frac{1}{2} \ln \left( \frac{2D}{\omega a^2} \right) + 3. \quad (4.20)$$

The quantity  $l_D = (\ln(2D/\omega a^2))/2$  represents the length scale beyond which pairs are unable to equilibrate with the external field.

There are several standard techniques for obtaining accurate numerical solutions to coupled first order differential equations with two point boundary conditions. It turned out that the so called ‘relaxation method’ proved the most effective in this case (the commonly used alternative ‘shooting’ method was also tried, but failed to provide a rapidly convergent solution). The particular implementation of the relaxation method used was adapted from that described in the book, ‘Numerical Recipes’ by Press et al. [64]. Essentially the technique involves transforming the coupled ordinary differential equations into a series of finite difference equations spanning a grid of 800 points, spaced between  $l = 0$  and  $l = l_f$ , which incorporate the boundary conditions at the edges. An initial guess is made at the values of the functions  $f(l)$  and  $g(l)$  at each of the grid points, the values are then substituted into the finite difference equations, leading to corrections to the initial values which are then altered accordingly and substituted back into the FDEs and so on recursively until the values converge. In practice, the initial values were chosen using Ambegaokar and Teitel’s approximate form of  $g(l)$ , and the values ‘relaxed’ to convergent solutions within two or three iterations. Care

was also taken to space the grid points to greatest effect — the majority of the points were distributed over the region where  $g(l)$  was anticipated to vary most strongly (i.e.  $l > l_f/2$ ), an approach which was readily justified *a posteriori*.

The only complicating feature in the calculation was the need to obtain  $\kappa(l)$  at each of the grid points. This was achieved using a sequence of subroutines that performed an adaptive 4th–5th order Runge-Kutta numerical integration. The differential equations involved were sufficiently straightforward to make this process routine and issues such as step size proved to be relatively unimportant.

The final integration to obtain the dynamic dielectric function (from eqn 4.15) was then performed using a simple minded trapezoidal method. This step was again straightforward, though it proved necessary to use double precision arithmetic to obtain accurate results as the quantities involved were quite small.

#### 4.2.2 Results

Starting with the initial values  $y(0) = 0.1$  and  $l_D = 10$  the value of  $K(0)$  was varied from 1.32 to 1.34 and integration performed over the range  $l = 0$  to  $l = l_D + 3$ , thus sweeping through the transition region, as can be seen from the plot of Timm's recursion relations in figure (4.1). As the recursion relations were integrated the quantity  $l_+$ , which is related to the correlation length of the system, was measured using the definition  $K(l_+) = 1/\pi$  (this gives a value roughly half the size quoted by Timm as he uses the definition  $K(l_+) = 2/\pi$ ; however, this is unimportant as it is the relative differences in this quantity, not its absolute values, which are of interest). The differential equations for  $g(l)$  were then solved numerically, as described above, and the real and imaginary parts of the inverse of the dynamic dielectric function were then calculated. The same procedure was then repeated for differing initial values of the fugacity:  $y(0) = 0.2$  and  $0.3$ , the values of  $K(0)$  being chosen in each case to sweep through the transition; then the value of  $l_D$  was altered to 8 and the calculation again repeated.

The real and imaginary parts of the function  $g(l)$ , calculated using  $y(0) = 0.1$ , are shown in figures (4.2) and (4.3) respectively for the three values of  $K(0)$ : 1.34, 1.33 and 1.32. The real part of the function dips slightly as  $K(0)$  is reduced before returning to almost its initial shape. The behaviour of the imaginary part is similar but not identical; again as  $K(0)$  is reduced the peak in  $\text{Im}(g(l))$  initially decreases, but on further reduction of  $K(0)$  it increases, to a slightly greater height than initially and with a broader shape.

The variation of the real and imaginary parts of the quantity  $K(0)\varepsilon^{-1}(\omega)$  with  $l_+$  for different values of the bare fugacity,  $y(0)$ , is shown in figures (4.4) and (4.5) respectively. As expected, the real part shows a rapid increase over a short range, before levelling out: this is just the superfluid jump. The imaginary part is similarly predictable in shape, displaying a clear dissipation peak. However, what is new here is that the curves obtained are relatively independent of the exact value of  $y(0)$  chosen (the value was kept within a

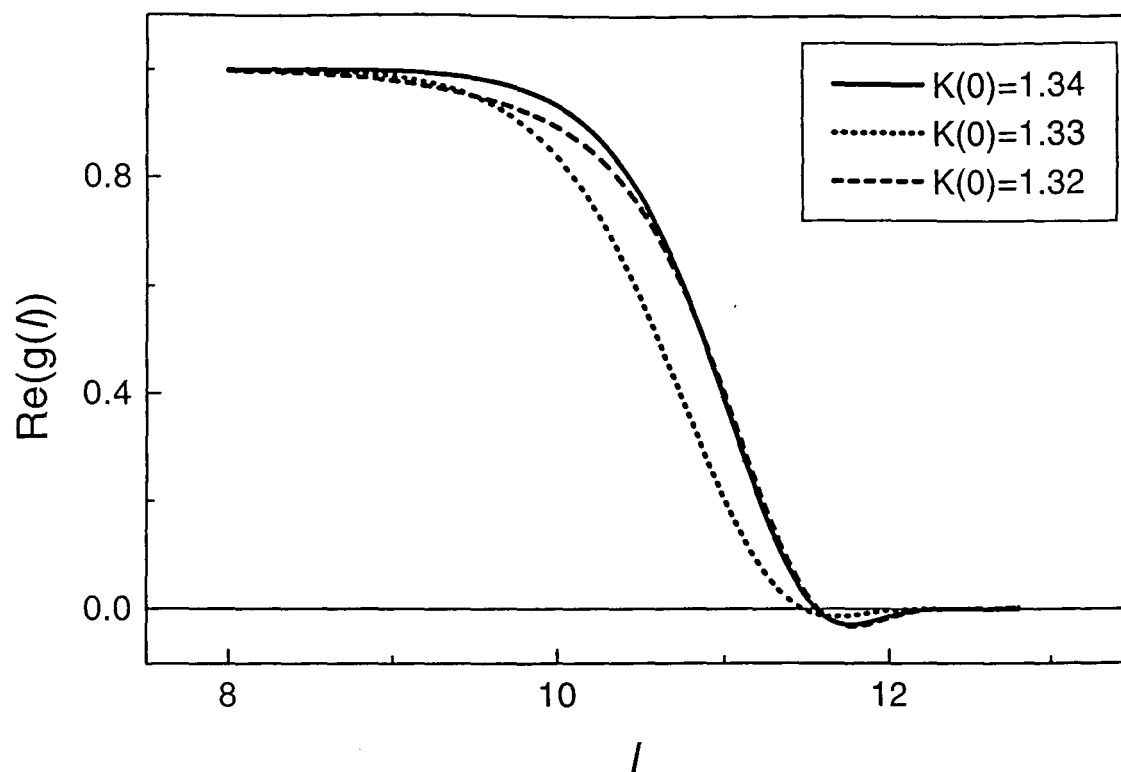


Figure 4.2 The real part of  $g(l)$  for  $K(0)=1.34$ , 1.33 and 1.32

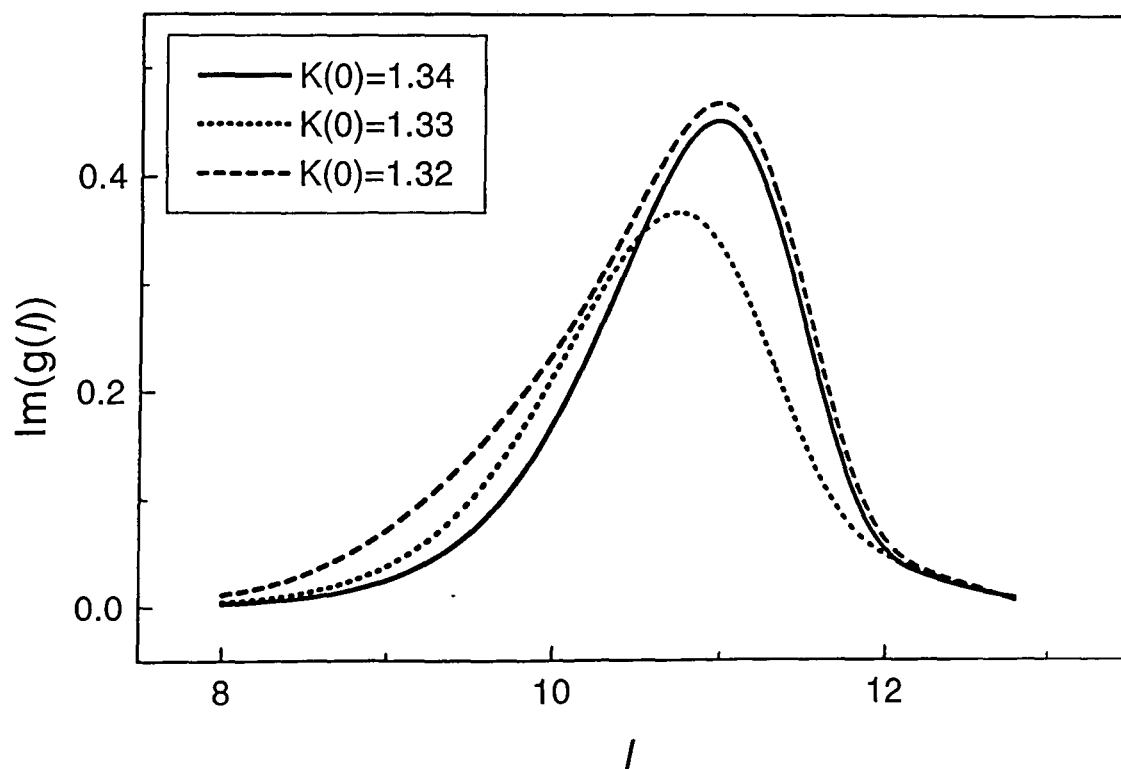


Figure 4.3 The imaginary part of  $g(l)$  for  $K(0)=1.34$ , 1.33 and 1.32

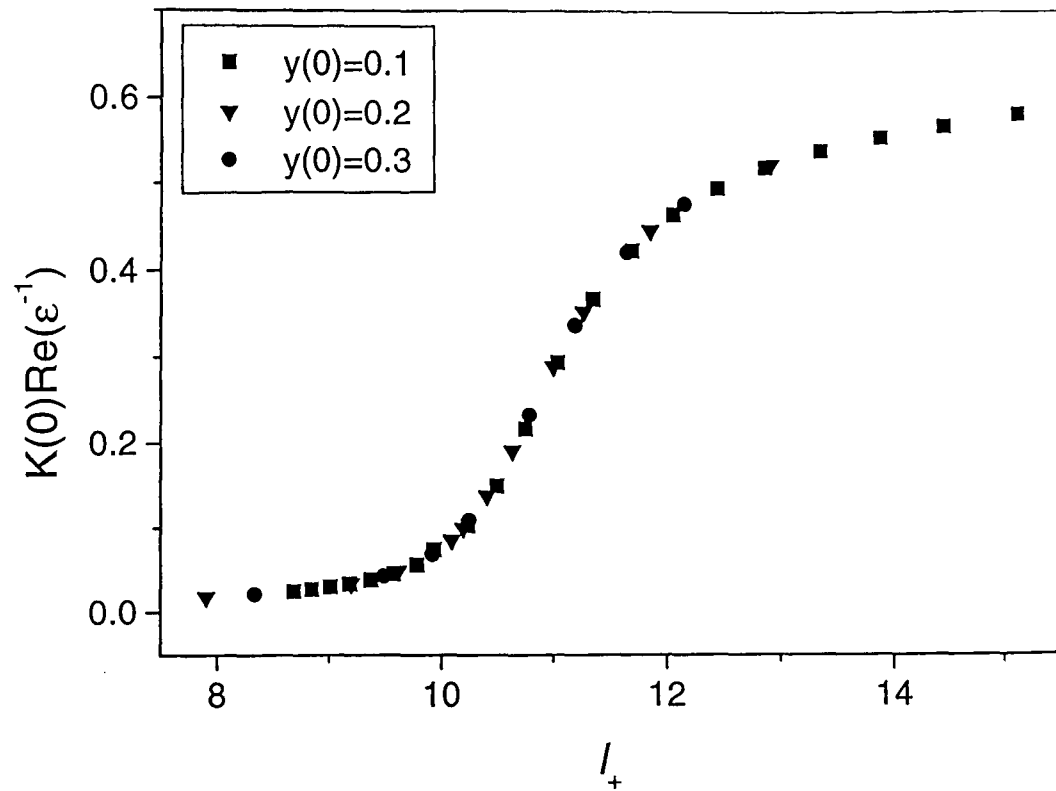


Figure 4.4 The variation of the real part of  $K(0)\varepsilon^{-1}(\omega)$  with  $l_+$  for  $y(0)=0.1, 0.2$  and  $0.3$

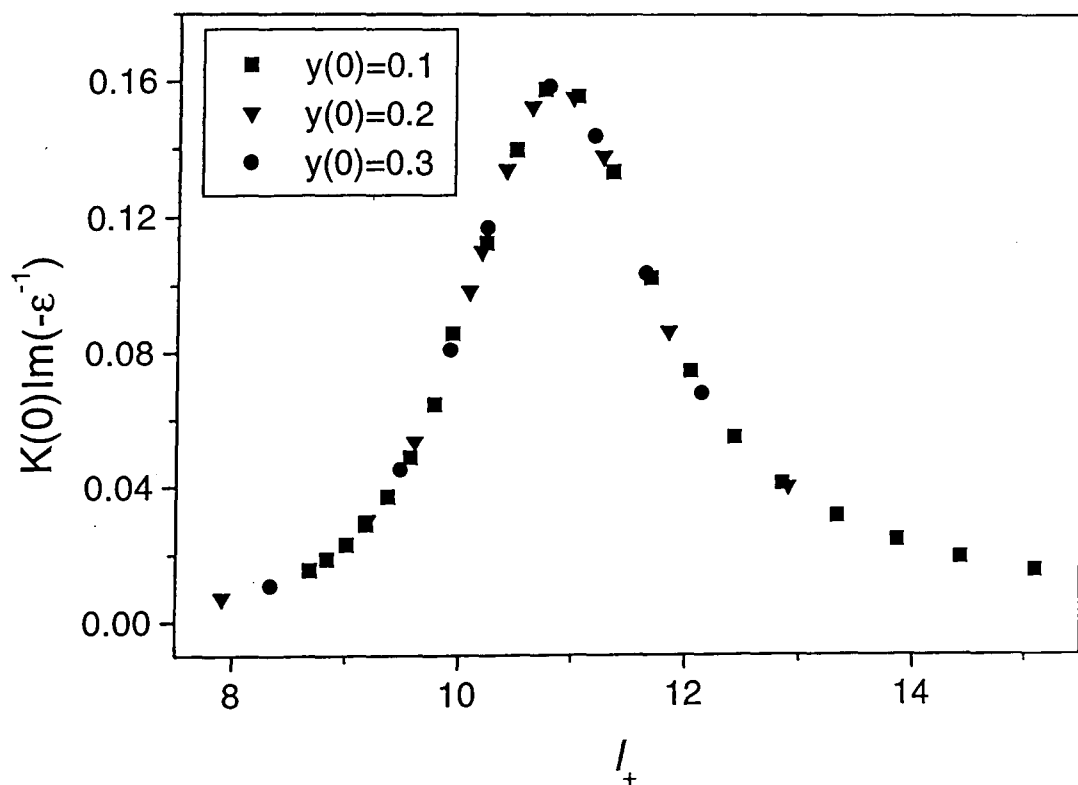


Figure 4.5 The variation of the imaginary part of  $K(0)\varepsilon^{-1}(\omega)$  with  $l_+$  for  $y(0)=0.1, 0.2$  and  $0.3$

limited range because the calculation is still based on the assumption that it is a small quantity). In fact this apparent universality extends to variations in the values of the other key parameter,  $l_D$ , as is shown in figures (4.6) and (4.7). This implies that the theory predicts a single universal curve which does not need to be tuned by altering the values of microscopic parameters, it offers the prospect of a fit to experiment with few if any fitting parameters.

A major complication which arises in fitting to experiment concerns the temperature dependence of the quantity  $l_+$ . The usual method employed is to model its variation with temperature using a set of arbitrary parameters, chosen to fit experiment. However, there is another way of looking at the results which obviates this problem [65], that is to plot the real and imaginary parts of the response function directly against each other, on an Argand diagram. Thus the whole problem of assigning a temperature dependence to  $l_+$  is avoided. Figure (4.8) shows the response function of the refined dynamic theory,  $K(0)\varepsilon^{-1}(\omega)$ , plotted in this way. The maximum in the imaginary part has a value of 0.158 and the ratio of the imaginary to real parts at the maximum is  $0.64 \pm 0.01$ . Now the fit to experiment can, in principle, be performed without adjustable parameters if the values of  $A/M$  and  $\chi$  can be measured accurately.

#### 4.2.3 Finite Size Effects

In the refined theory the length scale associated with the dynamics,  $l_D$ , is implicitly assumed to be the most important length scale in the problem. Accordingly, the integrations are performed up to a scale described by  $l_f = l_D + 3$  in each case. For an inhomogeneous substrate this may not be a safe assumption: there may be an additional length scale characterizing the disorder in the surface which proves more relevant than  $l_D$ . The effect of the disorder can be described crudely by stopping the renormalization at a length scale associated with the inhomogeneity. Such an approach would be in the same spirit as the use of a finite cut-off on the inter-vortex interaction,  $\lambda_c$ , introduced by Minnhagen.

The refined theory can easily be adjusted to gauge the effect of a finite size cut-off in the recursion relations. If instead of integrating up to  $l_f = l_D + 3$ , the integrations are performed up to  $l_f = l_D + C$  with  $C < 3$  then a curve with a rather different shape is obtained. As shown in figure (4.9) the main effect of reducing the cut-off  $C$  is to reduce the size of the imaginary component. This is consistent with the effect of a finite interaction cut-off,  $\lambda_c$ , in Minnhagen's theory.

The method is certainly crude, but it does provide a qualitative picture of how the theory is changed if the length scale of substrate disorder becomes shorter than the length scale associated with the dynamics.

### 4.3 Comparison with Minnhagen

The theory of Minnhagen was compared by Wallin with the results of experiments on superconducting wire networks performed by Jeanneret et al., which are analogous to the torsional oscillator experiments performed on superfluid films [27]. Jeanneret et al. measured the complex a.c. conductance

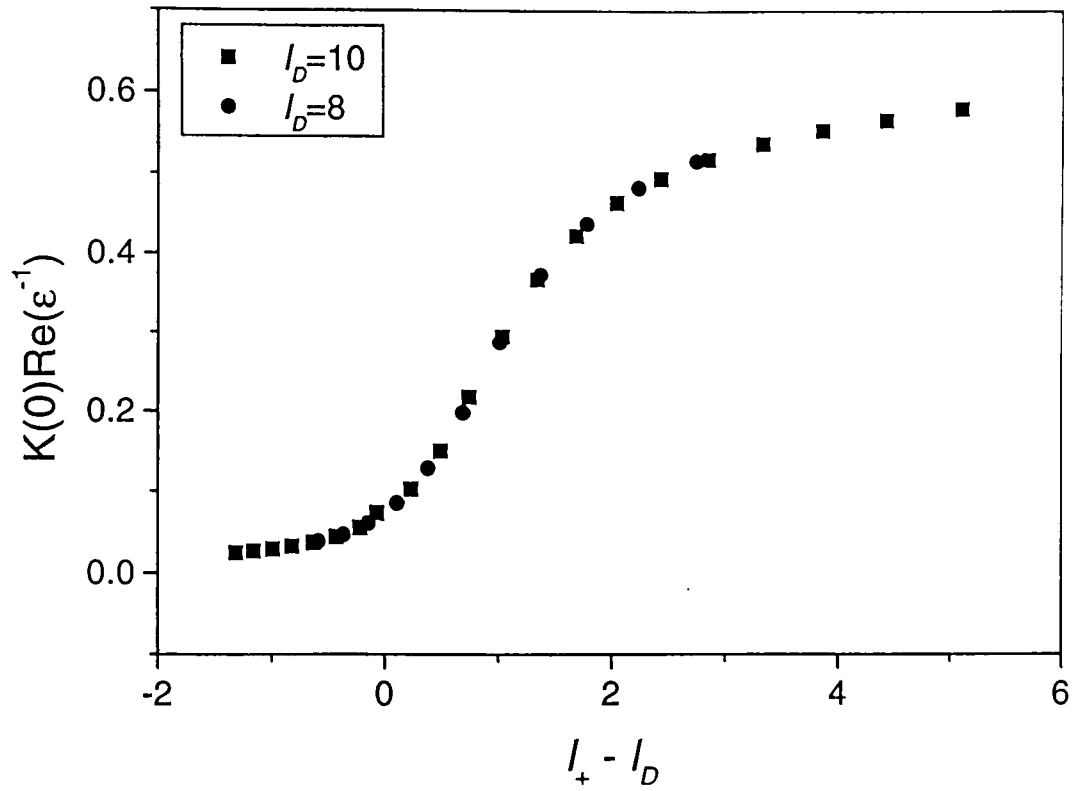


Figure 4.6 The variation of the real part of  $K(0)\varepsilon^{-1}(\omega)$  with  $l_+$  for  $l_D=10$  and 8

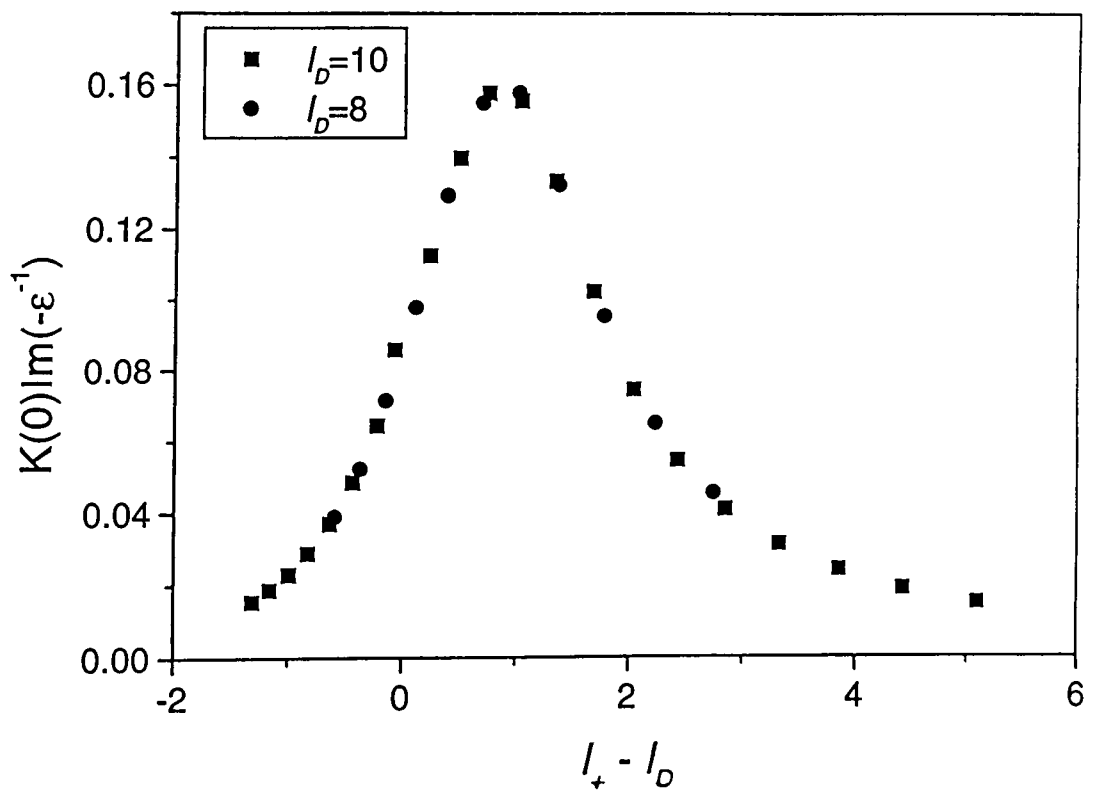


Figure 4.7 The variation of the imaginary part of  $K(0)\varepsilon^{-1}(\omega)$  with  $l_+$  for  $l_D=10$  and 8

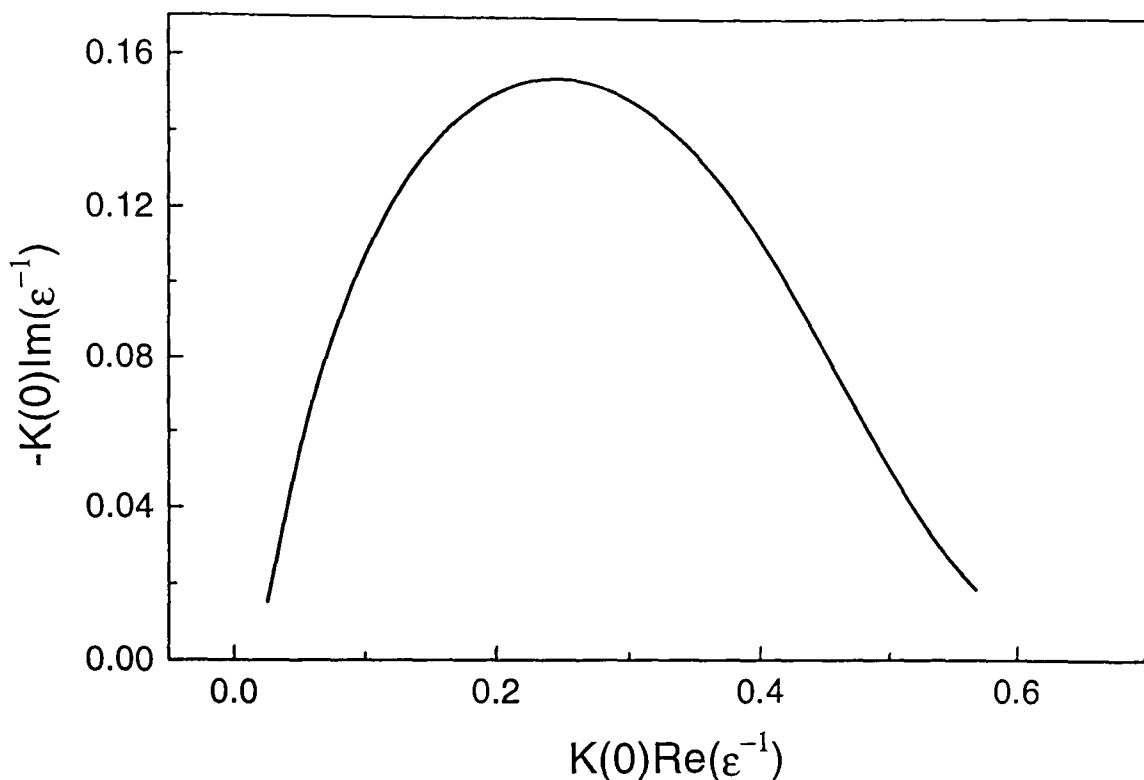


Figure 4.8 The universal curve predicted by the theory, the real and imaginary parts of  $K(0)\epsilon^{-1}(\omega)$  are plotted parametrically.

of networks of superconducting wires whose real and imaginary parts correspond to the quantities  $\text{Im}(-\epsilon^{-1}(\omega))$  and  $\text{Re}(\epsilon^{-1}(\omega))$  respectively. The prediction of the refined theory is compared, via a parametric plot, with the experimental curve and with the fit performed by Wallin [62] in figure (4.10). The universal curve from the refined theory has been scaled arbitrarily to fit at the static transition temperature, as the factor corresponding to  $A/M$  could not readily be obtained from the experimental data. Whilst the fit is not as good as that obtained by Wallin, it is quite reasonable considering that only one fitting parameter has been used (it is not clear how many fitting parameters Minnhagen's theory would require to fit just the parametric form of the data used here, as Wallin's approach is based around the temperature dependence of the quantities involved, but it is very unlikely to be just one).

The ratio of the real and imaginary parts of  $\epsilon^{-1}(\omega)$  at the dissipation peak for Minnhagen's theory is  $2/\pi$  in excellent agreement with the data of Jeanneret et al. A value of  $0.64 \pm 0.01$  is predicted for this quantity by the refined theory, a value which is consistent with that obtained by Minnhagen. In addition, the peak ratio in both theories is reduced by the introduction of an additional length scale to model disorder.

In summary, it seems that there is no major difference between the predictions of the refined theory and Minnhagen's phenomenological approach. However, even this close agreement does not guarantee that the refined theory will be able to describe the features of torsional oscillator experiments accurately.

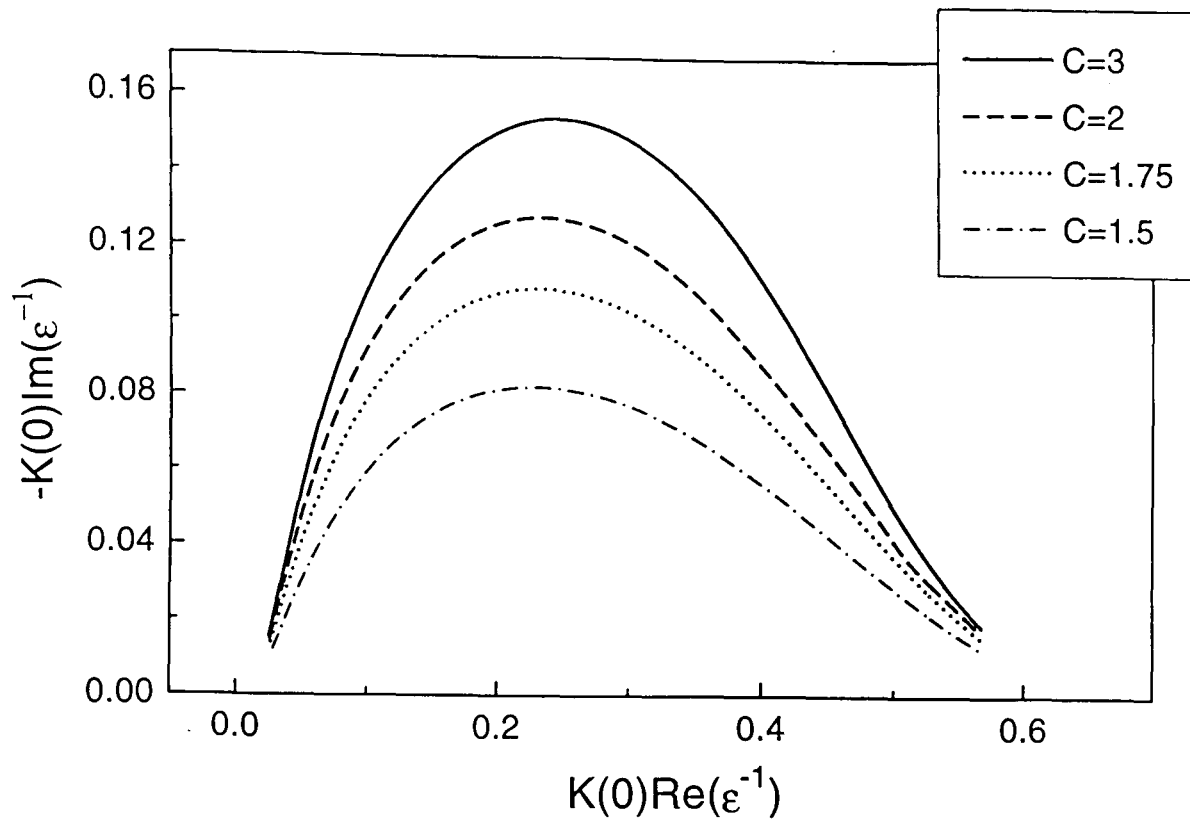


Figure 4.9 Variation in the parametric plot of the real and imaginary parts of  $K(0)\epsilon^{-1}(\omega)$  plotted parametrically with cut-off parameter  $C$ .

#### 4.4 Comparison with Experiment

Since the theory of AHNS was published in 1978 [7] along with the pioneering experimental study of Bishop and Reppy [51], numerous similar experiments have been performed on superfluid films using a variety of substrates. In this section the refined theory is compared with results from two sets of experiments: one performed using a Mylar substrate and the other using a Grafoil substrate pre-plated with Hydrogen Deuteride (HD).

The frequency shift and inverse  $Q$ -factor measured in torsional oscillator experiments are related to the quantities calculated in the theory by the relations

$$\frac{2\Delta P}{P} = \frac{Am^2k_B T}{M\hbar^2} K(0)\text{Re}(\epsilon^{-1}(\omega)), \quad (4.21)$$

$$\Delta Q^{-1} = \frac{Am^2k_B T}{M\hbar^2} K(0)\text{Im}(-\epsilon^{-1}(\omega)), \quad (4.22)$$

where  $A$  is the area of the film,  $m$  the mass of an atom of  $\text{He}^4$  and  $M$  is the sum of the mass of the cell and substrate.

As discussed in the previous chapter, the comparison between theory and experiment is complicated by the fact that some coupling occurs between the substrate and the superfluid component. It is believed that imperfections in the substrate allow it to entrain some of the superfluid component; the mechanism by which this occurs is unclear, but it is known to depend very strongly on the morphology of the substrate. The effect is accounted for

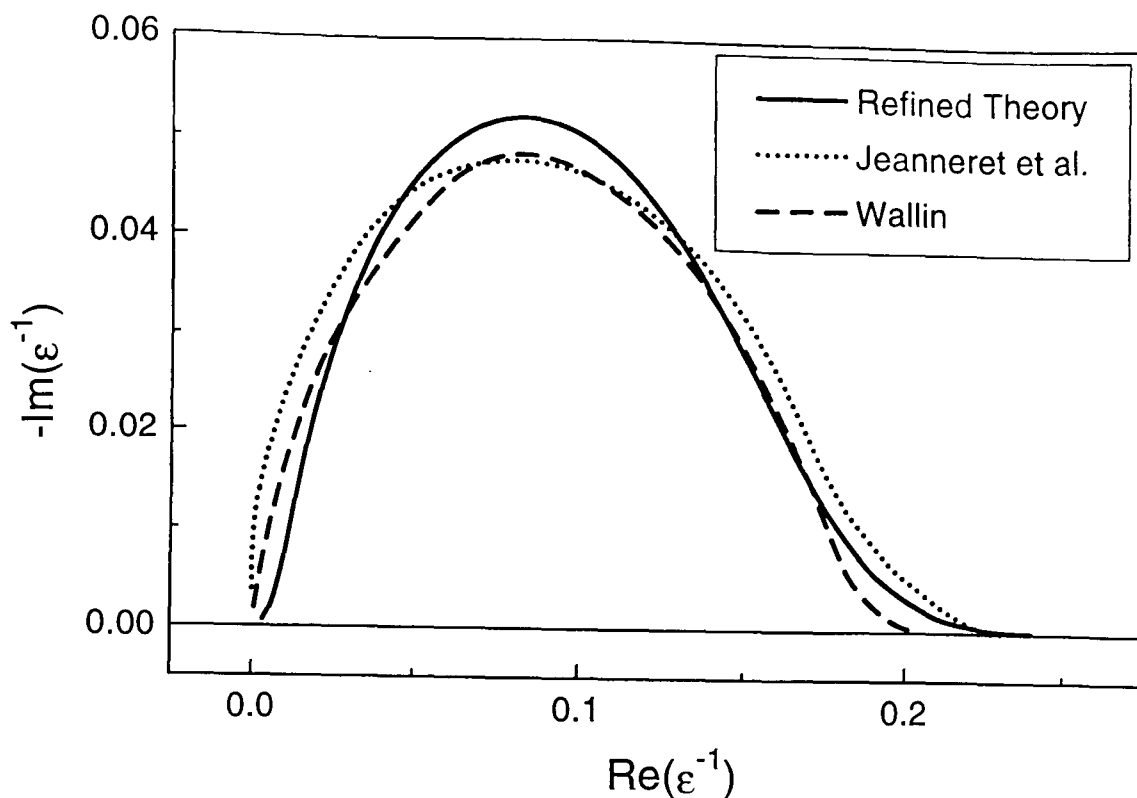


Figure 4.10 Comparison of the theoretical curve for  $\epsilon(\omega)^{-1}$  derived here with that obtained by Wallin [62] and the experimental data of Jeanneret et al. [27].

by the inclusion of an extra factor,  $\chi$ , in the equations for the period shift and inverse  $Q$ -factors. For Mylar about 15% of the superfluid component is entrained but for Grafoil the figure is as high as 95%.

#### 4.4.1 Mylar Substrate

Here the results from a series of torsional oscillator experiments carried out by McQueeney using a Mylar substrate [61] are analysed in the light of the predictions of the refined dynamic theory. His work is particularly interesting as he measured the response of helium films with a whole range of different thicknesses.

The results from torsional oscillator experiments are usually presented in the form of curves of  $2\Delta P/P$  against  $T$  and  $\Delta Q^{-1}$  against  $T$ . The problem with this method is that in order to make a comparison with the theory the temperature dependence of  $K(0)\text{Re}(\epsilon(\omega)^{-1})$  and  $K(0)\text{Im}(\epsilon(\omega)^{-1})$  have to be modelled in an essentially arbitrary way which introduces several fitting parameters. However, as discussed earlier in this chapter, the problem can be avoided if instead a parametric plot is used and the real and imaginary parts of  $K(0)\epsilon(\omega)^{-1}$  are plotted against each other.

McQueeney performed experiments on films of 28 different thicknesses which he referred to as coverages 1 to 28. They corresponded to films containing between 55 and 107  $\mu\text{moles}$  of helium of which 52.13  $\mu\text{moles}$  was estimated to form an inert (solid) layer atop the substrate. In order to analyse the data a series of representative points were taken from the graphs in McQueeney's thesis and plotted in a parametric form. Figure (4.11) shows the parametric

plots of the dielectric function for a wide range of different coverages, excluding only the thinnest films, scaled by the temperature of the dissipation peak in each case,  $T_p$ . Whilst there is significant variation in the sizes of the peaks in the curves, they show remarkably similar behaviour for much of the range of values. Interestingly there is an oscillation in the peak value of  $\Delta Q^{-1}$  with film thickness, as shown in figure (4.12). This suggests that atomic layering effects may play a significant role in modifying the behaviour of superfluid films on Mylar.

In figure (4.13) the results from a series of the thicker curves is compared with the prediction of the refined theory, using no fitting parameters. The value of  $A/M$ , corrected for the  $\chi$  factor is,  $266 \text{ m}^2\text{kg}^{-1}$  and was obtained from measurements performed by Agnolet, McQueeney and Reppy [60] on the same apparatus later used by McQueeney. Although the curves are displaced with respect to each other, their sizes and shapes are very similar except at one end, as can be seen from figure (4.14) where the theoretical curve has been translated to the left as an aid to the eye. The agreement between theory and experiment after a translation has been performed is striking, in particular the dissipation peak has the correct height, in effect this is a one parameter fit (as compared to the 5 or 6 usually employed). The problem lies in the steepness of the increase in the imaginary part of the experimental data at the left hand side: a feature which is not reproduced in the theoretical curve. The gradual increase in  $-K(0)\text{Im}(\varepsilon(\omega)^{-1})$  in the theoretical curve leads directly to the lateral displacement between theoretical and experimental curves.

It is not yet clear whether a rapid increase in  $-K(0)\text{Im}(\varepsilon(\omega)^{-1})$  is a feature of all the torsional oscillator experiments performed using helium on Mylar. It occurs consistently in McQueeney's data, but is not so obvious in the earlier data of Agnolet et al. [60]. However, this discrepancy at the left hand side of the parametric plots corresponds to the high temperature end of the response: the fit is poor here because of the distance from the static critical temperature. The refined theory discussed here is still based on recursion relations which describe the static transition which are, by construction, only valid close to the critical point, thus it is to be expected that the theory will become increasingly invalid in regions further away from  $T_{KT}$ . This problem was obscured in the theory of AHNS because they chose the magnitude of their free vortex contribution precisely to fit experiment at the high temperature end (though this meant that they could not fit the dissipation peak correctly), thus masking a fundamental weakness in the theory.

The similarity in the general shapes of the experimental and theoretical curves was only found for a limited range of film thickness ( $76\text{--}92\mu\text{moles}$ , i.e. coverages 16 to 24). A possible explanation for the large discrepancy that arises for the thinner films concerns the fugacity of the vortices. Even the refined theory is based on an expansion in the fugacity so it is bound to be more effective for systems with larger core energies — that is for the thicker films which contain longer vortices. The reason for the breakdown in agreement at the high coverage end is even less clear, but may be because the films are not behaving in an entirely two-dimensional way.

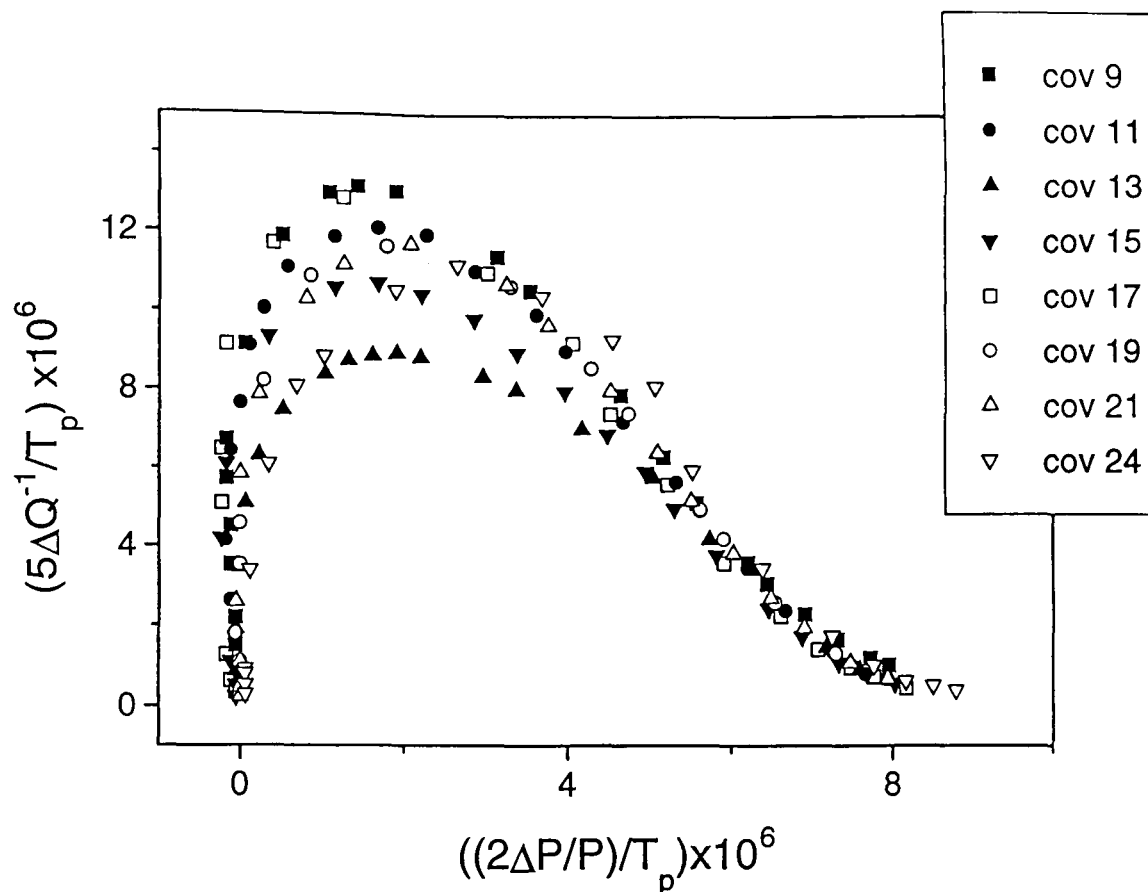


Figure 4.11 Parametric plots of  $5\Delta Q^{-1}/\Gamma_p$  versus  $2\Delta P/(P \times T_p)$  for a variety of thicker films, using the data from McQueeney's thesis

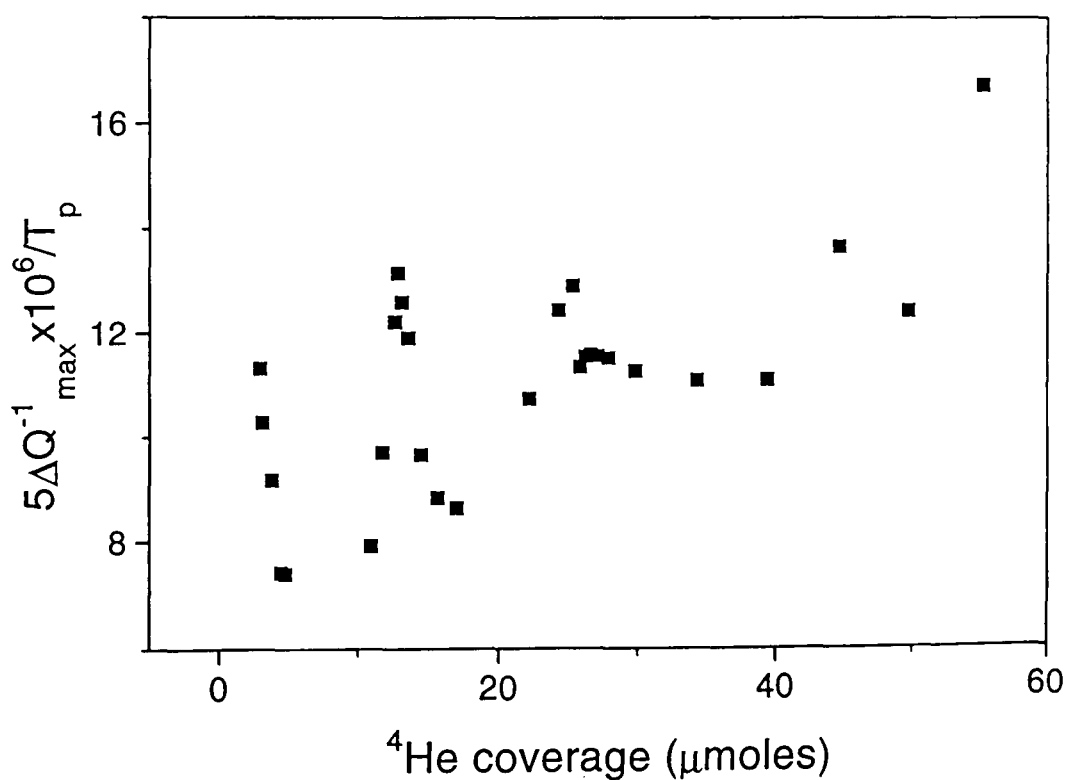


Figure 4.12 Variation of the maximum in  $\Delta Q^{-1}$  with film thickness, using data from McQueeney's thesis

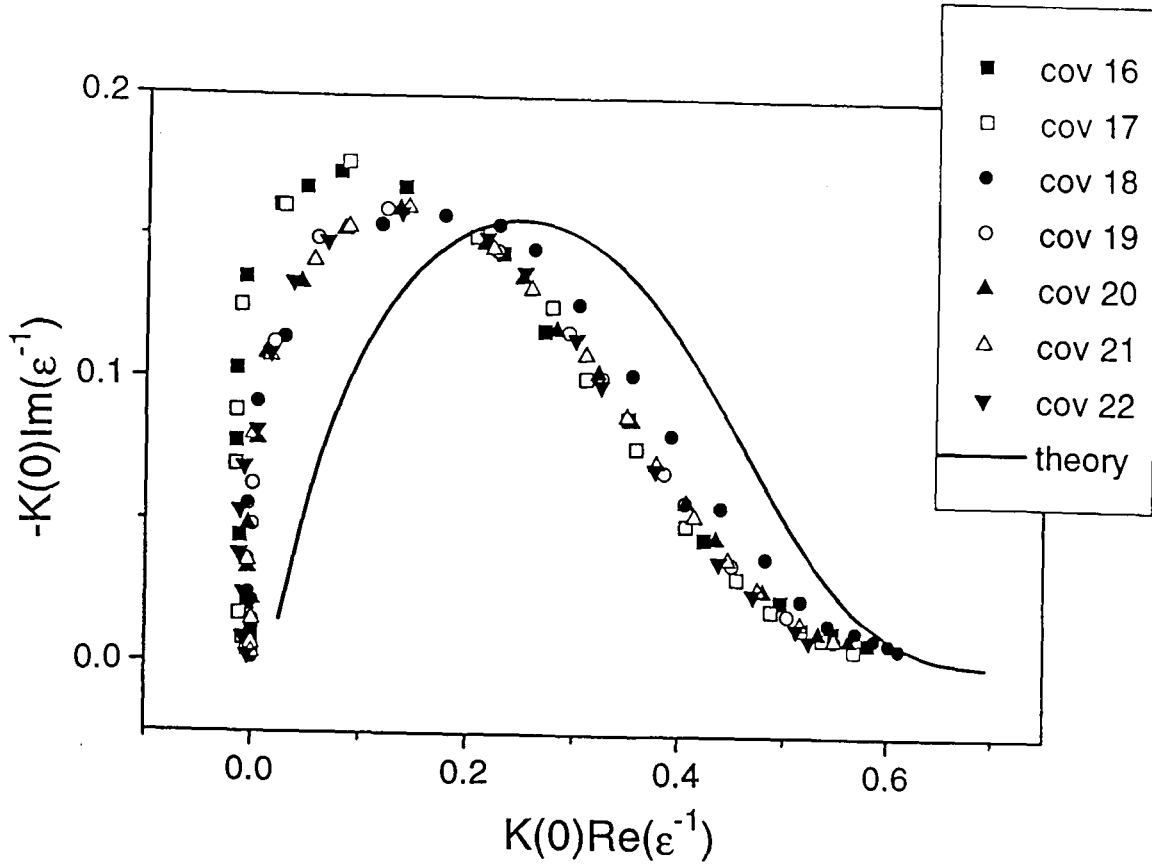


Figure 4.13 Comparison of plots of the real and imaginary parts of  $K(0)\varepsilon^{-1}(\omega)$  for thicker films, from McQueeney's thesis, and the theoretical prediction

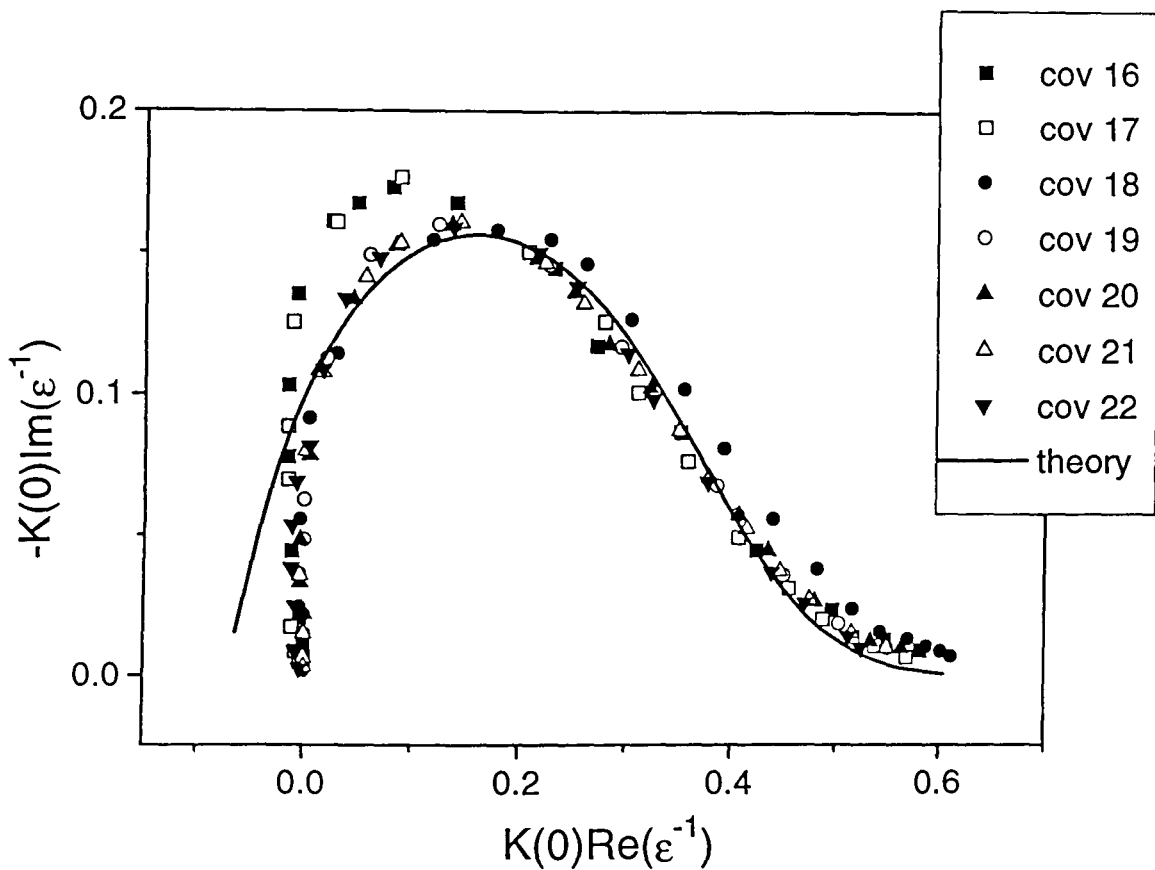


Figure 4.14 Comparison of plots of the real and imaginary parts of  $K(0)\varepsilon^{-1}(\omega)$  for thicker films, from McQueeney's thesis, compared with a translated version of the theoretical curve

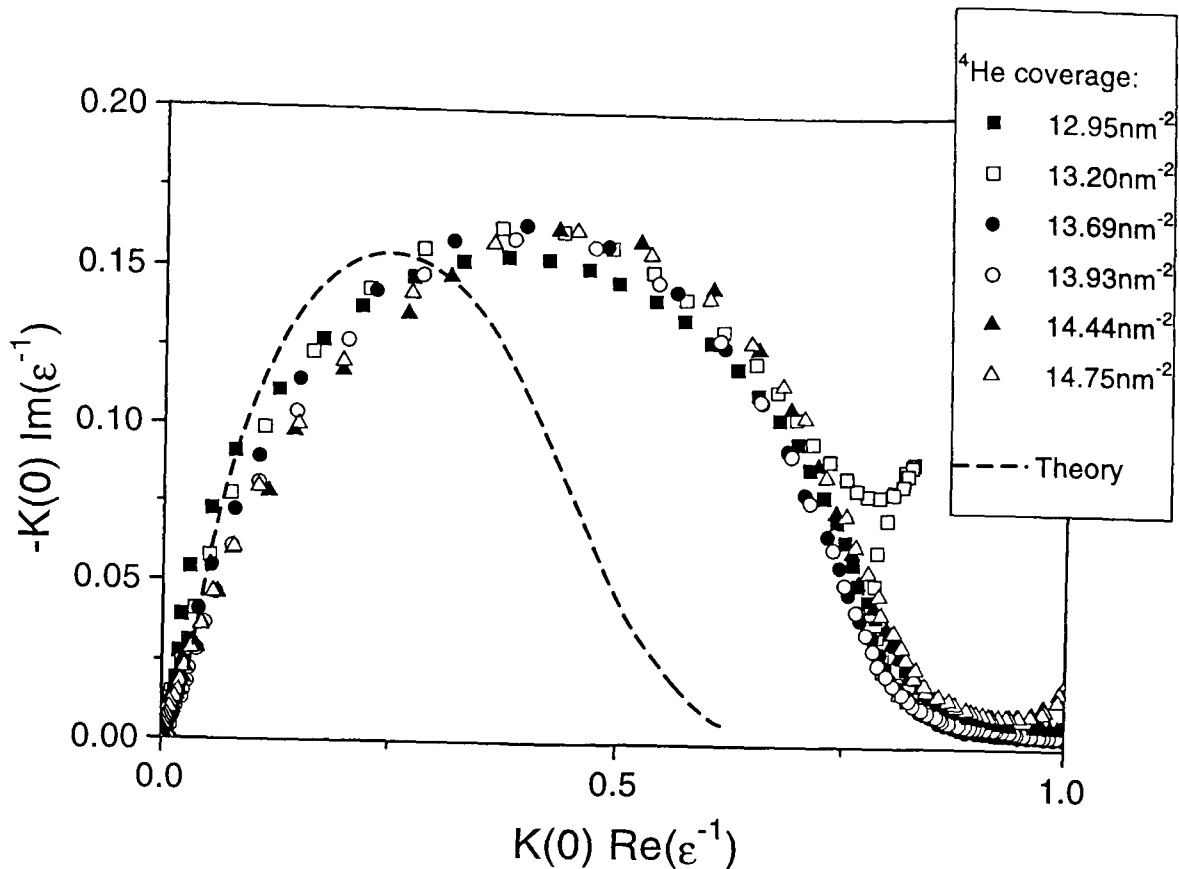


Figure 4.15 Plot of the theoretical curve for  $K(0)\varepsilon(\omega)^{-1}$  and the data of Nyéki et al. for Helium films on Grafoil pre-plated with an HD bilayer

#### 4.4.2 Grafoil Substrate

Torsional oscillator experiments have recently been performed using a Grafoil substrate, either on its own, or pre-plated with one or more layers of HD [63, 66]. The purpose of the pre-plating is to screen the effect of the substrate potential in the hope that this will allow the intrinsic properties of the film to be observed more easily.

Grafoil forms a series of atomically flat plaquettes with dimension of order 100–200Å which join together in an entirely disordered manner. Nyéki et al. examined the behaviour of helium films of various thicknesses and for two different types of pre-plating [66]. The  $\chi$ -factor for the system was measured to lie between 0.9519 and 0.9617 — depending on the exact details of the pre-plating. The very high value of the  $\chi$ -factor reflects the poor connectivity of the surface and is a strong indicator that the behaviour of the film is dominated by the morphology of the substrate.

In particular, Nyéki et al. studied superfluid transitions in a temperature range from 0.8K to 1.4K for films with thicknesses ranging from a submonolayer to 3 fluid layers on top of Grafoil pre-plated with either a bilayer or a trilayer of HD. For film thicknesses of greater than one fluid layer the data comes close to collapsing onto a single curve, as can be seen in the parametric plot of some of the data for the bilayer pre-plating, figure (4.15). Although the general shape and universal properties of the experimental curves are in line with the theoretical prediction the size and positions of the curves differ greatly [67]. Furthermore, there is a systematic variation in the value of the dissipation peak: it increases and then decreases with increasing coverage as the second fluid layer is built up towards completion as shown in figure

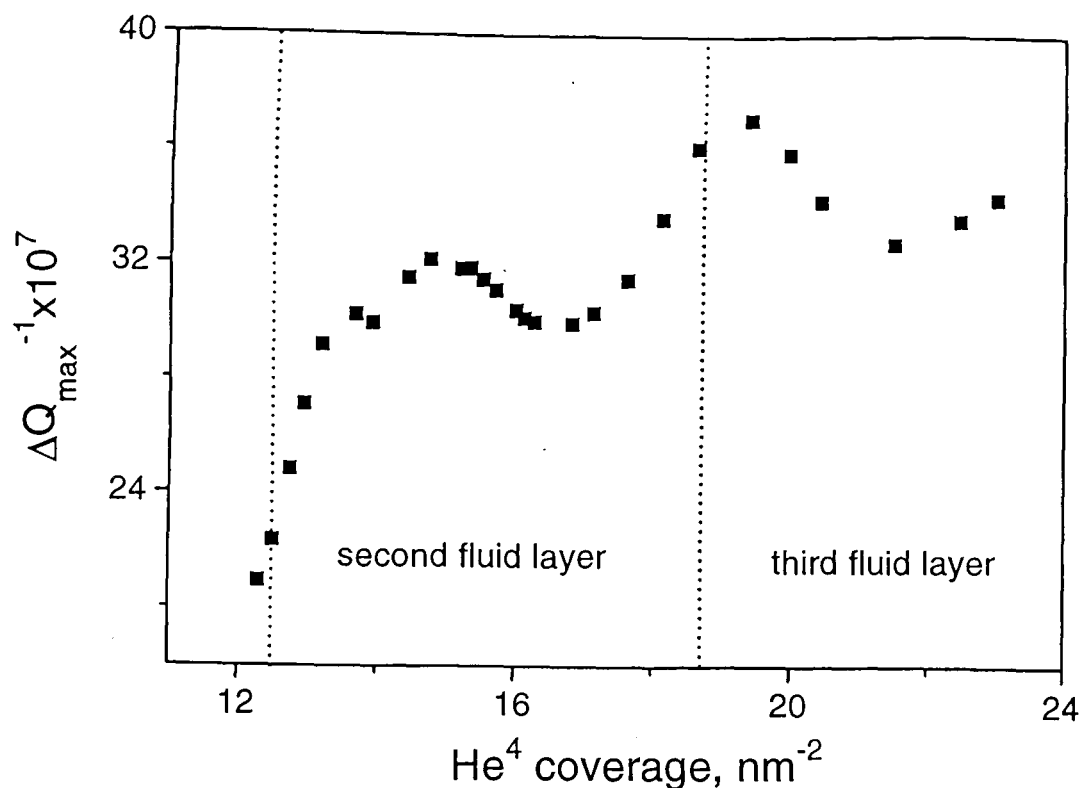


Figure 4.16 Variation of the maximum in  $\Delta Q^{-1}$  with film thickness for helium films on preplated Grafoil, using the data of Nyéki et al.

(4.16).

## 4.5 Discussion

McQueeney's data for superfluid films on Mylar allows a detailed comparison with the refined dynamic theory. It is found that the general shape of the parametric plot calculated using the refined theory agrees well with the results from a series of different film thicknesses, though there is always a serious discrepancy in the high temperature region. However, McQueeney found that there was significant variation in the behaviour of the dynamic dielectric function for different film thicknesses: a feature which cannot be reconciled with the prediction of a single curve which the refined theory leads to.

The comparison of the refined theory with results obtained using a Grafoil substrate proves even more problematic. This time the results lie much closer to a single universal curve, but its shape differs strongly from the predictions of the refined theory. The fact that the  $\chi$ -factor is so large for Grafoil (of order 0.95) suggests that the morphology of the substrate is playing a dominant role in the behaviour of the film. Indeed the dissipation sets in at a point far removed from that suggested by the theory, implying that the transition may not even be in the Kosterlitz-Thouless universality class.

Comparison with the work done by Wallin, based on Minnhagen's theory, suggests that there is very good agreement between the two approaches. This is perhaps to be expected as despite the fact that they differ somewhat in detail, they rely on essentially the same phenomenological basis.

---

The refined theory allows the predictions of the phenomenological model of AHNS to be made precise by removing almost entirely the need for fitting parameters. Using the refined theory makes the disagreement between theory and experiment transparent: it becomes apparent that the phenomenological approach to the dynamics of superfluid films cannot account satisfactorily for a number of the central features in the available data.

Any comprehensive theoretical framework which seeks to provide an understanding of all the data will need to contain at least two new additional features. Firstly, comparing the results obtained using Mylar and Grafoil substrates, it is clear that the disordering effect of the substrate on the superfluidity of films cannot be isolated and so must be incorporated into the theoretical picture. Secondly, a way of modelling the systematic variation in the dissipation and period shift with coverage needs to be developed.

---

## Chapter 5 Roughening and Super-Roughening Transitions

---

This chapter summarizes the theory of the roughening and super-roughening transitions in preparation for the description of the effect of disorder on crystal surfaces which follows in chapter 6. It turns out that the sine-Gordon model provides a very effective description of the behaviour of crystal surfaces close to the roughening transition. The renormalization group treatment of the roughening transition due to Nozières and Gallet is described in some detail as it leads to recursion relations which differ from those of Kosterlitz, despite the underlying duality of the sine-Gordon model and the two-dimensional Coulomb gas.

The roughening and super-roughening transitions are concerned with the way in which the morphology and growth of a crystal surface is affected by the underlying periodicity of the bulk crystal structure. In both cases, for temperatures below the transition temperature the surface is dominated on large length scales by the lattice, which seeks to pin it to discrete ‘planes’ separated by the lattice constant. For temperatures above the transition, the surface wanders freely across the planes of the lattice: it is a translational symmetry in the direction of the crystal height which is broken at the transitions. The essential difference between the two transitions lies in the nature of the underlying crystal ‘planes’ involved. If the bulk crystal structure is perfectly periodic, the behaviour of its surface is described by the roughening transition: the atoms of the solid lie in discrete layers which are truly planar. If instead the translational symmetry in the plane of the substrate is broken, so that although the atoms of the crystal lie in discrete layers, these layers are very strongly distorted from the planar, then the behaviour of the surface is described by the super-roughening transition.

The modern theory of the roughening transition is based on a renormalization group treatment of a sine-Gordon model [68, 18]. Careful experiments carried out on the surfaces of several types of crystal and extensive computer simulation work, based on a variety of growth models, give detailed confirmation of all the important predictions of the renormalization group approach. The most sophisticated version of the theory is due to Nozières and Gallet [19, 20, 69, 21] and their exposition is used as the basis of the description of the transition given here.

The super-roughening transition was initially predicted by Toner and Di Vincenzo [23], via an extension of previous work on the random phase sine-Gordon model [70, 71], for the surfaces of crystals containing quenched bulk disorder or equivalently crystals grown on disordered substrates. The behaviour of such systems in the linear response regime was analysed by Tsai and Shapir [24]. These works, though not yet exposed to the rigours of experimental test, have been the subject of a good deal of computer simulation work which has confirmed the existence of the transition despite continuing

controversy over some aspects of the theory [72, 73].

This chapter summarises the main ideas of both theories. It begins with a description of how the sine-Gordon model may be used to describe the behaviour of a crystal surface close to the roughening transition and how the random-phase sine-Gordon model can be used to describe the super-roughening transition. There then follows an outline of the renormalization group treatment of the sine-Gordon model developed by Nozières and Gallet. Next the predictions of the theory are compared with the results of experiment. Finally there is a brief summary of how renormalization group has been applied to the random-phase sine-Gordon model, leading to recursion relations for the super-roughening transition.

## 5.1 Formulation of a Continuous Model

For crystals with both ordered and disordered types of bulk lattice structures the thermodynamics of the interface between a crystal and its melt can only be understood correctly if the equilibrium fluctuations are considered since in two-dimensions they dominate the behaviour. At low temperatures the important modes of the surface are those with long wavelengths, the melting freezing waves, so called because the interface transmits them by melting slightly then freezing in turn. Their importance arises from the fact that their excitational energy goes to zero as their wavelength becomes infinitely long: they are the Goldstone modes of the system [74].

As usual where long wavelength fluctuations dominate, a coarse-grained continuous model is developed which is then analysed using the renormalization group. In order to formulate such a model, the interface between the solid phase and its melt is defined in a necessarily arbitrary way by the function  $z(\mathbf{r})$ , which represents the height of the crystal above a point in the crystal substrate with position vector  $\mathbf{r}$ : all atoms above this height are taken to be in the liquid phase whilst those below are in the solid phase. Any model of pinned interfaces must contain two basic terms: a local curvature term that represents the surface tension and an harmonic potential energy term that models the effect on the surface of the pinning to the underlying lattice. Thus the simplest expression for a crystal surface energy is the functional

$$E[z(\mathbf{r})] = \int d^2\mathbf{r} \left( \tilde{\gamma} \left( 1 + (\nabla z(\mathbf{r}))^2 \right)^{\frac{1}{2}} + V(z(\mathbf{r})) \right), \quad (5.1)$$

where  $\tilde{\gamma}$  is the surface stiffness and  $V(z(\mathbf{r}))$ , the pinning potential, has period the lattice spacing,  $b$ , and is minimized at the lattice ‘planes’. Clearly the functional  $V(z(\mathbf{r}))$  can be written as a cosine Fourier series, but only the first term is required since higher order harmonic terms turn out to become rapidly less relevant as their frequency increases. If in addition the interface is assumed to be reasonably smooth (so that  $\nabla z \ll 1$ ) then the surface tension term can be expanded in a MacLaurin series and only the lowest order term retained (in the language of the renormalization group it is simply a matter of discarding all but the most relevant terms). Thus in the case of the roughening transition, the model Hamiltonian is just that of the sine-

Gordon model,

$$\mathcal{H}_R = \int d^2\mathbf{r} \left( \frac{\tilde{\gamma}(\nabla z(\mathbf{r}))^2}{2} - V_0 \cos\left(\frac{2\pi z(\mathbf{r})}{b}\right) \right) \quad (5.2)$$

where  $V_0$  is the strength of the periodic pinning potential.

The Hamiltonian used to model the super-roughening transition is very similar,

$$\mathcal{H}_{SR} = \int d^2\mathbf{r} \left( \frac{\tilde{\gamma}(\nabla z(\mathbf{r}))^2}{2} - V_0 \cos\left(\frac{2\pi}{b}(z(\mathbf{r}) + z_1(\mathbf{r}))\right) \right). \quad (5.3)$$

The extra term in the periodic potential,  $z_1(\mathbf{r})$ , is essentially an extra phase, representing disorder in the lattice. It defines the position of the crystal interface in the absence of any fluctuations, i.e. at absolute zero temperature. In most studies of the super-roughening transition it is entirely uncorrelated so that  $\langle z_1(0)z_1(\mathbf{r}) \rangle = \delta(\mathbf{r})$ , representing the growth of a crystal on a substrate which is completely disordered on length scales greater than the atomic scale [23, 24]. However, the same Hamiltonian may be used to introduce a disordering phase term with *any* type of correlation [25]. In particular, if the disorder is due to the presence of screw dislocation pairs, then the correlation functions of  $z_1(\mathbf{r})$  depend strongly on the distribution of the pairs.

Implicit in this continuous description of the transition is the exclusion of modes of wavelength the lattice spacing,  $b$ , or less. Thus there is a built in ultraviolet cut-off: only degrees of freedom with wavenumber less than  $\Lambda_0 = 2\pi/b$  need be included when calculating the partition function.

In practice it proves impossible to renormalize the exact Hamiltonian so a further approximation must be made: the coupling is taken to be weak in the neighbourhood of the transition, so that a perturbative approach in powers of  $V_0$  is valid. Such an approximation of course makes sense in the study of a transition from a coupled to an uncoupled state. Following this approach, the rough state is clearly identified with a Gaussian Hamiltonian: inclusion of the pinning potential then represents a perturbation away from this state.

The excitational modes of the surface are most readily analysed by considering the surface height in terms of its Fourier components:

$$z(\mathbf{r}) = \sum_{k < \Lambda_0} z_{\mathbf{k}} e^{i\mathbf{k}\cdot\mathbf{r}}. \quad (5.4)$$

In terms of these the Hamiltonian given by eqn (5.2) becomes

$$\mathcal{H}_R = \sum_{k < \Lambda_0} \frac{1}{2} \tilde{\gamma} k^2 |z_{\mathbf{k}}|^2 - \int d^2\mathbf{r} V_0 \cos\left(\frac{2\pi z(\mathbf{r})}{b}\right). \quad (5.5)$$

Thus for a free interface, controlled solely by surface tension, the equipartition theorem leads to the relation

$$\langle |z_{\mathbf{k}}|^2 \rangle = \frac{k_B T}{\tilde{\gamma} k^2}. \quad (5.6)$$

The presence of the pinning potential leads to a non-trivial coupling of these surface modes.

The dynamics is obtained from the static behaviour in the usual way: by formulating a Langevin type equation. Since the surface height,  $z$ , is a non-conserved quantity, the system has model A dynamics; the dynamical equation takes the form

$$\eta \dot{z}(\mathbf{r}) = -\frac{\delta \mathcal{H}[z(\mathbf{r})]}{\delta z(\mathbf{r})} + R, \quad (5.7)$$

with  $R$  a random noise term with the usual Gaussian white spectrum,

$$\langle R(\mathbf{r}, t) R(\mathbf{r}', t') \rangle = 2D \delta(\mathbf{r} - \mathbf{r}') \delta(t - t') \quad (5.8)$$

to ensure that the system relaxes towards equilibrium.  $\eta^{-1}$  is the surface mobility.

The dynamic picture is to be preferred to the static one because it is more intuitive and leads to a systematic joint renormalization of both  $\tilde{\gamma}$  and  $\eta$ . Furthermore, the dynamic theory is more readily generalised to include other physical effects such as a slight over pressure on the crystal surface.

Nozières and Gallet also extended their version of the sine-Gordon theory to consider the roughening transition on a vicinal surface. They showed that the effect of a slight angle between the surface and the underlying crystal planes could be accounted for by an extra phase in the harmonic term of the Hamiltonian which leads to an anisotropy in the renormalized surface stiffness. However, the theory may be extended even further: to include the effect of a dynamic overpressure on the crystal surface [75], or to incorporate the effects of screw dislocations on the roughening transition (as is described in the following chapter).

## 5.2 Renormalization

Renormalization techniques have been applied very successfully to both of the systems described by the coarse grained models outlined above. In the case of the roughening transition renormalization has been carried out to second order in the potential in both static and dynamic pictures [18, 19, 21]. Nozières and Gallet also considered the response of the system to a weak external drive: in contrast to the AHNS approach Nozières and Gallet used an explicitly dynamic renormalization scheme based on the equation of motion to calculate the linear response of the system. In this section the static renormalization scheme, which is the least complex, is described and the main results from the dynamic approach are outlined, along with some of the consequences of the theory.

The static renormalization scheme proceeds by successively summing over the large wavevector modes in the partition function of the system. The surface modes,  $z_{\mathbf{k}}$ , are separated into two groups: a thin shell with wavevectors of magnitude in the range  $\Lambda < k \leq \Lambda_0$  (which will be averaged over) and the longer wavelength components with wavevectors  $k \leq \Lambda$ . Thus the surface height  $z(\mathbf{r})$  is split into two parts:

$$z(\mathbf{r}) = \bar{z}(\mathbf{r}) + \delta z(\mathbf{r}) \quad (5.9)$$

where

$$\bar{z}(\mathbf{r}) = \sum_{k \leq \Lambda} z_{\mathbf{k}} e^{i\mathbf{k} \cdot \mathbf{r}} \quad (5.10)$$

and

$$\delta z(\mathbf{r}) = \sum_{\Lambda < k \leq \Lambda_0} z_{\mathbf{k}} e^{i\mathbf{k} \cdot \mathbf{r}}. \quad (5.11)$$

After the short wavelength modes have been summed over  $\Lambda$  becomes the new cutoff, replacing  $\Lambda_0$ . Subsequent renormalization sums over the modes from  $\Lambda$  to  $\bar{\Lambda}$ .

The summation over the short wavelength modes leads to a new energy term in the partition function,

$$\mathcal{Z} = \int \mathcal{D}\bar{z}(\mathbf{r}) \int \mathcal{D}\delta z(\mathbf{r}) e^{-\mathcal{H}(\bar{z}(\mathbf{r}), \delta z(\mathbf{r}))/k_{\text{B}}T} \quad (5.12)$$

$$= \int \mathcal{D}\bar{z}(\mathbf{r}) e^{-\bar{\mathcal{H}}(\bar{z}(\mathbf{r}))/k_{\text{B}}T}. \quad (5.13)$$

This expression for the energy,  $\bar{\mathcal{H}}$ , contains the surface tension term due to the long wavelength modes and a potential energy term which, because of the summation, is averaged over the short wavelength modes with Gaussian weight. Thus,

$$\bar{\mathcal{H}} = \sum_{k < \Lambda} \frac{1}{2} \tilde{\gamma} k^2 |\bar{z}^2(\mathbf{r})| - \int d^2\mathbf{r} k_{\text{B}} T \ln \langle e^{V/k_{\text{B}}T} \rangle_0 \quad (5.14)$$

where the average  $\langle e^{V/k_{\text{B}}T} \rangle_0$  is carried out with weight  $e^{(-\tilde{\gamma}(k\delta z(\mathbf{r}))^2/k_{\text{B}}T)}$  over the range of  $\delta z(\mathbf{r})$ .

In the weak pinning regime the logarithmic term may be expanded perturbatively in terms of the pinning potential strength. The expansion has traditionally been performed up to second order as there is a finite correction to both the potential and surface tension operators at this level (the surface tension is marginal in a first order calculation). The cumulant expansion to this order is

$$k_{\text{B}}T \ln \langle e^{V/k_{\text{B}}T} \rangle_0 = \langle V \rangle_0 - \frac{1}{2k_{\text{B}}T} \left\{ \langle V^2 \rangle_0 - \langle V \rangle_0^2 \right\}. \quad (5.15)$$

The first order term leads to a renormalization of the potential,

$$\bar{V} = \langle V \rangle_0 = V(\bar{z}(\mathbf{r})) \left\langle \cos \left( \frac{2\pi\delta z(\mathbf{r})}{b} \right) \right\rangle_0 \quad (5.16)$$

$$= V(\bar{z}(\mathbf{r})) e^{-\frac{2\pi^2}{b^2} \langle (\delta z(\mathbf{r}))^2 \rangle_0} \quad (5.17)$$

where the correlation function is given by  $\langle (\delta z(\mathbf{r}))^2 \rangle_0 = k_{\text{B}}T dl / 2\pi\tilde{\gamma}$ , with  $dl = \ln(\Lambda/\bar{\Lambda})$ .

The second order terms lead to a renormalization of the surface tension,  $\tilde{\gamma}$ . When irrelevant operators have been eliminated the remaining term has the form

$$\alpha \bar{V}_0^2 \cos \left( \frac{2\pi}{a} (\bar{z}(\mathbf{r}') - \bar{z}(\mathbf{r})) \right)$$

where  $\alpha$  is a constant and  $\mathbf{r}' = \mathbf{r} + \boldsymbol{\rho}$ . A simple expansion of this cosine term to second order is appealing as the quadratic part is immediately identifiable with the surface stiffness operator. However, this approach is incorrect as the variable in the expansion,  $(\bar{z}(\mathbf{r}') - \bar{z}(\mathbf{r}))$ , is not necessarily small. The correct treatment of this term was first given by Knops and Den Ouden [18]. They recognized that the higher order terms thrown away when only the quadratic order is kept each contain a linear combination of an irrelevant operator and the quadratic operator (which is marginal). Thus for a term of  $2n^{\text{th}}$  order in the expansion of the cosine,

$$(\bar{z}(\mathbf{r}') - \bar{z}(\mathbf{r}))^{2n} = \tilde{O}_{2n}(\mathbf{r}) + a_{2n}(\mathbf{r}' - \mathbf{r})(\bar{z}(\mathbf{r}') - \bar{z}(\mathbf{r}))^2 + b_{2n}(\mathbf{r}' - \mathbf{r}) \quad (5.18)$$

where  $\tilde{O}_{2n}$  is an irrelevant operator and  $b_{2n}$  a constant which only contributes to the renormalized free energy. The key term is the coefficient of the quadratic operator,  $a_{2n}(\mathbf{r}' - \mathbf{r})$ , which gives the renormalization of the surface stiffness.

Nozières and Gallet use essentially the same method whilst providing a rather more physical argument for it [19]. They perform a further subdivision of the wave modes of the system splitting  $\bar{z}$  into two parts: a small term  $\xi$ , which may be considered as a weak external driving motion (the response to which is calculated) and a second part  $z^{eq}$  which represents all the other thermal fluctuations at equilibrium, such that  $\bar{z} = \xi + z^{eq}$ . By hypothesis  $z^{eq}$  has a Gaussian equilibrium distribution, thus

$$\cos\left(\frac{2\pi}{b}(\bar{z}(\mathbf{r}') - \bar{z}(\mathbf{r}))\right) = \cos\left(\frac{2\pi}{b}(z^{eq}(\mathbf{r}') + \xi(\mathbf{r}') - z^{eq}(\mathbf{r}) - \xi(\mathbf{r}))\right) \quad (5.19)$$

$$= \cos\left(\frac{2\pi}{b}(\xi' - \xi)\right) \left\langle \cos\left(\frac{2\pi}{b}(z^{eq}(\mathbf{r}') - z^{eq}(\mathbf{r}))\right) \right\rangle, \quad (5.20)$$

the term  $\cos(2\pi(\xi' - \xi)/b)$  may safely be expanded as a Taylor series and its second order component identified with the surface stiffness. The coefficient of this term is thus the correlation function

$$C(z', z) = \left\langle \cos\left(\frac{2\pi}{b}(z^{eq}(\mathbf{r}') - z^{eq}(\mathbf{r}))\right) \right\rangle, \quad (5.21)$$

where the average is taken with a Gaussian weight.

The recursion relations for the potential and surface stiffness are then readily obtained from the first and second order expressions respectively. The recursion relation for the pinning potential strength is written in terms of  $U = V_0/\Lambda^2$ , the pinning energy per area  $(1/\Lambda)^2$ . The relations have the form

$$\frac{dU}{dl} = U(2 - n) \quad (5.22)$$

$$\frac{d\tilde{\gamma}}{dl} = \frac{2\pi^4}{\tilde{\gamma}b^4} U^2 A(n), \quad (5.23)$$

where  $n = \pi k_B T / \tilde{\gamma} b^2$  and  $A(n)$  is given by the expression

$$A(n) = \int_0^\infty d\tilde{\rho} \tilde{\rho}^3 J_0(\tilde{\rho}) e^{-2nh(\tilde{\rho})}, \quad (5.24)$$

which may be evaluated numerically.

The starting point for the dynamic calculation is the Langevin equation for the interface, obtained from the model Hamiltonian (eqn 5.2) via eqn (5.7). It has the form,

$$\eta \dot{z} = \tilde{\gamma} \nabla^2 z - \frac{2\pi V_0}{b} \sin\left(\frac{2\pi z}{b}\right) + R. \quad (5.25)$$

The random force is separated into two parts:  $R = \bar{R} + \delta R$ , where  $\delta R$  represents fluctuations with wavenumbers lying in the thin shell from the lattice cutoff  $\Lambda_0 = 2\pi/b$ , to the value  $\Lambda$ . Further renormalization proceeds over the shell from  $\Lambda$  to  $\bar{\Lambda}$ .

Once separated out, the effect of  $\delta R$  is averaged over, effectively thinning the degrees of freedom of the system. The surface height after this average has been performed is defined as

$$\bar{z}(\bar{R}) = \left\langle z(\bar{R} + \delta R) \right\rangle_{\delta R}. \quad (5.26)$$

If  $\delta z = z - \bar{z}$ , then the equation of motion for  $\bar{z}$  may be written as

$$\eta \dot{\bar{z}} = \tilde{\gamma} \nabla^2 \bar{z} + \bar{R} - \frac{2\pi}{b} V_0 \left\langle \sin\left(\frac{2\pi}{b}(\bar{z} + \delta z)\right) \right\rangle_{\delta R} \quad (5.27)$$

and that for  $\delta z$  as,

$$\eta \delta \dot{z} = \tilde{\gamma} \nabla^2 \delta z + \delta R - \frac{2\pi}{b} V_0 \left\{ \sin\left(\frac{2\pi}{b}(\bar{z} + \delta z)\right) - \left\langle \sin\left(\frac{2\pi}{b}(\bar{z} + \delta z)\right) \right\rangle_{\delta R} \right\}. \quad (5.28)$$

Renormalization proceeds by rewriting the equation of motion for  $\bar{z}$  in the same form as eqn (5.25), and then extracting the dependence of the scaling parameters  $\tilde{\gamma}$  and  $V_0$  on the infinitesimal flow variable  $dl$  to obtain recursion relations. In the weak coupling approximation,  $\delta z$  is expanded as series of terms of the form:

$$\delta z = \delta z^{(0)} + \delta z^{(1)} + \dots \quad (5.29)$$

with the superscript denoting the power dependence on  $V$ . Clearly to calculate the renormalized equation of motion (eqn 5.27) to second order in the pinning strength calculation of the terms  $\delta z^{(0)}$  and  $\delta z^{(1)}$  is required. These terms are calculated progressively by an iterative solution of the relevant equation of motion, eqn (5.28), thus

$$\delta z^{(0)}(r, t) = \int d^2 \mathbf{r}' \int_{-\infty}^t dt' \chi_0(r - r', t - t') \delta R(r', t'), \quad (5.30)$$

where  $\chi_0$  is the response function for the diffusion equation. The expression for  $\delta z^{(1)}$  is then found by substituting  $\delta z^{(0)}$  into the harmonic term of the equation of motion.

Writing  $c = \cos(2\pi\delta z/b)$  and  $s = \sin(2\pi\delta z/b)$  and using the notation  $c^{(i)}$  and  $s^{(i)}$  for the  $i$ th order terms in their expansion in powers of  $V_0$ , the harmonic term in eqn (5.27) can be rewritten (up to second order) as

$$-\frac{2\pi}{b}V \left\{ \sin\left(\frac{2\pi}{b}\bar{z}\right) \left( \langle c^{(0)} \rangle + \langle c^{(1)} \rangle \right) + \cos\left(\frac{2\pi}{b}\bar{z}\right) \langle s^{(1)} \rangle \right\}$$

since the average of  $s^{(0)}$  proves to be zero. The term  $-V_0 \sin(2\pi\bar{z}/b) \langle c^{(0)} \rangle$  is first order in  $V_0$  and so leads to a correction to the pinning potential. The terms in  $\langle s^{(1)} \rangle$  and  $\langle c^{(1)} \rangle$  are the second order correction:

$$\Delta^{(2)} = -\frac{2\pi}{b}V_0 \left\{ \sin\left(\frac{2\pi}{b}\bar{z}\right) \langle c^{(1)} \rangle + \cos\left(\frac{2\pi}{b}\bar{z}\right) \langle s^{(1)} \rangle \right\} \quad (5.31)$$

$$= -\frac{2\pi}{b}V_0 \left\{ \sin\left(\frac{2\pi}{b}\bar{z}\right) \left\langle -\frac{2\pi}{b} \sin\left(\frac{2\pi}{b}\delta z^{(0)}\right) \delta z^{(1)} \right\rangle \right. \\ \left. + \cos\left(\frac{2\pi}{b}\bar{z}\right) \left\langle \frac{2\pi}{b} \cos\left(\frac{2\pi}{b}\delta z^{(0)}\right) \delta z^{(1)} \right\rangle \right\}, \quad (5.32)$$

which eventually renormalizes  $\eta$  and  $\tilde{\gamma}$ .

The calculation proceeds in a similar way to the static one: irrelevant operators are separated out and neglected. What remains is a term which depends on  $\sin(2\pi(\bar{z}' - \bar{z})/b)$ , again a separation of variables is made into the equilibrium fluctuations and the response to a weak external drive. This leads to corrections to both the surface stiffness and the mobility because the difference  $(\bar{z}' - \bar{z})$  now depends on time as well as position.

The recursion relations for the pinning potential and surface stiffness obtained in the dynamic renormalization programme take the same form as in the static case: eqns (5.22) and (5.23). However, in the dynamic picture the mobility is also renormalized

$$\frac{d\eta}{dl} = \frac{8\pi^4\eta}{\tilde{\gamma}b^4}U^2B(n), \quad (5.33)$$

and the functions  $A(n)$  and  $B(n)$  now take the form:

$$A(n) = n \int_0^\infty d\tilde{\rho}\tilde{\rho}^3 J_0(\tilde{\rho}) \int_0^\infty \frac{dx}{x} e^{-\frac{1}{4x}} e^{-2nh(\tilde{\rho},x)} e^{-\tilde{\rho}^2x} \quad (5.34)$$

$$B(n) = n \int_0^\infty d\tilde{\rho}\tilde{\rho}^3 J_0(\tilde{\rho}) \int_0^\infty dx e^{-\frac{1}{4x}} e^{-2nh(\tilde{\rho},x)} e^{-\tilde{\rho}^2x}, \quad (5.35)$$

with the quantity  $h(\tilde{\rho}, x)$  given by

$$h(\tilde{\rho}, x) = \int_0^1 \frac{dk}{k} \left[ 1 - J_0(k\tilde{\rho})e^{-x\tilde{\rho}^2k^2} \right]. \quad (5.36)$$

Clearly there is a fixed point at  $n = 2$  which corresponds to a roughening temperature given by

$$T_R = \frac{2\tilde{\gamma}b^2}{k_B\pi}.$$

A simple transformation to the reduced variables  $X = 2\tilde{\gamma}b^2/\pi k_B T$  and  $Y = 4\pi U/k_B T$  allows the recursion relations for the pinning potential and surface stiffness to be rewritten explicitly in the form of the Kosterlitz-Thouless universality class:

$$\frac{dY}{dl} = 2Y \left[ 1 - \frac{1}{X} \right] \quad (5.37)$$

$$\frac{dX}{dl} = \frac{Y^2}{2X} A(2/X). \quad (5.38)$$

This of course is to be expected given the equivalence of the sine-Gordon and two-dimensional Coulomb gas models. What is interesting is that the recursion relations are not exactly the same as those derived by Kosterlitz (see chapter 2): the presence of the term  $A(2/X)/X$  is new here. This discrepancy arises because the operator product expansion of Knops and Den Ouden [18] has been used. Earlier treatments of the roughening transition which used the incorrect expansion of the cosine function, described above, led to recursion relations identical to those of Kosterlitz [9].

Nozières and Gallet comment on the difference between their recursion relations and those of Kosterlitz, ‘In the  $(U, \gamma)$  plane, they are the usual Kosterlitz-Thouless hyperbolae near the fixed point. Away from  $n = 2$ , they depart from that shape, even to order  $U^2$ ’. Furthermore they observe that, ‘such corrections considerably improve the theoretical fit of curvature and step energy measurements’ [19]. Hence it can be concluded that the recursion relations derived by Kosterlitz for superfluid films and still used widely in that context may well not be as accurate as those derived by Nozières and Gallet.

As usual in the Kosterlitz universality class, there are essentially two lines of fixed points. For initial conditions corresponding to temperatures above the roughening temperature,  $T_R$ ,  $Y$  flows to zero at a finite value of  $X$ ; for temperatures below the roughening transition the value of  $Y$  eventually diverges. Since  $Y = 4\pi U/k_B T$  measures the strength of the periodic pinning potential, this implies that above the transition temperature there exists no length scale on which the pinning potential is relevant to the interface while below it such a finite length scale will always exist. The critical value of the scaling parameter,  $l = l_c$ , at which the pinning potential becomes relevant for  $T < T_R$  cannot be determined exactly. It is usually estimated to occur when the pinning strength is of the same order as the thermal fluctuations of the surface so that  $Y(l_c) \sim 4\pi$ .

The correlation length of the system simply defines the length scale on which the pinning potential becomes relevant

$$\xi = \frac{e^{l_c}}{\Lambda_0}, \quad (5.39)$$

so that it remains finite for all temperatures below the transition and is infinite above. However, the correlation length has another obvious interpretation in the context of a crystal surface: it represents the approximate width of a step on the interface. Since the step width and the step energy,

$\beta$ , are related by the relation

$$\beta \sim \frac{\tilde{\gamma}b^2}{\xi}, \quad (5.40)$$

it is clear that the step energy vanishes at the roughening transition. A more refined calculation using the recursion relations also allows the exact behaviour of the step energy as the transition is approached to be determined [19].

The behaviour of the height-height correlation function of the system may also be predicted using  $l_c$ . Again the recursion relations must be integrated to obtain an accurate result, but if the interface is considered as unpinned up to a length scale equal to the correlation length,  $\xi$ , then it follows that for shorter distances the correlation function will simply be that of a free interface:

$$G(r) = \langle (z(0) - z(r))^2 \rangle = b^2 \ln |\Lambda_0 r|. \quad (5.41)$$

Thus above the transition temperature, when  $\xi$  diverges, the correlation function will diverge logarithmically with distance. However, below the roughening temperature — where  $\xi$  is finite — the interface may only be regarded as free for lengths  $r < \xi$ , so that the height-height correlation function remains bounded even for very large separations with the form

$$G(\infty) = \langle (z(0) - z(\infty))^2 \rangle = b^2 \ln |\Lambda_0 \xi|. \quad (5.42)$$

### 5.3 Comparison with Experiment

A roughening transition might be expected to occur in a wide variety of crystals in equilibrium with their melts. However, the release of latent heat is frequently sufficient to prevent the system from reaching equilibrium and furthermore, because the transition is of infinite order, it is easily broadened. The most conclusive experiments performed to date have been on  $\text{He}^4$  crystals though electronic and x-ray scattering off the surfaces of certain metal crystals [76] and investigations of organo-halide crystals [77] have also revealed the presence of roughening transitions in the systems concerned.

Computer simulations have also proved a useful tool in testing the predictions of the theory. Such simulations seek to isolate the essential physical details of a system and provide details of their statistical behaviour.

#### 5.3.1 Experiments on Helium Crystals

Several important studies of the roughening transition in  $\text{He}^4$  crystals in contact with the superfluid phase have been performed, in particular by Wolf et al. [78], Gallet et al. [22] and Rolley et al. [79].  $\text{He}^4$  is particularly suitable for the investigation of the thermodynamics of crystal interfaces because it has some unique properties which make the transition particularly accessible [80, 81]: it has quasi-infinite thermal conductivities which allow equilibrium to be achieved quickly and any departures from it are easily controlled; the superfluid phase has zero viscosity so that there is no resistance to mass transport; equally importantly, a very high level of purity can be achieved.

Three very different sets of measurements have been performed on such systems: the energy of steps at temperatures just below the transition, the average curvature of crystals and the variation of the growth rate in the critical region. Each of these give results which are entirely consistent with theoretical expectations. The Nozières-Gallet theory requires three different fitting parameters which are usually taken to be as follows: the roughening temperature,  $T_R$ ; the ratio of the unrenormalized parameters  $V_0(0)/\tilde{\gamma}(0)$ ; and the cut-off,  $\Lambda_0$ . However, it is found that the same choice of values leads to a good fit for each of the three types of experiment, a result which provides strong support for the Nozières-Gallet theoretical picture.

The step energy for crystals close to the roughening temperature was measured successfully by Wolf et al. [78]. They examined the variation in the growth velocity of crystals grown by a two-dimensional nucleation process with the difference in chemical potential between the crystal and its melt,  $\Delta\mu$ . In this regime the growth velocity,  $v(\mu)$ , is given by the expression

$$v(\mu) = k\Delta\mu \exp\left(\frac{-\pi\beta^2}{3b\Delta\mu\rho_S k_B T}\right), \quad (5.43)$$

where  $\rho_S$  is the bulk density of the solid phase and  $k$  the surface mobility. The step energy was found to decay towards zero as the roughening transition was approached in precisely the way predicted by the theory, as is shown in figure (5.1).

Gallet et al. extended this work to investigate the growth rate of crystals close to and above the roughening temperature [22]. They found that the growth evolved smoothly from a non-linear rate below  $T_R$ , to a linear one at and above  $T_R$ . This experiment provided a sensitive test of the dynamic theory which proved to be in good qualitative and quantitative agreement.

The third series of experiments which have been performed to test the theory measure the dispersion and damping of melting freezing waves on vicinal surfaces [79]. Such experiments allow the surface stiffness to be measured and clearly reveal the anisotropy predicted by Nozières and Gallet for vicinal surfaces.

### 5.3.2 Computer Simulation Work

Much of the computer simulation work on the behaviour of crystal surfaces has centred around the solid-on-solid (SOS) model. The idea is to treat the crystal as a series of columns of various heights so that the assignment of energies to different interface configurations is straightforward. The substrate is divided into an array of squares and the height of the crystal above each is recorded, in integer units, in the array  $h_i$  — this leads to a simplified interface which contains no overhangs or voids. The energy of the surface is taken to be lowest when all the columns have the same height so that the SOS Hamiltonian takes the form

$$H_{\text{SOS}} = \sum_{i,\delta} f |h_i - h_{i+\delta}|, \quad (5.44)$$

where the summation runs over all the nearest neighbours for each of the height columns. The function  $f|x|$  is generally an increasing function of its

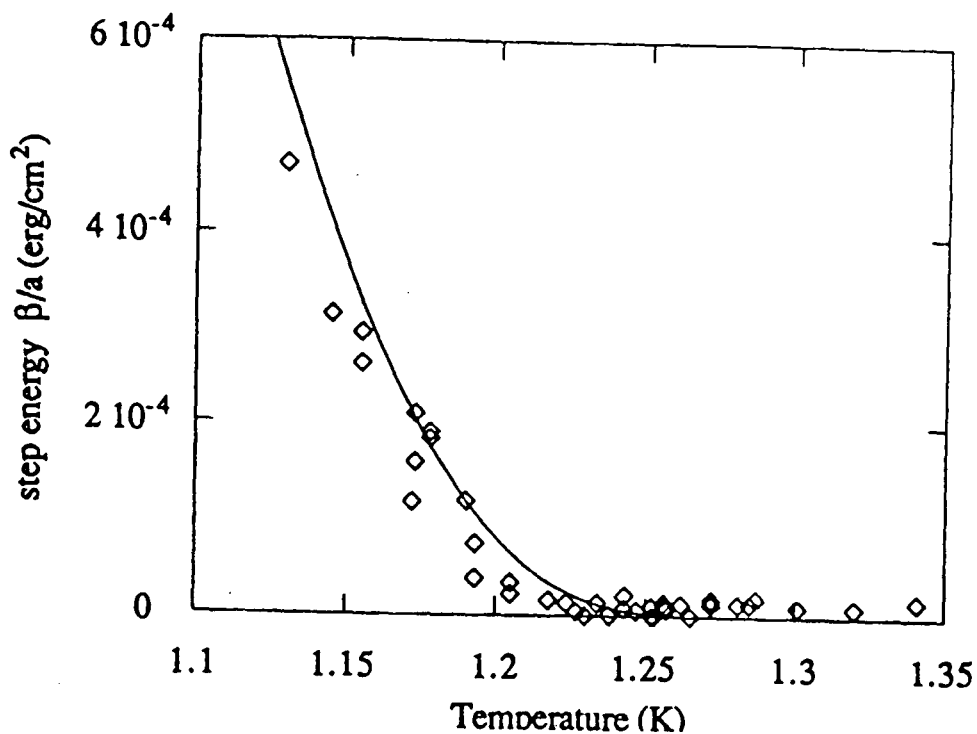


Figure 5.1 Variation of step energy with temperature close to the roughening transition, reproduced from the review in the work of Balibar et al. [82].

variable, but its exact form varies depending on the particular details of the model which is used. The two most commonly studied forms are:  $f|x| = |x|$  (known as the absolute solid-on-solid model) and  $f|x| = x^2$  (called the discrete Gaussian model). In all cases quantities of interest are obtained by using the Hamiltonian as a Boltzmann weighting in Monte-Carlo simulations [83]. That the relevance of such models goes beyond their original formulation as simplistic attempts to mimic real crystal growth processes was demonstrated by Chui and Weeks [30] who showed that the discrete Gaussian model is dual to the two-dimensional Coulomb gas model and hence equivalent to the sine-Gordon model.

The crystal surfaces modelled in such simulations have been shown to undergo the roughening transition. The behaviour of the height-height correlation function may be determined in a straightforward way using the columnar heights. The behaviour of the correlation function for large separations changes at the transition: below the transition temperature it takes a finite value, but above the transition temperature it diverges logarithmically [84]. It has also been demonstrated that the step energy vanishes above the transition in such models [85].

## 5.4 Super-Roughening

Renormalization group methods have also been applied to the model used to describe crystal surfaces where disorder is present (eqn 5.3). For a crystal grown on a disordered substrate a super-roughening transition replaces the roughening transition in both the static and dynamic regimes; however, the exact details of the calculations are not directly relevant to what follows and so the interested reader is referred to the original works for them [23, 24]. The treatments are essentially extensions of earlier work on the random phase sine-Gordon model [70, 71]. Both are based on the weak coupling approximation so that a perturbative expansion in powers of the pinning potential is used. The dynamic renormalization is carried out using field-theoretic methods. It uses the so-called Martin-Siggia-Rose (MSR) formalism which enables a dynamic theory in  $d$ -dimensions to be transformed into a static one in  $(d+1)$ -dimensions [86].

The static recursion relations, first obtained by Toner and Di Vincenzo [23], can be written in the form

$$\frac{dg}{dl} = 2g(1 - n) - \frac{A_g}{\Lambda_c^2} g^2 \quad (5.45)$$

$$\frac{d\tilde{\gamma}}{dl} = 0 \quad (5.46)$$

$$\frac{d\tilde{\gamma}'}{dl} = A_K \frac{\pi n \tilde{\gamma}}{\Lambda_c^4} g^2, \quad (5.47)$$

where  $A_g$  and  $A_K$  are dimensionless constants of order one and the notation  $g = U^2 e^{-2l}$  has been used.  $\Lambda_c$  is a short wavelength cut-off which is inversely proportional to the correlation length for translational order in the plane parallel to the substrate. The quantity  $\tilde{\gamma}'$  is an off-diagonal element of the surface stiffness matrix which arises because the translational symmetry in the plane of the crystal substrate has been broken by the presence of disorder; it does not affect the renormalization of the other parameters and so is not essential for a basic understanding of the transition. These relations show that there is a fixed point at  $n = 1$ , hence the super-roughening transition occurs at a temperature  $T_{SR} = \tilde{\gamma} b^2 / \pi k_B$ . Renormalization was carried out in the dynamic picture by Tsai and Shapir who obtained recursion relations which reduce to those of Toner and Di Vincenzo in the static limit [24].

The dynamic recursion relations for the super-roughening transition lead to important predictions for the behaviour of the height-height correlation function [24]. It is found that the correlation function diverges logarithmically above the transition temperature (as expected in the rough state), but diverges even more strongly below the transition temperature, with the form  $G(R) \propto (\ln R)^2$ .

SOS models can also be used to investigate the super-roughening transition, since the mechanics of the model remains applicable once the disorder has been incorporated in the initial configuration. This is done by displacing the

baseline from which each column height is measured. The height in the  $i$ th column,  $h_i$ , is given by

$$h_i = d_i + n_i b, \quad (5.48)$$

where the quenched height  $d_i$  is chosen randomly and independently on the interval  $(-b/2, +b/2]$  and  $n_i$  is an integer. Monte Carlo simulations based on the discrete Gaussian model confirm the presence of the super-roughening transition, which is identified from a change in the behaviour of the height-height correlation function. The transition is found to occur exactly at the temperature predicted by renormalization group methods [87]. However, the results of simulations have not yet confirmed the predicted behaviour of the height-height correlation function [87, 88].

---

## Chapter 6 Roughening and Disorder

---

This chapter describes how the behaviour of a crystal surface is modified by the presence of dislocations. It is found that the surface still undergoes a roughening transition when the disordering caused by the dislocations is weak. In contrast, when the underlying crystal lattice is strongly disordered by dislocations, the surface can undergo a super-roughening transition. In both cases the weak-coupling regime may be modelled successfully using an extension of the Nozières-Gallet theory. However, the behaviour in the strong coupling regime is less well understood: it seems that there must be a low temperature transition from a facet to the super-rough state, but under exactly what circumstances it occurs remains unclear.

This chapter is organized as follows. In the first section there is a discussion of how the morphology of a crystal surface is changed by screw dislocations. Then there is a description of the way in which the change in morphology can be accounted for in the weak coupling limit by adapting the sine-Gordon model of the interface. Next the Nozières-Gallet renormalization group treatment is repeated in the presence of screw dislocations and the behaviour of the interface calculated for different distributions of the dislocations. There then follows an analysis of the effect of thermally generated dislocation loops on crystal surfaces in the weak coupling limit. Then there is a section which considers the effect of disorder on interfaces which are strongly coupled to the underlying lattice. Finally, the chapter concludes with a section in which there is a discussion of the results obtained and a phase diagram for a crystal surface threaded by screw dislocations is proposed.

### 6.1 Screw Dislocations

The effect of screw dislocation pairs on the behaviour of the crystal surface they thread depends crucially on their distribution. Each of the dislocations acts as a source or sink for a step. The steps on the interface join each screw with another screw of opposite sense of rotation and so the dislocations form pairs, as illustrated in figure (6.1).

If the screws are distributed as pairs, with steps between them of average length  $l_l$ , then the degree to which the crystal surface is disordered can, in principle, be controlled by varying the separation  $l_l$ . The disordering effect of the dislocations may then be investigated by considering crystals with the screws distributed in different ways, that is crystals threaded by screw dislocation pairs with differing average separations  $l_l$ . This parameter can vary from almost zero, the case which leads to an ordered surface (the screw pairs have no effect), up to a value equal to the average distance between screws of the same sign i.e. a separation of  $d_{++} = (L^2/M)^{1/2}$  where  $L^2$  is the area of the substrate and  $M$  the number of each type of screw present. Strongly correlated screw pairs, for which  $l_l \ll d_{++}$ , lead to a shift in the

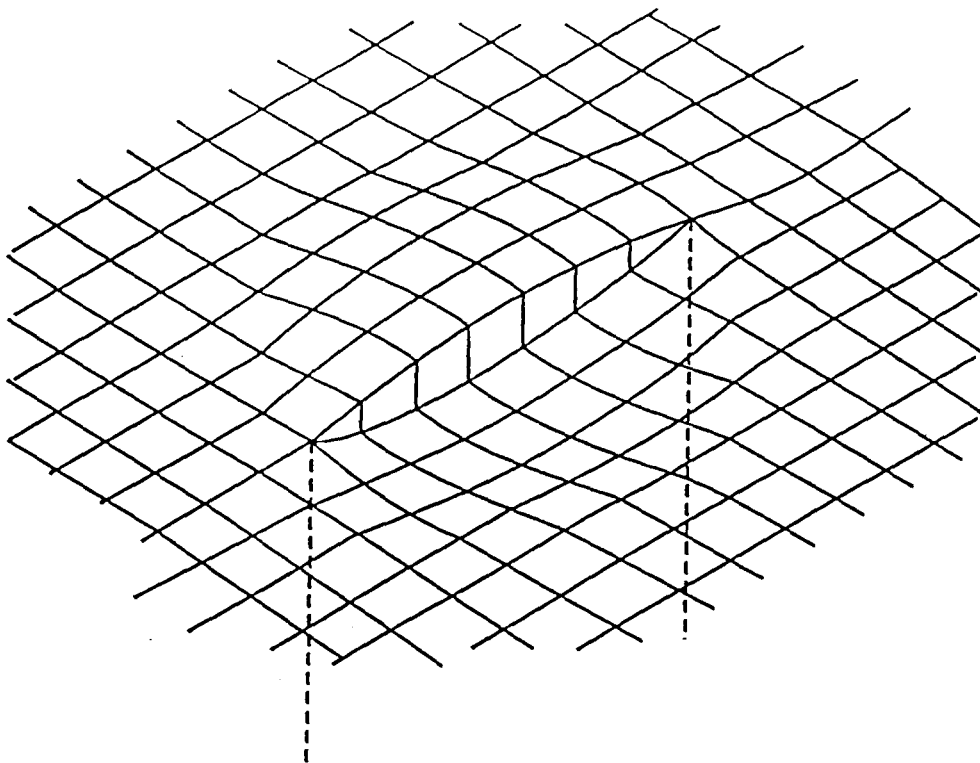


Figure 6.1 Two screw dislocations of opposite sign which pierce the surface normally form a pair with a step on the interface running between them

position of the roughening transition, but crucially they do not alter the universality class of the transition. Weakly correlated pairs, where  $l_l \approx d_{++}$ , on the other hand, destroy the roughening transition and lead to a super-roughening transition [26].

The screw dislocation pairs are imagined to be sown somehow into the nascent crystal. This might be done by growing it on a suitably treated substrate, by exposing it to strain fields, or a combination of such methods. However, once formed with screw dislocations in a particular distribution, the crystal would be allowed to grow in conditions close to equilibrium. The dislocations are assumed to be effectively quenched and to run right through the crystal from its base to the interface parallel to the  $z$ -axis. Crucially the pairings between screws, and hence the distribution of the steps they induce, are not necessarily fixed as the crystal grows.

When a crystal surface is threaded by screw dislocations the crystal planes lose their individual identity since rotation about a dislocation leads smoothly from one plane to the next. The average positions of the atoms are no longer those of the perfect planes,  $z = nb$ , with  $n$  a positive integer, instead they are shifted by the dislocations from these by an amount,  $z_1(\mathbf{r})$ , which depends on the number and distribution of the dislocations. This means that the minima of the pinning potential will be shifted by this amount at each point over the crystal surface, though of course the periodicity of the potential is unaffected. In terms of the model Hamiltonian  $z_1(\mathbf{r})$  simply acts as an extra phase.

The displacement,  $z_1(\mathbf{r})$ , induced by a single screw dislocation is  $\delta z_1 = \pm \phi b / 2\pi$  [89], where  $\phi$  is the azimuthal angle of rotation about the dislocation

(the sign depends on the sense of rotation of the screw). Now consider a pair of screw dislocations of opposite sign with a step between them described by the vector  $\mathbf{l}_l$ . The elastic displacement due to the pair at a point  $\mathbf{r}$ , measured from an origin at the midpoint between the dislocations, is  $\delta z_1(\mathbf{r}) = \gamma b/2\pi$ , where  $\gamma$  is the angle subtended by the vector  $\mathbf{l}_l$  at the point  $\mathbf{r}$ . If  $r \gg l_l$ , then this reduces to  $\delta z_1(\mathbf{r}) = l_l \sin \theta b/2\pi r$  where  $\theta$  is the angle between  $\mathbf{l}_l$  and  $\mathbf{r}$ . The total displacement of the interface at any point is then obtained by simply summing over the contributions of each pair of screw dislocations that have a step between them. Thus  $z_1(\mathbf{r})$  depends not only on the actual positions of the dislocations, but also on the particular distribution of steps between them.

## 6.2 Renormalization with Disorder

The Hamiltonian for an interface with disorder arising from screw dislocations can be renormalized using the Nozières-Gallet framework. The potential term is simply modified to include the extra phase due to the screw dislocations,  $z_1(\mathbf{r})$ ,

$$\mathcal{H} = \int d^2\mathbf{r} \left( \frac{\tilde{\gamma}(\nabla z(\mathbf{r}))^2}{2} - V_0 \cos \left( \frac{2\pi}{b} (z(\mathbf{r}) - z_1(\mathbf{r})) \right) \right). \quad (6.1)$$

Since the disorder induced phase shift,  $z_1$ , is independent of the thermal fluctuations in the surface height, its presence has no effect on the way in which the surface height,  $z$ , is split into two parts:

$$z(\mathbf{r}) = \bar{z}(\mathbf{r}) + \delta z(\mathbf{r}). \quad (6.2)$$

This means that the first order term renormalizes in the same way as before,

$$\bar{V} = \langle V \rangle_0 = V_0 \left\langle \cos \left( \frac{2\pi}{b} (\bar{z}(\mathbf{r}) + \delta z(\mathbf{r}) - z_1(\mathbf{r})) \right) \right\rangle_0 \quad (6.3)$$

$$= V (\bar{z}(\mathbf{r}) - z_1) \left\langle \cos \left( \frac{2\pi \delta z(\mathbf{r})}{b} \right) \right\rangle_0 \quad (6.4)$$

$$= V (\bar{z}(\mathbf{r}) - z_1) e^{-\frac{2\pi^2}{b^2} \langle (\delta z(\mathbf{r}))^2 \rangle_0}. \quad (6.5)$$

At second order averages over the equilibrium distribution arise and these are affected by the disorder phase. In particular it is the correlation function  $C(z, z')$  which is altered, in the presence of disorder it has the form:

$$C = \left\langle \cos \left( \frac{2\pi (\bar{z}' - z_1' - \bar{z} + z_1)}{b} \right) \right\rangle, \quad (6.6)$$

where the unprimed quantities are evaluated at  $\mathbf{r}$  and the primed ones at  $\mathbf{r} + \boldsymbol{\rho}$ . The average is taken over the Fourier components of the equilibrium distribution of the interface displacement and hence depends on  $z_1$ . Thus the correlation function may be rewritten as,

$$C = G_D(\boldsymbol{\rho}) e^{-2\pi^2 \langle (\bar{z}' - \bar{z})^2 \rangle / b^2}, \quad (6.7)$$

with the function  $G_D(\rho) = \langle \cos(2\pi(z'_1 - z_1)/b) \rangle$  due to the disorder. The average in  $G_D(\rho)$  is taken over a random placement of dislocations and the average value of  $(\bar{z}' - \bar{z})^2$  is given by

$$\langle (\bar{z}' - \bar{z})^2 \rangle = \frac{k_B T}{\pi \tilde{\gamma}} \int_0^{\Lambda_0} \frac{dk}{k} [1 - J_0(k\rho)] = \frac{k_B T}{\pi \tilde{\gamma}} h(\rho). \quad (6.8)$$

The function  $G_D$  is assumed to depend on the position  $\rho$ , but not on the time. The dislocations are considered to be effectively fixed in place: it is true that their positions and the pairings between them do evolve over time, but the time scales for these processes are assumed to be so long as to be irrelevant.

The new term  $G_D(\rho)$  modifies the renormalization of the surface stiffness to

$$\frac{d\tilde{\gamma}}{dl} = \frac{\pi^3 \bar{V}_0^2}{\tilde{\gamma} b^4} \int_0^\infty d^2 \rho \rho^2 J_0(\Lambda \rho) e^{-2nh(\rho)} G_D(\rho). \quad (6.9)$$

Thus the static recursion relations take the form

$$\frac{dU}{dl} = U(2 - n) \quad (6.10)$$

$$\frac{d\tilde{\gamma}}{dl} = \frac{2\pi^4}{\tilde{\gamma} b^4} U^2 A(n, l), \quad (6.11)$$

with

$$A(n, l) = \int_0^\infty d\tilde{\rho} \tilde{\rho}^3 J_0(\tilde{\rho}) e^{-2nh(\tilde{\rho})} G_D(\tilde{\rho} e^l / \Lambda_0) \quad (6.12)$$

When the calculation is performed in the dynamic regime the renormalization of both the surface stiffness and the mobility are altered by the dislocations. The recursion relations for the potential and surface stiffness have the same form as in the static case (eqns 6.10 and 6.11) and the behaviour of  $\eta$  is given by

$$\frac{d\eta}{dl} = \frac{8\pi^4 \eta}{\tilde{\gamma} b^4} U^2 B(n, l). \quad (6.13)$$

The function  $G_D$  is present in the integration over  $\tilde{\rho}$  in both the expressions for  $A(n, l)$  and  $B(n, l)$  so they are altered:

$$A(n, l) = n \int_0^\infty d\tilde{\rho} \tilde{\rho}^3 J_0(\tilde{\rho}) G_D(\tilde{\rho} e^l / \Lambda_0) \int_0^\infty \frac{dx}{x} e^{-\frac{1}{4x}} e^{-2nh(\tilde{\rho}, x)} e^{-\tilde{\rho}^2 x} \quad (6.14)$$

$$B(n, l) = n \int_0^\infty d\tilde{\rho} \tilde{\rho}^3 J_0(\tilde{\rho}) G_D(\tilde{\rho} e^l / \Lambda_0) \int_0^\infty dx e^{-\frac{1}{4x}} e^{-2nh(\tilde{\rho}, x)} e^{-\tilde{\rho}^2 x}. \quad (6.15)$$

The existence and character of any surface phase transition in the presence of dislocation induced disorder are thus controlled by  $G_D(\rho)$ , and its behaviour in turn is entirely determined by the distribution of the dislocations.

There are three important forms that the function  $G_D(\rho)$  can take. Firstly, if  $G_D(\tilde{\rho} e^l / \Lambda_0)$  tends to some constant value as  $l \rightarrow \infty$ , then there is no essential

change in the transition that occurs. A simple roughening transition occurs, with slightly altered values of the parameters  $A(n)$  and  $B(n)$ . If on the other hand  $G_D(\tilde{\rho}e^l/\Lambda_0)$  varies as  $(l_l/\rho)^{2\alpha}$ , with the parameter  $2\alpha < 1$ , then there is still a roughening transition, but a distinct shift in the critical point occurs [25]. Finally, if the correlation function decays to zero rapidly with increasing  $l$ , then the recursion relations for  $\tilde{\gamma}$  and  $\eta$  are effectively terminated at a finite length scale and no longer describe a transition in the Kosterlitz-Thouless universality class.

### 6.3 Calculation of Correlation Functions

The calculation of the correlation functions involving screw dislocations is complicated because there is no simple analytical way of calculating the function  $G_D(\rho)$ . In order to determine the actual behaviour of particular distributions of screw dislocations, computer simulations were used to calculate  $G_D(\rho)$  for all  $\rho$  in the two limits  $l_l \ll d_{++}$  and  $l_l \approx d_{++}$ . The model used was based on the simple ansatz that steps form between screw dislocations of opposite sign in such a way as to minimize the total step length. Although, as will be seen, this is not quite the same as minimizing the surface energy it leads to a state which is close to (within the range of thermal fluctuation at least) the minimum energy configuration. In the limiting cases for which the simulation is used the simple model on which it is based is perfectly sufficient.

#### 6.3.1 Computational Method

The average values of the height-height correlation function for different distributions of screw dislocations were calculated in the following way. Screw dislocations were placed on a square crystal surface of side  $L$ , either entirely at random (the random distribution) or as closely spaced pairs, of opposite sign, distributed randomly across the surface (the paired distribution). In the case of the random distribution the dislocations of opposite sign were paired up in such a way that swapping over the steps between any two pairs always led to an increase in the total step length. This leads to a state which is close to a local minima in the total step energy, though not necessarily close to the global minimum. For closely paired dislocations the system is in its lowest energy state when steps form between members of the same pair and so no rearrangement was necessary.

The correlation function  $G_D(\rho) = \langle \cos(2\pi(z_1(\rho) - z_1(0))/b) \rangle$  was calculated in the following way. First of all two sample points a distance  $\rho$  apart on the interface were selected at random (within a square of side  $L/2$  at the centre of the system, so that neither of the points could approach the edges too closely). The total phase due to all the dislocations paired together by steps was then calculated at the points. This was done using simple coordinate geometry and the total obtained by simply adding together the contributions of all the dislocations. The cosine of the difference in phase between the two points was then calculated. Finally, the process was repeated for a variety of different values of  $\rho$  and for different distributions of the screw dislocations.

For the randomly placed distribution between 12 and 80 screw dislocations

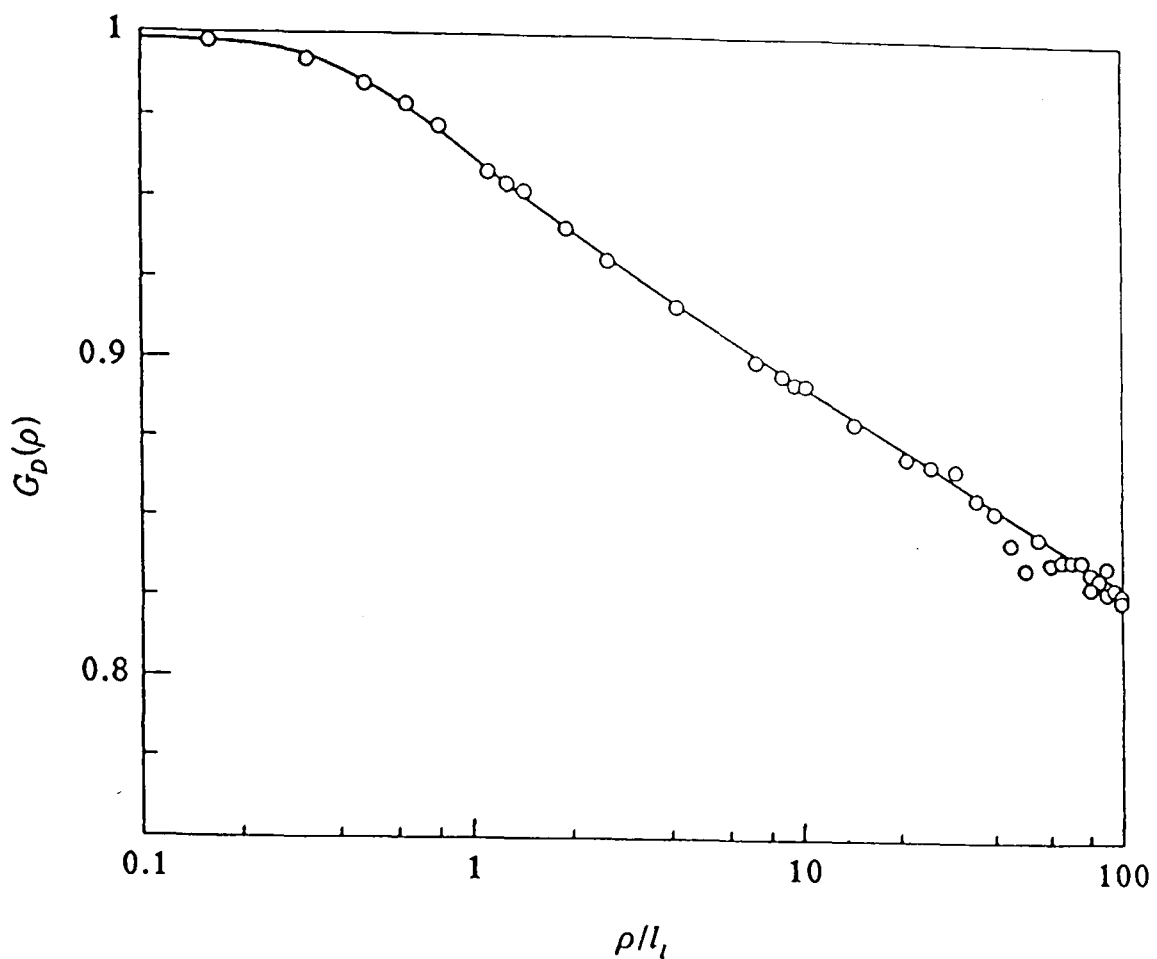


Figure 6.2 The function  $G_D(\rho)$  as a function of  $\rho/l_l$  for closely spaced pairs of dislocation lines, where  $l_l/d_{++} = 0.01$

of each kind were used. Averages were taken over up to 500 different choices of the sample points' positions and then the process was repeated between 50 and 100 times for differing random placements of the dislocations. For the paired distributions the members of each pair were separated by a distance  $0.1d_{++}$ . Averages in this case were taken over more than 10000 different random placements of pairs and were repeated for systems containing between 25 and 100 pairs.

### 6.3.2 Closely Spaced Pairs

The results of the simulations for closely spaced pairs are shown in figure (6.2). The correlation function takes the form  $G_D(\rho) \sim (l_l/\rho)^{2\alpha}$ , with  $2\alpha = \pi l_l^2/d_{++}^2$ . In the static picture this leads to a modification of the parameter  $A(n)$  which now depends on the renormalization parameter  $l$ : for  $\rho \gg l_l$  it may be written as  $A(n, l) = A'(n)e^{-2\alpha l}$  where

$$A'(n) = \int_0^\infty d\tilde{\rho} \tilde{\rho}^3 J_0(\tilde{\rho}) e^{-2nh(\tilde{\rho})} (\Lambda_0 l_l / \tilde{\rho})^{2\alpha}. \quad (6.16)$$

This then leads to modified static recursion relations of the form:

$$\frac{dU'}{dl} = U'(2 - \alpha - n) \quad (6.17)$$

$$\frac{d\tilde{\gamma}}{dl} = \frac{2\pi^4}{\tilde{\gamma}b^4} (U')^2 A'(n) \quad (6.18)$$

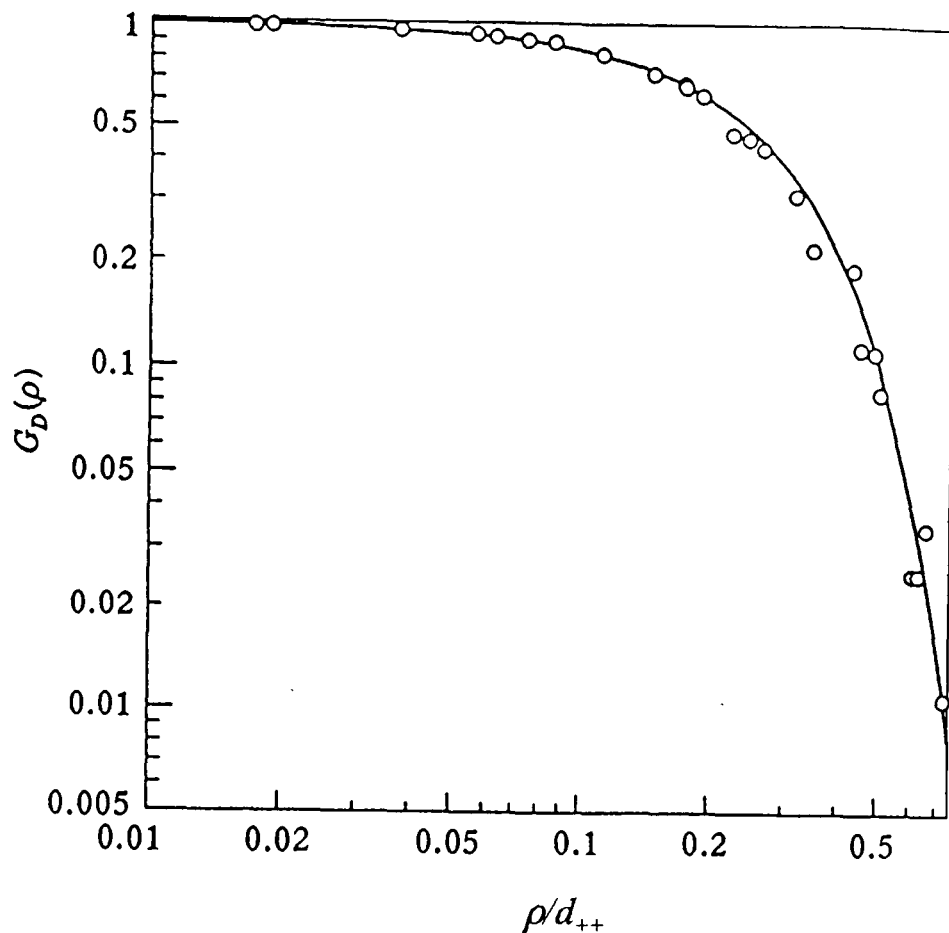


Figure 6.3 The function  $G_D(\rho)$  as a function of  $\rho/d_{++}$  for screw dislocations placed at random,  $l_l/d_{++} \simeq 1$

where  $U' = Ue^{-\alpha l}$ . They are still of the Kosterlitz-Thouless form, but the fixed point is shifted from the normal roughening transition value,  $n = 2$ , to  $n = 2 - \alpha$ . This behaviour was first encountered by Scheidl [25] who studied the case where  $z_1$  is just a random field with a spatial correlation function of the form  $\rho^{-2\alpha}$ . The calculation is easily repeated in the dynamic renormalization scheme, leading to the same result.

### 6.3.3 Randomly Placed Dislocations

When equal numbers of screw dislocations of opposite sign are placed entirely at random onto a crystal surface the correlation function  $G_D$  decays rapidly to zero as the length scale is increased. The actual decay is somewhat faster than  $e^{-\rho/d_{++}}$  so that within the error of the simulations  $G_D$  is zero for  $\rho \simeq 0.8d_{++}$  (see figure 6.3). Thus it is reasonable to model the function as a simple step at  $\rho = d_{++}$ : this leads to recursion relations which have a different form depending on the length scale.

When  $d_{++}\Lambda_0 e^{-l} \ll 1$  the coefficients in the dynamic renormalization scheme are modified,

$$A(n, l) = n \int_0^{d_{++}\Lambda_0 e^{-l}} d\tilde{\rho} \tilde{\rho}^3 J_0(\tilde{\rho}) \int_0^\infty \frac{dx}{x} e^{-2nh(\tilde{\rho}, x)} e^{-1/4x} e^{-\tilde{\rho}^2 x} \quad (6.19)$$

$$\simeq n \int_0^{d_{++}\Lambda_0 e^{-l}} d\tilde{\rho} \tilde{\rho}^3 J_0(\tilde{\rho}) \ln(1/\tilde{\rho}^2) \quad (6.20)$$

$$\simeq \frac{1}{2} n d_{++}^4 \Lambda_0^4 e^{-4l} \ln(e^l / d_{++} \Lambda_0) \quad (6.21)$$

and

$$B(n, l) = n \int_0^{d_{++} \Lambda_0 e^{-l}} d\tilde{\rho} \tilde{\rho}^3 J_0(\tilde{\rho}) \int_0^\infty dx e^{-2nh(\tilde{\rho}, x)} e^{-1/4x} e^{-\tilde{\rho}^2 x} \quad (6.22)$$

$$\simeq n \int_0^{d_{++} \Lambda_0 e^{-l}} d\tilde{\rho} \tilde{\rho} J_0(\tilde{\rho}) \quad (6.23)$$

$$\simeq \frac{1}{2} n d_{++}^2 \Lambda_0^2 e^{-2l}. \quad (6.24)$$

The term  $e^{-\tilde{\rho}^2 x}$ , in addition to  $e^{-2nh(\tilde{\rho}, x)}$ , cuts off the integrals for  $x \sim 1/\tilde{\rho}^2$ . For large values of  $l$  both  $A(n, l)$  and  $B(n, l)$  die off rapidly since they vary as  $l e^{-4l}$  and  $e^{-2l}$  respectively.

The crossover comes at a value of  $l$  given by  $l_d = \ln(d_{++} \Lambda_0)$ : for smaller values of  $l$  the renormalization proceeds almost as in the absence of disorder, but at  $l = l_d$  the renormalization of the surface stiffness is effectively stopped and that of  $\eta$  altered substantially. It is of course the large length scale behaviour which determines the critical behaviour of the system and for  $l \gg l_d$  the recursion relations can be approximated closely, up to second order, as

$$\frac{dU}{dl} = U(2 - n_\infty) \quad (6.25)$$

$$\frac{d\tilde{\gamma}}{dl} = \frac{\pi^4 n_\infty d_{++}^4 \Lambda_0^4}{\tilde{\gamma} b^4} U^2 e^{-4l} \ln(e^l / d_{++} \Lambda_0) \quad (6.26)$$

$$\frac{d \ln \eta}{dl} = \frac{4\pi^4 n_\infty d_{++}^2 \Lambda_0^2}{\tilde{\gamma}^2 b^4} U^2 e^{-2l}, \quad (6.27)$$

where  $n_\infty$  is the constant value to which  $n$  is renormalized when  $d\tilde{\gamma}/dl$  decays to zero for  $l \gg l_d$ . There is a very close correspondence between the recursion relations obtained for randomly placed dislocations and those of the super-roughening transition obtained by Tsai and Shapir in the dynamic regime [24]. This is seen most clearly if the potential  $U$  is redefined: defining the quantity  $g$  by the relation

$$g = U^2 e^{-2l}, \quad (6.28)$$

the recursion relations become,

$$\frac{dg}{dl} = 2g(1 - n_\infty) - \beta g^2 \quad (6.29)$$

$$\frac{d\tilde{\gamma}}{dl} = 0 \quad (6.30)$$

$$\frac{d \ln \eta}{dl} = \frac{4\pi^4 n_\infty d_{++}^2 \Lambda_0^2}{\tilde{\gamma}^2 b^4} g. \quad (6.31)$$

The term in  $g^2$  has been introduced here without proof, but it would arise naturally in a higher order renormalization scheme. The functional form of

the coefficient  $\beta$  has not been determined, but it will not alter the character of the transition as it is not the leading term close to criticality. The fixed point of these relations occurs at  $n_\infty = 1$ : for  $n_\infty < 1$ ,  $g$  renormalizes to a constant value and  $\eta$  diverges, leading to an interface which is pinned and immobile; in contrast if  $n_\infty > 1$ , then while  $g$  tends to a zero,  $\eta$  tends to a finite value, leading to an unpinned and mobile interface.

Although the recursion relations obtained have the same form as those of the super-roughening transition this does not necessarily mean that a sharp phase transition would be observed in practice. It may be that a crossover occurs instead [90]: such a possibility is consistent with the observation, made by Toner and Di Vincenzo, that the super-roughening transition is not a true thermodynamic phase transition and is in fact rounded on long length scales [23].

#### 6.4 Dislocation Loops

Another interesting type of disordering of crystal surfaces is that due to the thermally generated dislocation loops which always arise in real crystals. These objects consist of two short sections of screw dislocation which pierce the surface normally and are joined in the bulk of the crystal by an edge dislocation and on the surface by a step. Dislocation loops differ topologically from screw dislocation pairs because the loops are entirely closed objects. The size of the loops is very small in comparison with the average distance between them as their energy cost is proportional to the length of the edge dislocation in the bulk of the crystal.

Because dislocation loops are present at all finite temperatures, it was argued by Andreev that crystal surfaces should always be disordered so that a roughening transition of the Kosterlitz-Thouless type cannot occur [35, 36]. Andreev's argument centres on the way in which the height of a crystal surface is defined when the crystal is threaded by dislocation loops. The height above a particular point on the substrate can be seen as the sum of two contributions: a growth height due to the addition of layers of atoms, and a component due to elastic distortions in the underlying crystal planes. In this picture the surface height of a defect free crystal is entirely due to the growth component.

The problem arises over the appropriate choice of 'height' when the calculation of the height-height correlation function is considered. Andreev argues that when there are defects present it is the growth height which should be used to calculate the height-height correlation function. He finds that in the presence of dislocation loops, which lead to steps of length  $l_l$ , spaced an average distance  $d$  apart, the height-height correlation function has the form

$$\langle [z_A - z_B]^2 \rangle = \frac{L l_l b^2}{d^2}, \quad (6.32)$$

where the points A and B lie a distance  $L$  apart. Clearly this function is strongly divergent, implying that crystal surfaces will always have an infinite width and so be rough since dislocation loops must always be present to some extent.

It was on the basis of the divergence of the height-height correlation function, calculated in this way, that Andreev claimed that ‘there can be no roughening phase transitions ... to which the Kosterlitz-Thouless picture actually applies’ [35]. However, Andreev’s method is not the only way of defining the height of a crystal surface threaded by dislocations [90]. For instance one could define the height by counting the number of crystal planes that are crossed in travelling directly upwards from the substrate to the surface. Where a dislocation loop is present the number of planes is only altered in the region between the line dislocation, running inside the crystal, and the step to which it joins on the surface. Since the effects of the line dislocation and the step parts of the loop are equal and opposite, according to this definition the loops warp the crystal planes, but certainly do not lead to any divergences in the correlation function. However, the matter can be investigated more thoroughly by incorporating the dislocation loops into the Nozières-Gallet theory — in much the same way as with screw dislocations.

If the crystal surface is pierced by thermally generated dislocation loops the correlation function,  $G_D(\rho)$ , takes on a third distinct form. The dislocation loops are modelled as a semicircular dislocation, of radius a few lattice spacings, whose ends are linked by a small step in the interface forming a closed object. As the loops are thermally generated and the energy required to generate them is typically much larger than  $k_B T$ , they form a dilute gas on the interface and so can be assumed to be non-interacting. The elastic displacement produced by a single loop is rather less than that due to a pair of screw dislocations,  $\delta z_1 \simeq \sin \theta / r^2$ , because the underlying dislocation cancels out the effect of the step on long length scales.

Since the loops act independently the correlation function is given by

$$G_D(\rho) = \left\langle \cos \left( 2\pi \sum_{\lambda=1}^N (\delta z_{1\lambda} - \delta z'_{1\lambda}) / b \right) \right\rangle \quad (6.33)$$

for  $N$  loops in an area  $S$ , where  $\delta z_{1\lambda}$  and  $\delta z'_{1\lambda}$  are the contributions from the loop labelled by ‘ $\lambda$ ’ to the total elastic displacement at the points  $\mathbf{r}$  and  $\mathbf{r}'$  respectively. The average is taken over all configurations of each of the  $N$  loops. However, when the cosine is expanded all those terms containing at least one sine vanish on the average, hence the expression simplifies to the form

$$G_D(\rho) = \prod_{\lambda=1}^N \langle \cos (2\pi (\delta z_{1\lambda} - \delta z'_{1\lambda}) / b) \rangle. \quad (6.34)$$

Each of the terms in this product are equal so

$$G_D(\rho) = \langle \cos (2\pi (\delta z_1 - \delta z'_1) / b) \rangle^N \quad (6.35)$$

$$= \left\langle 1 - \frac{1}{S} \int d^2 \mathbf{r} (1 - \cos (2\pi (\delta z_1 - \delta z'_1) / b)) \right\rangle^N, \quad (6.36)$$

where now the average is over the configurations of a single loop. In the thermodynamic limit, where  $N$  tends to infinity with  $n = N/S = 1/d^2$  fixed, the correlation function is

$$G_D(\rho) = \exp \left( -n \int d^2 \mathbf{r} \langle 1 - \cos (2\pi (\delta z_1 - \delta z'_1) / b) \rangle \right). \quad (6.37)$$

If the origin is taken to be at the centre of a loop of length  $l_i$  then the two points  $\mathbf{r}$  and  $\mathbf{r}'$  lie at distances  $r$  and  $r'$  from it. There is only a contribution to the integral in eqn (6.37) when the value of the cosine term differs from 1, this occurs when a dislocation loop is within a distance  $l_i$  of the point  $\mathbf{r}$ . Further away, each loop contributes an amount  $\delta z_{1\lambda} \approx \alpha l_i^2 \sin \theta b / r^2$  to the total  $\delta z_1$ , where  $\alpha$  is a constant. Thus when the separation,  $\rho$ , is much larger than the size of the loop, the integral over  $r$  converges rapidly in the region  $l_i < r < \rho$ . This means that the integral tends to a constant value for large  $\rho$ , thus the correlation function  $G_D(\rho)$  tends to  $e^{-\alpha n l_i^2}$ . Since the energy of a dislocation loop increases sharply with length, it is clear that in practice the value of the ratio of loop length to inter-loop spacing will be very small. Hence  $G_D(\rho)$  decreases only slightly from unity when  $\rho > l_i$  so that the roughening transition is essentially unaffected by the presence of the loops.

## 6.5 The Strong Coupling Regime

In the weak coupling limit the roughening transition exists in the low-disorder regime, but when the underlying crystal lattice is strongly disordered a super-roughening transition occurs instead. This leads to the hypothesis that in the strong coupling limit, at  $T = 0$ , there must be a phase transition at which the ground state of a crystal surface changes from faceted to super-rough [37]. However, there are two important questions which need to be addressed before the nature of such a transition can be elucidated for a crystal where the disorder arises from screw dislocations. First, the traditional definition of a facet as ‘flat’ becomes ambiguous in the presence of dislocations: a more general picture of what is meant by a facet is needed. Second, for a surface threaded by dislocations the morphology of the surface is determined by the way in which steps form on the interface between the dislocations. In order to model the behaviour of the interface, what is required is a clear understanding of how the steps are likely to form for a given distribution of screws.

This section begins with a description of how the definition of a facet may be generalized to situations where the underlying crystal lattice is disordered. Next there is discussion of how the steps on the interface arising from screw dislocations are most likely to be distributed in the low temperature limit. Finally results are presented from an attempt to use a simple computer simulation to determine exactly where the proposed transition from a facet to the super-rough state occurs.

### 6.5.1 Definition of a Facet

For a perfect crystal structure a ‘facet’ is synonymous with the ground state of the surface and can be unambiguously defined in terms of either a height-height correlation function,  $\langle (z(r) - z(r + \rho))^2 \rangle$ , which remains finite as  $\rho \rightarrow \infty$ , or simply a finite step energy (which means it costs a finite amount of energy to tilt the surface). However, in the presence of dislocations the surface becomes rugged: the crystal ‘planes’ are no longer planar and cannot be uniquely defined. Therefore the traditional definition of a

facet is ambiguous and can lead to misconceptions. A clear understanding of both how a facet may be defined in the presence of disorder and the nature of the ground state of such systems is essential to any understanding of the behaviour of disordered crystal surfaces in the low temperature limit [37].

Here a crystal surface is defined as faceted if, in the thermodynamic limit, a finite amount of energy is required to tilt the surface by even an infinitesimal amount. Put another way, a crystal surface of area  $L^2$  is faceted if there is a cusp in the variation of the free surface energy density,  $E(\theta)/L^2$ , with tilt angle,  $\theta$ , in the limit  $\theta \rightarrow 0$ . This means that if a step that runs right across the interface is added and allowed to interact with the steps between any dislocations already present, then the change in the surface energy density will be proportional to  $L$  if the crystal is faceted. If the energy of the system grows less rapidly with  $L$  when steps are added to the interface, for example as  $\ln L$  or as  $L^\alpha$  with alpha less than 1, then there is no cusp in the free energy and the interface is not faceted according to this definition.

In the low temperature regime the dominant contribution to the surface energy comes from the step energy: steps on the interface have a finite energy per unit length. The longer the total length of steps between dislocations the higher the surface energy. However, when the surface is threaded by dislocations an accurate calculation of the free energy must also include the contribution due to the strain introduced in the interface by the dislocations [90]. The energy due to the elastic strain is taken to be much weaker than that arising from the steps, but its inclusion may lead to a lifting of the degeneracy of various arrangements of steps between screw dislocations which, whilst leading to differing surface morphologies, have the same total step length.

When screw dislocations are distributed as closely spaced pairs the steps that form between them are short in comparison with the average distance between any two pairs. As a consequence the cost of creating a step running right across the crystal is the same as in the absence of dislocations: certainly the long step is broken into pieces wherever it crosses dislocation-induced steps, but since these steps are randomly oriented the effect of breaking the long step into pieces will be to increase the total step length as often as it is to decrease it.

For dislocations distributed at random, the steps that form on the interface are simply as long as their average separation. This means that when an extra step which runs right across the interface is added, a good deal of rearrangement of the steps will tend to occur, as the crystal is grown slowly, before 'equilibrium' is reached (that is to say an arrangement that does not alter as further layers are gradually added to the surface [91]). Certainly the energy of the surface increases when the extra step is added, but it is not obvious that the energy density varies with  $L$ , in the limits of  $L \rightarrow \infty$  and  $\theta \rightarrow 0$ , in a way that ensures that there is a cusp in the free energy.

An interesting comparison can be made between the case of randomly placed screw dislocations and that of solid-on-solid models with disordered substrates. It has been established that in the weak coupling limit the solid-on-solid model with atoms growing on a disordered substrate undergoes the

super-roughening transition. Recent work on such systems in the low temperature limit has shown that the increase in the free energy of the surface when an extra step is added scales with the size of the system as  $\ln L$  implying that the ground state is non-faceted [72, 73]. The standard solid-on-solid model and the undistorted sine-Gordon model of crystal surfaces (or that which includes the effects of paired dislocations) are known to display the same characteristics in both weak and strong coupling limit [92]. Furthermore, the theoretical model of an interface threaded by screw dislocations undergoes a super-roughening transition in the weak coupling limit, as does the disordered solid-on-solid model. This suggests that the ground state of a crystal surface threaded by randomly distributed screw dislocations should be unfaceted.

Parallels may also be drawn with the Mott-transition of hydrogen atoms or excitons [93, 94]. For both systems  $+$  and  $-$  charges are present. A transition occurs when, and if, the charges are able to dissociate. When the distance between positive charges is much smaller than the Bohr radius such a dissociation does not occur, the charges remain paired in neutral dipoles. However, if the dipoles start to overlap (i.e. if the distances between like and unlike charges are similar) then the system becomes a plasma. At  $T = 0$  there is a sharp transition from the insulating state to the conducting state, but it is blurred at finite temperatures. The dilute screw pairs are analogous to the paired state in the Mott-transition. As the density is increased so that  $l_i \approx d_{++}$  a transition to a non-faceted state which is nevertheless still pinned occurs. The analogy breaks down at finite temperatures where a sharp transition is expected to persist in the case of dislocations. The transition is not blurred for crystal surfaces because steps are macroscopic objects which can stretch across the whole crystal width, while atoms are highly localised and so are more susceptible to fluctuations.

### 6.5.2 Step Distribution

In the low temperature limit the distribution of dislocation induced steps on a crystal surface is determined entirely by the distribution of the dislocations over the surface. When the screw dislocations exist as pairs, the key parameter is the ratio of the intra-pair separation  $l_i$ , to the inter-pair separation  $d_{++}$ . When  $l_i/d_{++} \ll 1$  the steps form short sections which always join members of the same pair and are well separated on the surface of the crystal; if instead  $l_i/d_{++} \approx 1$ , then it is no longer obvious how the steps should form as the screw dislocation pairs become indistinct and blend together. However, the distribution of steps is somewhat constrained by the topological requirement that no two steps can cross.

When the density of screw dislocations is large the pairings between them, and hence the way in which the steps will form, are not obvious by inspection. A good idea of how the steps are distributed under these circumstances can be obtained by considering how their positions change as a crystal grows. Consider a single pair of screw dislocations with a step of length  $l$  joining them. As a slight over-pressure is applied to the crystal the step bows out by an amount  $s \simeq l^2 F/\beta$ , where  $\beta$  is the energy per unit length of the step and  $F$  the force applied to the surface. If the crystal grows at the expense

of its melt then the step will bow out further as atoms add to the edge of the step, until eventually it intersects with itself forming a terrace.

If there are several pairs of screw dislocations then as growth proceeds the steps will intersect with each other from time to time as they expand, and so rearrange. The degree to which this happens depends on the rate at which the crystal is grown as this affects the distance which the steps bow out between the dislocations. For a crystal being grown at a very slow rate the most likely distribution of the steps on the interface is one in which the total step length is a minima: that is the steps form between dislocations in such a way that the pairs so formed are as small as possible. The step length evolves towards a minimum because the rearrangement of steps as the crystal grows is intrinsically a one way process. Large steps bow out a long way as the crystal grows, interacting with any steps they encounter in the process, where as smaller steps sweep out smaller areas, therefore they are less likely to interact with another step and so are more likely to maintain their configuration as growth proceeds. However, there is no reason why the configuration of the steps should be the one, amongst all possible pairings, which minimizes the total step length. The bias in the evolution of the step distribution is always towards a reduction in step length, but there is no guarantee that the system will find its way to the state where the total step length is the absolute minimum.

### 6.5.3 Computer Simulation Method

A simple computer simulation was developed to try and determine exactly when the proposed low temperature transition from a faceted to super-rough state occurs. In this model all attention is focused on the behaviour of the steps between screw pairs: the rest of the thermodynamics of the surface is ignored since in the strong coupling limit the fluctuations in the interface are negligible. Furthermore, it is assumed that because the energy of the surface is dominated by the steps, the strain energy associated with the dislocations can be neglected.

The question that the simulations were designed to consider is this: for a given distribution of screw pairs is there a cusp in  $E(\theta)/L^2$  in the limit  $\theta \rightarrow 0$ ? The question is answered by measuring the average energy required to tip surfaces threaded by screw dislocations by increasing amounts. The tilting is achieved — as it would be in practice — by adding steps which stretch across the whole width of the crystal (known as ‘long steps’) to the interface. These ‘long steps’ are then allowed to rearrange with the steps already present, due to the screw dislocation pairs themselves, until a locally minimum energy configuration is achieved. By simply recording the change in ground state energy as the ‘long steps’ are added successively, the curve of change in surface energy versus tilt angle can be plotted. Also, by investigating the behaviour of crystals of different size, the relationship between the change in energy when a single ‘long step’ is added and the size of the crystal surface may be determined. The hope was that this simple model would show a change in behaviour with different distributions of screw dislocations.

In the simple model considered here the dislocations are placed across a

square crystal surface of side  $L$ , as randomly distributed pairs of + and - screws, each separated by a much shorter distance  $l_l$  and with a step between them. To ensure that none of the screws lie outside the crystal surface the centre of each pair is distributed within a square of side  $L_0 = L - l_l$ . When  $M$  pairs are placed, the average distance between screws of the same type is approximately  $d_{++} = \sqrt{L^2/M}$ . The relaxation of the system to a local energy minimum is simulated by allowing the pairings of sets of two screws to interchange wherever this leads to a lower energy state. In practice the relaxation is done by cycling through all the screws in turn and swapping over the pairings between them (and hence the associated steps) where this reduces the total step length. The simulation also allows screws to pair with the edge of the substrate if this leads to a reduction in energy (for distributions where  $l_l \simeq d_{++}$  this is a realistic possibility).

Once a local minimum energy state of the system is found, 'long steps' are added one at a time that run across the whole width of the crystal to test the stability of the ground state. Each time a 'long step' is added the new minimum energy configuration is worked out, using the same methods as before, and the total energy of the system calculated.

The whole procedure was repeated for between 200 and 2000 different random arrangements of the screws for values of  $l_l/d_{++} = 0.2, 0.4, 0.6, 0.78, 0.9$  and  $1.0$ , as well as for an entirely random distribution of screws. For each type of distribution simulations were performed using values of  $L$  from 7071 to 31423 (in arbitrary units) and the average increase in the energy of the system is calculated as up to seven 'long steps' are added successively. The variation of the number of screws and the size of the crystal gives sets of results from which the behaviour of the energy of the system may be extrapolated to the thermodynamic limit for each type of distribution.

At first it seemed that this simple method was sufficient to provide a reasonable picture of how a crystal surface disordered by dislocations behaves in the strong coupling limit. Unfortunately though, careful tests of the simulation revealed that the algorithm becomes inadequate for values of  $l_l/d_{++}$  close to 1. The problem is that the minimas in the energy become very shallow. Therefore when an extra 'long step' is added to the interface the relaxation algorithm frequently shifts the system to the vicinity of a different minima rather than pushing the system up the side of the well defined by the original minima. However, despite these difficulties the results from the simulations are still of some value because the breakdown in the algorithm is itself interesting as it may be associated with a change from the faceted to super-rough states.

#### 6.5.4 Results

The quantities that are of interest in the simulations are the changes in the surface energy density,  $\Delta E/L^2$ , when the crystal is tilted by an amount  $\theta/b$  (where  $\theta$  is the number of steps added divided by  $L$  and  $b$  is the crystal lattice parameter). According to the definition of a facet used here, a plot of  $\Delta E/L^2$  versus  $\theta/b$  should determine whether a crystal surface is faceted or not: if there is a cusp at the origin then the crystal is faceted, otherwise

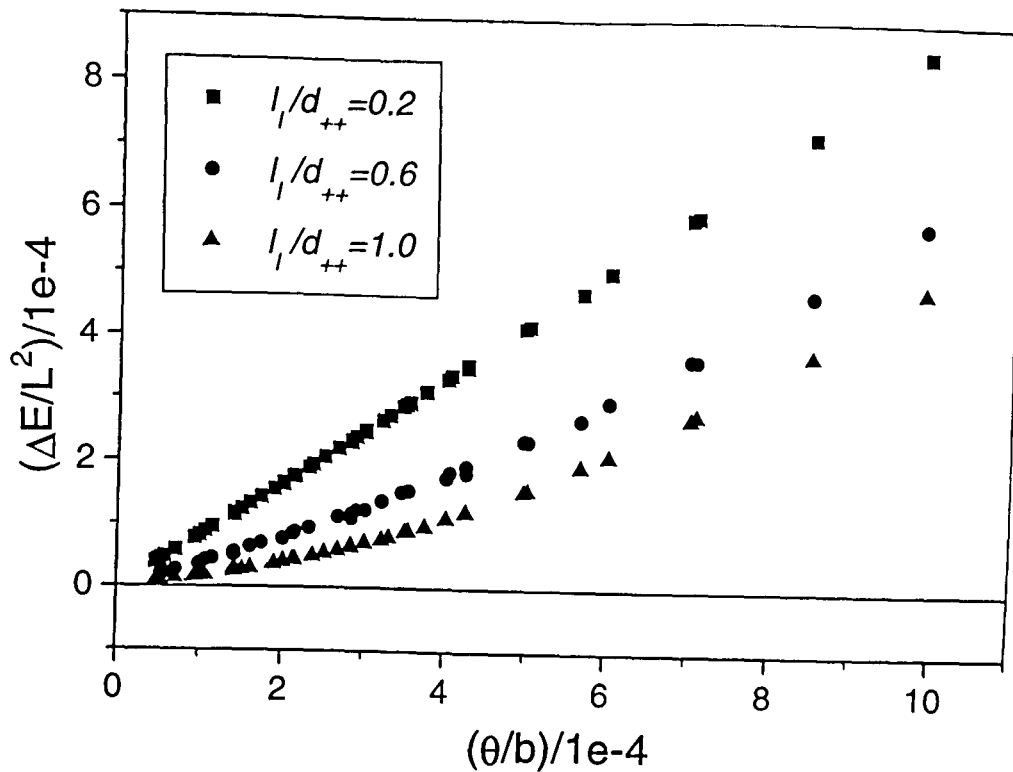


Figure 6.4 Variation of  $\Delta E/L^2$  with tilt angle for different distributions of screw dislocations defined by  $l_1/d_{++}$

it is super-rough.

A plot of  $\Delta E/L^2$  versus  $\theta/b$  for  $l_1/d_{++} = 0.2, 0.6$  and  $1.0$  combining the data from each value of  $L$  is shown in figure (6.4). At first sight it appears that the results collapse onto a single curve for each value of  $l_1/d_{++}$ . For small amounts of disorder ( $l_1/d_{++} = 0.2$  and  $0.6$ ) the behaviour is clearly predominantly linear, passing through the origin. In contrast, the plot for the largest value of disorder ( $l_1/d_{++} = 1.0$ ) is far from linear, although it still passes through the origin. However, since it is the region closest to the origin which is of interest, inspection is insufficient and an analytic analysis of the curves is required.

If the curves of  $\Delta E/L^2$  are assumed to have an analytic form then for small  $\theta$  they can be approximated by a power series in  $\theta$ :

$$\Delta E/L^2 = a_1\theta + a_2\theta^2 + a_3\theta^3 + a_4\theta^4 + \dots \quad (6.38)$$

For the data available the number of parameters required to obtain a good fit (which was defined by the value of the chi-squared divided by the degrees of freedom) increased from 2 to 4 with  $l_1/d_{++}$  varying from 0.2 to 1.0. Separate fits were performed for each value of  $L$  for each  $l_1/d_{++}$ . The purpose of fitting the sets of data from different sized crystals was to isolate the finite size effects which arise: both due to screws forming steps with the edges and the requirement that the centres of the screw pairs are placed at least a distance  $l_1/2$  away from any edge. In figure (6.5) the variation of the linear coefficient,  $a_1$ , with  $1/L$  is plotted for each value of  $l_1/d_{++}$ .

For  $l_1/d_{++} \leq 0.78$  the behaviour is clear: in each case the value of  $a_1$  increases linearly as  $1/L \rightarrow 0$ , the gradient being almost the same each time.

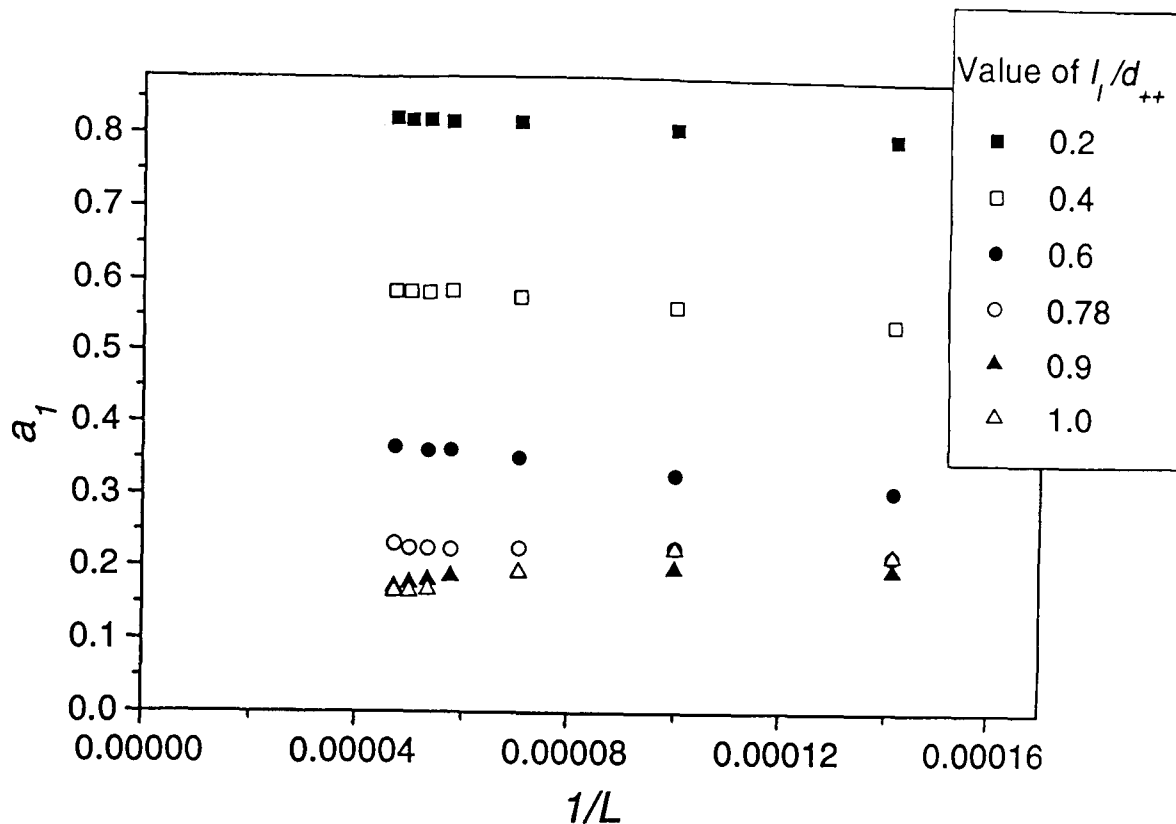


Figure 6.5 Variation of the linear coefficient,  $a_1$ , in the expansion of surface energy in powers of the tilt angle, with  $1/L$  for different distributions of screw dislocations defined by  $l_1/d_{++}$

This implies that these systems are all faceted as they each contain finite linear coefficients. In contrast, for larger values,  $l_1/d_{++} > 0.8$ , the value of  $a_1$  decreases with increasing  $L$ , although its exact behaviour in the limit  $1/L \rightarrow 0$  cannot be determined from the available data. This suggests that for values of  $l_1/d_{++}$  close to unity the linear coefficient may vanish in the thermodynamic limit, implying that under these circumstances the interface is super-rough. However, because the simulations were performed on such limited scales, the behaviour in the thermodynamic limit can only be conjectured. The safest conclusions to draw from these results are that for  $l_1/d_{++} \leq 0.78$ , the crystal surface is faceted, but for  $l_1/d_{++} > 0.8$  the algorithm used breaks down.

## 6.6 Conclusions and Discussion

The extension of the Nozières-Gallet theory of the roughening transition to include the effect of screw dislocations shows that the disorder can change the universality class of the phase transition. If the screw dislocations are distributed at random then instead of the roughening transition a super-roughening transition occurs instead. However, if the screw dislocations are distributed as closely spaced pairs then the interface still undergoes a roughening transition, but the critical point is shifted.

In the low temperature regime it is possible to define a facet, even in the presence of disorder, as any state for which there is a cusp in the surface energy density when the interface is tilted slightly. However, if the surface undergoes a super-roughening transition in the weak coupling limit then at

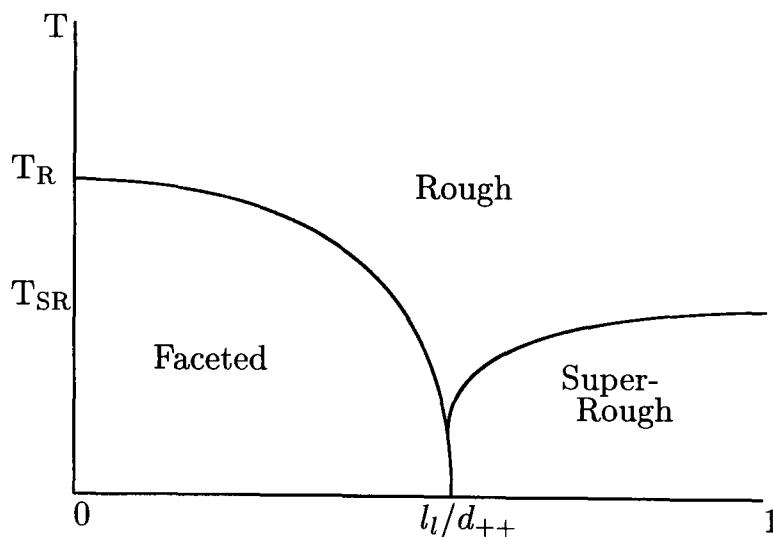


Figure 6.6 Schematic representation of the proposed phase diagram of a crystal surface which is disordered by screw dislocations.  $l_i/d_{++}$  represents the degree of disorder in the system,  $T_R$  and  $T_{SR}$  are the roughening and super-roughening temperatures respectively.

temperatures below the transition it must be in the super-rough state. This means that in the strong coupling regime there must be a critical level of disordering in the underlying crystal lattice at which a Mott-like transition occurs between the faceted and super-rough states.

These results suggest a phase diagram for the crystal surface of the general form illustrated in figure (6.6). The rough phase is the high temperature state of the system for all levels of disorder, whilst the low temperature phases for weak and strong disorder are faceted and super-rough respectively. Certain regions of the phase diagram have been modelled successfully: the far left side of the diagram represents the region described by the standard theory of the roughening transition and the right-hand side can be associated with the super-roughening transition. Part of the faceted-rough phase boundary for a crystal with a small amount of disorder in the crystal lattice has also been mapped when the disorder arises from screw dislocations [26]; in this case the transition point is shifted slightly.

The question of exactly when a Mott type transition occurs between the faceted and super-rough states remains open. In particular, the problem of how to work out the pairings between screw dislocations that lead to the ground state has not yet been solved.

---

## Chapter 7 New Dynamic Theory of Superfluid Films

---

This final chapter outlines the way in which the theory of Nozières and Gallet can be adapted to model the dynamics of superfluid films. The work is still at a relatively early stage, but preliminary results suggest that it may lead to an improved understanding of the experimental data.

As has been discussed in some detail already in this thesis, the current theories of superfluidity in thin films are insufficient to explain quantitatively the results of a variety of torsional oscillator experiments. The problem arises because there has not been a satisfactory theoretical framework in which to discuss the dynamics of these systems. The dynamics have always been tacked on in an essentially ad-hoc way to a static (that is, equilibrium) renormalization treatment. There are no recursion relations for the renormalization of the noise or a time dependent external drive. Furthermore, there is no obvious way of describing the effects of atomic layering in the film or disorder in the substrate, though both have been shown to affect the results of real experiments considerably. What is required is a renormalization procedure which has the dynamics built into it: just such a procedure was developed by Nozières and Gallet in the context of the roughening transition [19].

It has been appreciated for some time that the dynamic renormalization scheme of Nozières and Gallet is more systematic than any of the methods currently used to describe the dynamics of superfluid films [75]. Their scheme was extended to consider the effect of an harmonically varying overpressure on the crystal surface by Giorgini and Bowley [75], who came close to recognizing the application to superfluid films. They identified and calculated a ‘dielectric constant’ for the crystal system. However, they perceived an analogy between the two systems where in fact there is an identity. Using the Hubbard-Stratonovich transformation the duality of the two-dimensional Coulomb gas and sine-Gordon models can be proved and so an exact translation from the language of the roughening transition to that of superfluid films is possible [9]. Hence, a fully self-consistent dynamic renormalization scheme may be formulated for superfluid systems in which the noise and external oscillating field are renormalized and which may be extended to include the effects of disorder or discrete layering.

This chapter contains a description of preliminary work on the adaptation of the Nozières-Gallet scheme to superfluid systems. After a brief discussion of the details of the duality of the two models, the way in which the electric field can be ‘translated’ into the language of the sine-Gordon model is shown along with the derivation of its recursion relation. This is followed by details of how the dielectric function can be calculated. Some preliminary results using a simple calculational scheme based on the work of Giorgini and Bowley [75] are then presented. Next there is a description of some of the ways in which the basic model may be extended, in particular to take into account

the effects of disorder and discrete layering in the films. Finally there is a discussion of how the work outlined might be extended in the future in order to develop a comprehensive theory of the dynamics of superfluid films.

## 7.1 Comparison of Models

The duality of the two-dimensional Coulomb gas model, which is used to describe superfluid films, and the sine-Gordon model was discussed in chapter 2 and is demonstrated in appendix C. Each term in either of the models has a direct counterpart in the other one.

The starting point is the grand partition function for the two-dimensional Coulomb gas (which is used to describe superfluid films),

$$\mathcal{Z} = \sum_{N^+} \frac{1}{N^+!} \sum_{N^-} \frac{1}{N^-!} \prod_{\alpha=1}^{N^+} \int \frac{d^2\mathbf{r}_\alpha}{a^2} \prod_{\beta=1}^{N^-} \int \frac{d^2\mathbf{r}_\beta}{a^2} y^{N^+} y^{N^-} \exp\left(\frac{-\mathcal{H}_{CG}}{k_B T}\right), \quad (7.1)$$

where  $N^+$  and  $N^-$  are the number of positive and negative charges, and the Coulomb gas Hamiltonian is given by

$$\frac{\mathcal{H}_{CG}}{k_B T} = -\pi K \int \int_{|\mathbf{r}-\mathbf{r}'|>a} d^2\mathbf{r} d^2\mathbf{r}' n_v(\mathbf{r}) \ln\left(\frac{|\mathbf{r}-\mathbf{r}'|}{a}\right) n_v(\mathbf{r}'), \quad (7.2)$$

where  $n_v(\mathbf{r})$  is the density of unit charges at  $\mathbf{r}$ . The duality transformation allows the grand partition function to be rewritten in the form

$$\mathcal{Z} = C \int \mathcal{D}\phi(\mathbf{r}) \exp\left(-\int d^2\mathbf{r} \left(\frac{1}{8\pi^2 K} (\nabla\phi(\mathbf{r}))^2 - \frac{2y}{a^2} \cos\phi(\mathbf{r})\right)\right). \quad (7.3)$$

Comparing this with the Hamiltonian used to describe the roughening transition, discussed in chapter 5,

$$\mathcal{H}_R = \int d^2\mathbf{r} \left(\frac{\tilde{\gamma}(\nabla z(\mathbf{r}))^2}{2} - V_0 \cos\left(\frac{2\pi z(\mathbf{r})}{b}\right)\right), \quad (7.4)$$

it is apparent that the pinning potential may be associated with the fugacity, and the surface stiffness with the Kosterlitz parameter, using the relations:

$$z \Leftrightarrow \frac{b\phi}{2\pi}$$

$$V_0 \Leftrightarrow \frac{2yk_B T}{a^2}$$

and

$$\tilde{\gamma} \Leftrightarrow \frac{k_B T}{Kb^2}.$$

Furthermore, the minimum length scale in the Coulomb gas problem,  $a$ , can be identified with the lattice cutoff length in the sine-Gordon model,  $\Lambda_0^{-1}$ : in particular, they scale in exactly the same way.

These connections make obvious physical sense: it is clear that the fugacity and pinning potential should be associated as they both constitute the expansion parameter in the renormalization group treatment of the respective

models. It is also clear from the above identifications that the low temperature phase of one system must be related to the high temperature phase of the other and vice-versa. This observation becomes clear when it is noted that the low temperature phase of the crystal surface has a large value of the pinning potential where as the fugacity is high for superfluid systems in the high temperature limit.

The dynamics of the sine-Gordon model is usually obtained by the formulation of a Langevin equation. This standard technique, which provides a valid description of the dynamics of the sine-Gordon model, is assumed to still be applicable when that model is used as an abstract representation of the superfluid system.

The description of the duality transformation which is common in the literature [9] essentially stops at this point. The question of how an analogue of the electric field in the two-dimensional Coulomb gas could be calculated for crystal surfaces remains, nor is there any attempt to see how disorder in superfluid systems might manifest itself in the sine-Gordon picture. If the Nozières-Gallet approach is to be adapted to analyse superfluid systems then answers to these questions become essential. However, the technique needed to do so is clear: a Hamiltonian for the superfluid system containing the electric field is postulated and then converted into the language of the sine-Gordon model via an Hubbard-Stratonovich transformation.

## 7.2 The Electric Field Analogue

The effect of a macroscopic electric field on the two-dimensional Coulomb gas is analogous to the effect of an oscillating substrate on a superfluid film. As was discussed in chapter 3, the force on the charges due to the macroscopic electric field,  $\mathbf{E}$ , is equivalent to the Magnus force on vortices which arises from the relative motion between normal and superfluid components in the film,

$$q\mathbf{E}\cdot\mathbf{r} \Leftrightarrow 2\pi\frac{\rho_s^0\hbar}{m}\mathbf{r}\cdot(\mathbf{k}\times(\mathbf{v}_n-\mathbf{u}_s)). \quad (7.5)$$

Therefore, in order to analyse the dynamics of the vortices in the sine-Gordon model the Hubbard Stratonovich transformation performed must be generalized to include the quantity corresponding to the electric field in the Coulomb gas picture.

The electric field can be seen as leading to an external chemical potential in the context of the two-dimensional Coulomb gas model. In the absence of such a field, the fugacity is just a function of the chemical potential,  $y = \exp(-\mu/k_B T)$ , and the chemical potential arises simply from the core energy of the charge. This definition may be extended in a straightforward way to take account of the presence of an electric field,  $\mathbf{E}$  [95]. The generalized fugacity,  $y'$ , which includes the effect of  $\mathbf{E}$  is written as

$$y' = \exp\left(-\frac{\mu}{k_B T} + \frac{1}{k_B T} \int d^2\mathbf{r} n_v(\mathbf{r})\mathbf{E}\cdot\mathbf{r}\right) \quad (7.6)$$

$$= y \exp\left(\frac{1}{k_B T} \int d^2\mathbf{r} n_v(\mathbf{r})\mathbf{E}\cdot\mathbf{r}\right). \quad (7.7)$$

The electric field term is simplified by putting the charges in explicitly and writing

$$\int d^2\mathbf{r} n_v(\mathbf{r}) \mathbf{E} \cdot \mathbf{r} = \int d^2\mathbf{r} \mathbf{E} \cdot \mathbf{r} \left( \sum_{\alpha} \delta(\mathbf{r}_{\alpha} - \mathbf{r}) - \sum_{\beta} \delta(\mathbf{r}_{\beta} - \mathbf{r}) \right) \quad (7.8)$$

$$= \sum_{\alpha} \mathbf{E} \cdot \mathbf{r}_{\alpha} - \sum_{\beta} \mathbf{E} \cdot \mathbf{r}_{\beta}, \quad (7.9)$$

where the positions of the positive and negative charges are represented by the sets of coordinates  $\{\mathbf{r}_{\alpha}\}$  and  $\{\mathbf{r}_{\beta}\}$  respectively.

When the generalized fugacity, which includes the electric field term (eqn 7.7), is included in the grand partition function and the duality transformation is performed, the sine-Gordon partition function obtained has the modified form:

$$\mathcal{Z} = C \int \mathcal{D}\phi(\mathbf{r}) \exp \left( -\frac{1}{8\pi^2 K} \int d^2\mathbf{r} (\nabla\phi)^2 + \frac{2y}{a^2} \int d^2\mathbf{r} \cos \left( \phi - i \frac{\mathbf{E} \cdot \mathbf{r}}{k_B T} \right) \right). \quad (7.10)$$

The electric field gives rise to an extra term in the sinusoidal expression; also because the new term involves the dot product of the position, it specifies a special direction in the plane of  $\mathbf{r}$ . This is very similar to the way in which a vicinal surface is described in the context of the roughening transition [19]: in that setting an extra term of the form  $hx$  is included in the argument of the cosine, where  $h = \langle \partial z / \partial x \rangle$  quantifies the amount of tilt along the  $x$  direction. However, the presence of  $i = \sqrt{-1}$  in eqn (7.10) is rather disquieting, although it is an inevitable consequence of the Hubbard-Stratonovich transformation for any system of charges whose fugacities are not always identical [96].

Some light is shed on the possible meaning of the imaginary term in eqn (7.10) by Samuel [97, 54]. The auxiliary field can be seen as a kind of coarse grained Coulomb potential; however, it is  $i\phi$  rather than  $\phi$  which is identified with a charge density. If, as Samuel suggests, the auxiliary field is pure imaginary then the Hamiltonian containing the electric field makes perfect sense. In fact the presence of the  $i$  should make no difference to the analysis: here it will be assumed that the imaginary term leads to no unusual behaviour. Instead a simple calculation is made which can be compared with experiment: if the results are successful then it will be worth attempting a more rigorous derivation.

In order to obtain the dynamics in the presence of the electric field model A dynamics is assumed. Furthermore, in order to avoid divergences an upper length scale,  $L$ , must be imposed on the problem such that  $EL/k_B T \ll 1$ . In principle this should lead to an extra surface term in the equation of motion [97]. However, here it is assumed that the size of  $L$  can be chosen to be much greater than all other length scales, in particular the dynamic length scale. When this is the case the boundaries will have a negligible effect on the bulk of the film and so the surface term can be neglected.

When the fugacity and Kosterlitz parameter have been 'translated' into the language of the roughening transition. using the associations described

above, a Langevin equation of the form

$$\eta\dot{z} = \tilde{\gamma}\nabla^2 z - \frac{2\pi}{b}V_0 \sin\left(\frac{2\pi}{b}z - i\frac{\mathbf{E}\cdot\mathbf{r}}{k_B T}\right) + R, \quad (7.11)$$

is obtained. The simplest way of proceeding is to renormalize this equation up to first order in the magnitude of the electric field, leading to a non-trivial recursion relation for the electric field. This recursion relation can then be integrated to give the dynamic dielectric function. A higher order treatment would also be of interest, but is considerably more complex and so is not considered here in any detail.

### 7.3 Renormalization

The renormalization procedure adopted here is the second order dynamic method of Nozières and Gallet which was described in the context of the roughening transition in chapter 5 and so the same notation has been used.

If the Langevin equation for the system is rewritten in terms of the variable

$$z_e = z - i\frac{E(t)xb}{2\pi k_B T}, \quad (7.12)$$

and the electric field is assumed to be given by  $E(t) = E_0 e^{-i\omega t}$ , then it takes the new form

$$\eta\dot{z}_e + \eta\frac{\omega xb E_0}{2\pi k_B T} e^{-i\omega t} = \tilde{\gamma}\nabla^2 z_e - \frac{2\pi}{b}V_0 \sin\left(\frac{2\pi}{b}z_e\right) + R. \quad (7.13)$$

Thus a term proportional to  $\eta\omega x e^{-i\omega t}$  arising in the renormalization scheme will lead to a correction to  $E_0$ .

Proceeding in the style of Nozières and Gallet, the short wavelength Fourier components of  $z$  are summed over. It is found that there is no change in the behaviour of the term which is first order in the potential, as in the case when disorder was included in the model of the roughening transition. At second order the most relevant term has the form

$$\begin{aligned} \Delta^{(2)} &= \frac{4\pi^3 \bar{V}_0^2}{b^3} \int d^2 \boldsymbol{\rho} \int_0^\infty d\tau \chi_0(\boldsymbol{\rho}, \tau) 2n \delta g(\boldsymbol{\rho}, \tau) \\ &\times \sin\left(\frac{2\pi}{b}(\bar{z}' - \bar{z}) + \frac{iE_0 b}{2\pi k_B T} (xe^{-i\omega t} - x'e^{-i\omega(t-\tau)})\right), \end{aligned} \quad (7.14)$$

where  $\boldsymbol{\rho} = \mathbf{r} - \mathbf{r}'$ ,  $\tau = t - t'$  and  $n = \pi k_B T / \tilde{\gamma} b^2$ . It is the expansion of this term which leads to renormalization of  $\tilde{\gamma}$ ,  $\eta$  and the electric field.

The next step is to expand the harmonic term using the trick of splitting  $z$  into two parts, so that  $\bar{z} = z^{eq} + \xi$  where  $z^{eq}$  has an equilibrium distribution. Thus if the shorthand

$$\alpha = \frac{iE_0 b}{2\pi k_B T} (xe^{-i\omega t} - x'e^{-i\omega(t-\tau)}) \quad (7.15)$$

is adopted, then the expansion of the harmonic term to first order in  $\xi$  becomes,

$$\sin\left(\frac{2\pi}{b}(\bar{z}' - \bar{z}) + \alpha\right) = \frac{2\pi}{b}(\xi' - \xi) \cos(\alpha) \left\langle \cos\left(\frac{2\pi}{b}((z^{eq})' - z^{eq})\right) \right\rangle + \sin(\alpha) \left\langle \cos\left(\frac{2\pi}{b}((z^{eq})' - z^{eq})\right) \right\rangle. \quad (7.16)$$

The first term in this expression is familiar, the difference  $(\xi' - \xi)$  is expanded as a Taylor series,

$$(\xi' - \xi) = -\tau \frac{\partial \xi}{\partial t} - \rho_i \frac{\partial \xi}{\partial r_i} + \frac{1}{2} \rho_i \rho_j \frac{\partial^2 \xi}{\partial r_i \partial r_j} + \dots \quad (7.17)$$

and so leads to corrections to the surface stiffness and the mobility from the coefficients of the  $\partial \xi / \partial t$  and  $\partial^2 \xi / \partial r_i \partial r_j$  terms respectively. These take almost the same form as in the Nozières-Gallet treatment except for the presence of the extra  $\cos \alpha$ :

$$d\tilde{\gamma}_{ij} = \frac{8\pi^4 \bar{V}_0^2 n dl}{b^4} \int d^2 \rho \rho_i \rho_j \int_0^\infty d\tau \chi_0(\rho, \tau) e^{-2n\bar{h}(\rho, \tau)} J_0(\Lambda \rho) e^{-\tilde{\gamma} \Lambda^2 \tau / \eta} \cos \alpha \quad (7.18)$$

$$d\eta = \frac{16\pi^4 \bar{V}_0^2 n dl}{b^4} \int d^2 \rho \int_0^\infty d\tau \tau \chi_0(\rho, \tau) e^{-2n\bar{h}(\rho, \tau)} J_0(\Lambda \rho) e^{-\tilde{\gamma} \Lambda^2 \tau / \eta} \cos \alpha. \quad (7.19)$$

The surface stiffness is generalized to take account of any possible anisotropy, taking the form:  $\tilde{\gamma}_{ij}$  with  $i, j = x, y$ . Usually when the angular integrals are carried out the off-diagonal elements of the stiffness matrix vanish and the sum of the diagonal elements takes a value which does not depend on the choice of axes. However, if there is any angular dependence in the  $\cos \alpha$  term then this will no longer be the case, implying that the electric field breaks the rotational symmetry in the  $xy$  plane. In the isotropic case terms in  $\partial \xi / \partial r_i$  vanish, but again if the rotational symmetry in the  $xy$  plane is broken by the  $\cos \alpha$  term then they will be finite and lead to an extra parameter in the renormalization scheme. Just such an anisotropy arises in the renormalization of the vicinal crystal surface. In terms of superfluid films such an anisotropy would lead to a generalization of the Kosterlitz parameter to a tensorial form and physically it would imply differing longitudinal and transverse momentum susceptibilities in the superfluid [9].

The second term in the harmonic expansion (eqn 7.16) must give rise to a correction to the electric field  $E_0$ , though how it does so is not immediately obvious. Labelling the part of  $\Delta^{(2)}$  which contains this term as  $Y$  leads to the expression

$$Y = \frac{16\pi^4 \bar{V}_0^2 n dl}{b^4} \int d^2 \rho \int_0^\infty d\tau \chi_0(\rho, \tau) e^{-2n\bar{h}(\rho, \tau)} J_0(\Lambda \rho) e^{\tilde{\gamma} \Lambda^2 \tau / \eta} \sin \alpha. \quad (7.20)$$

To obtain the linear response the term  $\sin \alpha$  must be simplified to include only terms up to and including linear order in  $E_0$ . Using the notation  $\rho_x =$

$x' - x$ ,

$$\alpha = \frac{iE_0 b}{2\pi k_B T} \left( x e^{-i\omega t} (1 - e^{i\omega\tau}) - \rho_x e^{-i\omega(t-\tau)} \right) \quad (7.21)$$

so that the sinusoidal term may be expanded as

$$\begin{aligned} \sin \alpha &= \sin \left( iX x e^{-i\omega t} (1 - e^{i\omega\tau}) \right) \cos \left( -iX \rho_x e^{-i\omega(t-\tau)} \right) \\ &\quad + \cos \left( iX x e^{-i\omega t} (1 - e^{i\omega\tau}) \right) \sin \left( -iX \rho_x e^{-i\omega(t-\tau)} \right), \end{aligned}$$

where  $X = E_0 b / 2\pi k_B T$ . However, when the angular integration in eqn (7.20) is performed the second term in the expansion of  $\sin \alpha$  vanishes because  $\rho_x = \rho \cos \theta$  and

$$\int_0^{2\pi} d\theta \sin(z \cos \theta) \equiv 0, \quad \forall z. \quad (7.22)$$

Thus to first order in  $E_0$ ,

$$\sin \alpha = \frac{iE_0 b}{2\pi k_B T} x e^{-i\omega t} (1 - e^{i\omega\tau}) + O(E_0^3). \quad (7.23)$$

The extra correction term arising at second order in the pinning potential and linear order in the electric field is given by

$$\begin{aligned} Y &= \frac{iE_0 b x e^{-i\omega t} 16\pi^4 \bar{V}_0^2 n dl}{2\pi k_B T b^4} \int d^2 \rho \int_0^\infty d\tau \chi_0(\rho, \tau) e^{-2n\bar{h}(\rho, \tau)} J_0(\Lambda\rho) e^{\tilde{\gamma}\Lambda^2\tau/\eta} \\ &\quad \times (1 - e^{i\omega\tau}). \end{aligned} \quad (7.24)$$

By comparing this expression with the electric field term in eqn (7.13), it is clear that

$$\begin{aligned} dE_0 &= -i \frac{16\pi^4 \bar{V}_0^2 n E_0 dl}{\eta b^4} \int d^2 \rho \int_0^\infty d\tau \chi_0(\rho, \tau) e^{-2n\bar{h}(\rho, \tau)} J_0(\Lambda\rho) e^{\tilde{\gamma}\Lambda^2\tau/\eta} \\ &\quad \times \frac{1}{\omega} (1 - e^{i\omega\tau}). \end{aligned} \quad (7.25)$$

Thus on making the change of variables  $\tilde{\rho} = \rho\Lambda$  and  $\kappa = \tilde{\gamma}\tau/\eta\rho^2$ , this becomes

$$\begin{aligned} dE_0 &= \frac{32\pi^5 \bar{V}_0^2 n E_0 dl}{b^4 \tilde{\gamma} \Lambda^4} \int d\tilde{\rho} \tilde{\rho}^3 \int_0^\infty d\kappa \chi_0(\tilde{\rho}, \kappa) e^{-2n\bar{h}(\tilde{\rho}, \kappa)} J_0(\tilde{\rho}) e^{-\tilde{\rho}^2 \kappa} \\ &\quad \times \frac{i}{\omega} (e^{i\omega\tau} - 1). \end{aligned} \quad (7.26)$$

If substitutions are now made for the kernel,  $\chi_0 = e^{-1/4\kappa} / 4\pi\tilde{\gamma}\tau$ , and for the pinning potential,  $U = V_0/\Lambda^2$ , then eqn (7.26) can be rewritten as

$$\begin{aligned} \frac{d \ln E_0}{dl} &= \frac{8\pi^4 U^2 n}{b^4 \tilde{\gamma}^2} \int_0^\infty d\tilde{\rho} \tilde{\rho}^3 \int_0^\infty d\kappa e^{-1/4\kappa} e^{-2n\bar{h}(\tilde{\rho}, \kappa)} J_0(\tilde{\rho}) e^{-\tilde{\rho}^2 \kappa} \\ &\quad \times \frac{i}{\tau\omega} (e^{i\omega\tau} - 1). \end{aligned} \quad (7.27)$$

Notice that the distinctions between  $V_0^2$  and  $\bar{V}_0^2$  as well as  $\eta$  and  $\bar{\eta}$  have been neglected in the change of variables, in each case using the exact expression

would lead to a correction which is both proportional to  $dl^2$  or higher order and fourth order in the pinning potential, hence their omission is quite acceptable in the context of this second order scheme.

To obtain recursion relations for  $\tilde{\gamma}$  and  $\eta$  that include the effects of the electric field up to just linear order, an expansion of the term in  $\cos \alpha$  similar to that employed for the  $\sin \alpha$  term is required. Once this has been done, the recursion relations are easily obtained by substituting the linearised expression into eqns (7.18) and (7.19). A straightforward expansion of the cosine term gives

$$\begin{aligned} \cos \alpha = & \cos \left( iXx e^{-i\omega t} (1 - e^{i\omega\tau}) \right) \cos \left( -iX\rho_x e^{-i\omega(t-\tau)} \right) \\ & - \sin \left( iXx e^{-i\omega t} (1 - e^{i\omega\tau}) \right) \sin \left( -iX\rho_x e^{-i\omega(t-\tau)} \right), \end{aligned} \quad (7.28)$$

where again  $X = E_0 b / 2\pi k_B T$ . Clearly there are no terms of linear order in the electric field present,

$$\begin{aligned} \cos \alpha = & 1 + \frac{1}{2} \left( \frac{E_0 b e^{-i\omega t}}{2\pi k_B T} \right)^2 \left( x^2 (1 - e^{i\omega\tau})^2 + \rho_x^2 e^{2i\omega\tau} \right) \\ & - \left( \frac{E_0 b e^{i\omega t}}{2\pi k_B T} \right)^2 \left( x\rho_x (1 - e^{i\omega\tau}) e^{i\omega\tau} \right) + O(E_0^4). \end{aligned} \quad (7.29)$$

Thus in the linear field approximation the renormalization equations for  $\tilde{\gamma}$  and  $\eta$  have exactly the same form as in the case of zero field so the system can be treated as isotropic. However, if instead an expansion to second order were performed then an expression containing the quantity  $\rho_x$  would be obtained, which would lead to anisotropy in the surface stiffness as discussed above.

The results derived in the second order treatment of Nozières and Gallet for  $U$ ,  $\tilde{\gamma}$  and  $\eta$ , along with the relation for the electric field obtained above, form a complete set of recursion relations for the system:

$$\frac{dU}{dl} = (2 - n) U \quad (7.30)$$

$$\frac{d\tilde{\gamma}}{dl} = \frac{2\pi^4 U^2}{\tilde{\gamma} b^4} A(n) \quad (7.31)$$

$$\frac{d\eta}{dl} = \frac{8\pi^4 \eta U^2}{\tilde{\gamma}^2 b^4} B(n) \quad (7.32)$$

and

$$\frac{d \ln E_0}{dl} = -\frac{8\pi^4 U^2}{\tilde{\gamma}^2 b^4} C(n, \omega\tau). \quad (7.33)$$

The functions  $A(n)$ ,  $B(n)$  and  $C(n, \omega\tau)$  are given by the relations

$$A(n) = n \int_0^\infty d\tilde{\rho} \tilde{\rho}^3 \int_0^\infty \frac{d\kappa}{\kappa} e^{-1/4\kappa} e^{-2n\tilde{h}} J_0(\tilde{\rho}) e^{-\tilde{\rho}^2 \kappa} \quad (7.34)$$

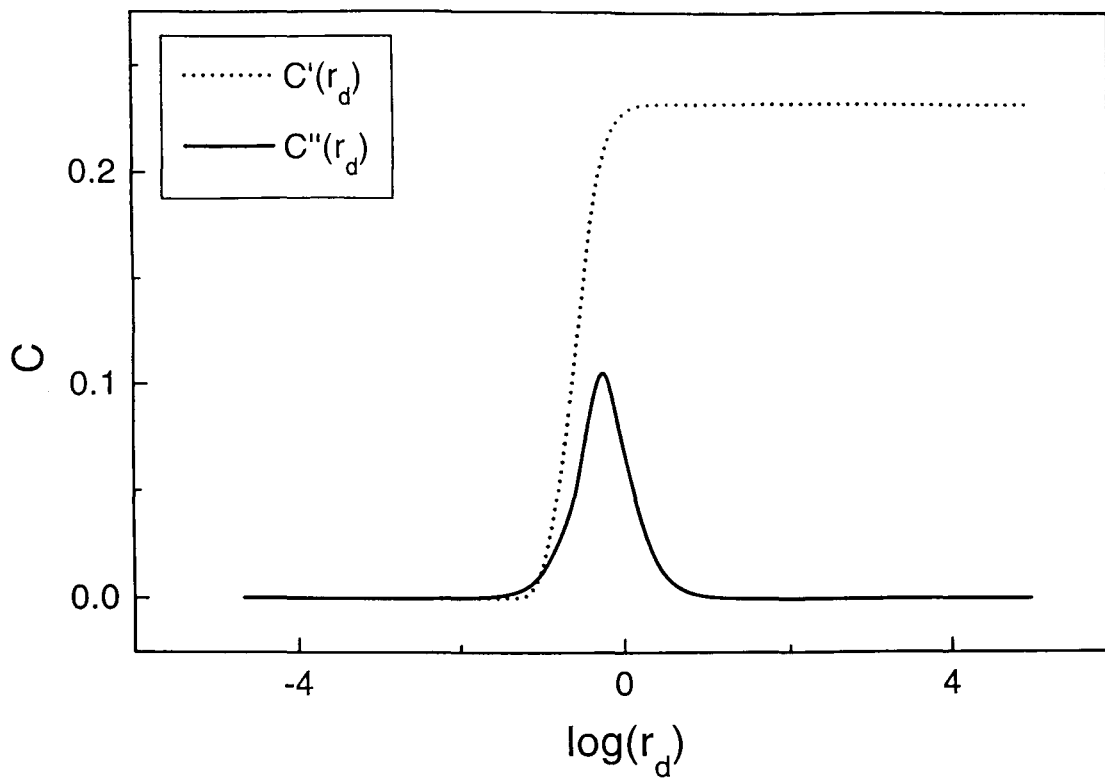


Figure 7.1 The variation of functions  $C'(n, r_d)$  and  $C''(n, r_d)$  with  $r_d$  for the case  $n = 2$

$$B(n) = n \int_0^\infty d\tilde{\rho} \tilde{\rho}^3 \int_0^\infty d\kappa e^{-1/4\kappa} e^{-2n\bar{h}} J_0(\tilde{\rho}) e^{-\tilde{\rho}^2 \kappa} \quad (7.35)$$

and

$$C(n, \omega\tau) = -in \int_0^\infty d\tilde{\rho} \tilde{\rho}^3 \int_0^\infty d\kappa e^{-1/4\kappa} e^{-2n\bar{h}} J_0(\tilde{\rho}) e^{-\tilde{\rho}^2 \kappa} \frac{(e^{i\omega\tau} - 1)}{\omega\tau}. \quad (7.36)$$

Making the change of variables  $\tau = \kappa \rho^2 \eta / \tilde{\gamma}$ , and introducing the quantity  $r_d = \Lambda (\tilde{\gamma} / \eta \omega)^{1/2}$ , equal to the ratio of the 'diffusion' length and  $\Lambda^{-1}$ , the  $C$  coefficient can be split into its real and imaginary parts,  $C'$  and  $C''$  respectively:

$$C'(n, r_d) = nr_d^2 \int_0^\infty d\tilde{\rho} \tilde{\rho} \int_0^\infty \frac{d\kappa}{\kappa} e^{-1/4\kappa} e^{-2n\bar{h}} J_0(\tilde{\rho}) e^{-\tilde{\rho}^2 \kappa} \sin\left(\frac{\tilde{\rho}^2 \kappa}{r_d^2}\right) \quad (7.37)$$

and

$$C''(n, r_d) = 2nr_d^2 \int_0^\infty d\tilde{\rho} \tilde{\rho} \int_0^\infty \frac{d\kappa}{\kappa} e^{-1/4\kappa} e^{-2n\bar{h}} J_0(\tilde{\rho}) e^{-\tilde{\rho}^2 \kappa} \sin^2\left(\frac{\tilde{\rho}^2 \kappa}{2r_d^2}\right). \quad (7.38)$$

These expressions have exactly the same form as those derived by Giorgini and Bowley who considered the response of a crystal interface to an harmonic over pressure. The behaviour of the  $C$  functions is readily investigated by numerical integration. The variation of  $C'(n, r_d)$  with  $r_d$  is very close to that of a step function: it increases rapidly from zero for small  $r_d$ , to a constant value of 0.246 at  $r_d \sim 0.5$ , for  $n = 1$ . However,  $C'(n, r_d)$  varies only slightly

with  $n$ , the height of the step varies from 0.246 for  $n = 1$ , to a value of 0.195 when  $n = 3$ . In contrast the function  $C''(n, r_d)$  takes the form of a sharp peak around the point  $r_d \sim 0.5$ , and has a value of zero elsewhere. The effect of variation in  $n$  is to modulate the value of the peak, but the change is only of order 10%. The behaviour of  $C'(n, r_d)$  and  $C''(n, r_d)$  for  $n = 2$  is shown in figure (7.1).

The recursion relations are readily 'translated' into the language of superfluid films that was used in chapters 3 and 4:

$$\frac{dy}{dl} = y(2 - \pi K) \quad (7.39)$$

$$\frac{dK^{-1}}{dl} = 4\pi^3 y^2 [2\pi K A(\pi K)] \quad (7.40)$$

$$\frac{d \ln \eta}{dl} = 32\pi^4 y^2 K^2 B(\pi K) \quad (7.41)$$

$$\frac{d \ln E_0}{dl} = -32\pi^4 y^2 K^2 C(\pi K, r_d). \quad (7.42)$$

Eqns (7.41) and (7.42) do not have counterparts in the static treatment of Kosterlitz which was described in chapter 2. However, eqns (7.39) and (7.40) do arise in Kosterlitz's scheme, though not in exactly the same form: the factor in the square brackets in eqn (7.40) is simply equal to one in Kosterlitz's work [1]. A value of one is close, but not identical, to the value of  $2\pi K A(\pi K)$  at the transition, which is 1.56.

### 7.3.1 Calculation of the Dielectric Function

The dielectric function is, in principle, obtained by simply integrating the recursion relation for the electric field

$$\ln \left( \frac{E_0(l = \infty)}{E_0(l = 0)} \right) = - \int_0^\infty dl \frac{8\pi^4 U(l)^2}{\tilde{\gamma}(l)^2 b^4} C(n, r_d), \quad (7.43)$$

hence

$$\varepsilon(\omega)^{-1} = \left( \frac{E_0(l = \infty)}{E_0(l = 0)} \right) = \exp \left( - \int_0^\infty dl \frac{8\pi^4 U(l)^2}{\tilde{\gamma}(l)^2 b^4} C(n, r_d) \right) \quad (7.44)$$

or, explicitly in the language of superfluid films,

$$\varepsilon(\omega)^{-1} = \exp \left( - \int_0^\infty dl \left( 32\pi^4 y(l)^2 K(l)^2 C(\pi K(l), r_d) \right) \right). \quad (7.45)$$

However, great care needs to be taken to ensure that the assumptions on which the derivation of the recursion relations are based do not become invalid. The most serious problem is that an increase in the magnitude of the coupling,  $U$ , as  $l \rightarrow \infty$  will make the weak coupling approximation invalid.

This question was considered by Giorgini and Bowley in their analysis of the mathematically identical problem of the roughening transition in the presence of an external harmonic drive. They were concerned with the renormalization of the part of the interface velocity fluctuating at the same frequency

as the external drive,  $u_0(\omega)$ . In their treatment they derive an expression which they identified as a dielectric function,

$$\varepsilon(\omega)^{-1} = \left( \frac{u_0(l = \infty)}{u_0(l = 0)} \right) = \exp \left( - \int_0^\infty dl \frac{8\pi^4 U(l)^2}{\tilde{\gamma}(l)^2 b^4} C(n, r_d) \right). \quad (7.46)$$

Their expression for the renormalization of the interface velocity is identical to that derived here for the renormalization of the electric field.

In an approach very similar to that of AHNS, Giorgini and Bowley calculate the dielectric function as a combination of two parts: a term from the short wavelength fluctuations, which is obtained via the renormalization approach, and a second term describing the long wavelength behaviour which is dominated by the pinning potential. In terms of the roughening transition this description is valid in the region just below the transition where the pinning potential is finite on a macroscopic scale. This corresponds to the region just above the superfluid transition in thin Helium films, which is exactly what is probed by torsional oscillator experiments.

To model the strong coupling regime Giorgini and Bowley use the simplest possible ansatz. They solve the equation of motion for the surface assuming that all displacements of the interface are small in this regime. They expand in terms of the displacement, retaining just the leading term. Then they use this result to calculate a contribution to the dielectric function of the system in the strong coupling limit which is added to the contribution arising from the weak coupling regime (obtained from renormalization). The crossover between the two contributions is not well defined in the theory and suffers from the same problems as the cut-off introduced by AHNS between bound and free vortices; it is assumed to be related to the correlation length of the system, but is in practice an adjustable parameter.

It is now recognized that the calculation of Giorgini and Bowley is unsatisfactory, both because of the imprecision it leads to in the crossover region and also because of the crude nature of the approximations it involves. A more satisfactory technique would use a renormalization group approach: either by obtaining recursion relations which are explicitly valid in the strong coupling regime, or by developing a renormalization scheme which remains valid over the whole range of integration, similar to that described in chapter 4.

However, in order to perform a preliminary calculation of the response of a superfluid film using the dynamic approach, the method of Giorgini and Bowley is sufficient. Therefore the expression for the dielectric function given above (eqn 7.44) is modified: the integration is performed up to a finite cutoff,  $l_c$ , and a separate term from the strong coupling regime is then added on. This strong coupling contribution is obtained from a solution in the long wavelength limit of the equation of motion for small displacements, which has the form

$$\eta \dot{z}_e = \tilde{\gamma} \nabla^2 z_e - \left( \frac{2\pi}{b} \right)^2 V_0 z_e - \eta \frac{\omega x b E_0}{2\pi k_B T} e^{-i\omega t} + R. \quad (7.47)$$

If the solution is further restricted to include only the component varying at the same frequency as the external field, then it is found that the expression for the dielectric function can be written as

$$\ln(\varepsilon(\omega)) = \int_0^{l_c} dl \frac{8\pi^4 U(l)^2}{\tilde{\gamma}(l)^2 b^4} C(n, r_d) + \ln \left( 1 + i \frac{4\pi^2 V_0(l_c)}{\omega \eta(l_c) b^2} \right). \quad (7.48)$$

The notation is considerably simplified by making the following change of variables

$$X \equiv \frac{2\tilde{\gamma}b^2}{\pi k_B T},$$

$$Y \equiv \frac{4\pi U}{k_B T}.$$

The equation for the dielectric function now takes the form

$$\ln(\varepsilon(\omega)) = \int_0^{l_c} dl \frac{2Y(l)^2}{X(l)^2} C(2/X, r_d) + \ln \left( 1 + i \frac{2Y(l_c)}{X(l_c)} r_d^2(l_c) \right), \quad (7.49)$$

with the real and imaginary parts of the coefficient  $C$  given by eqns (7.37) and (7.38) above, respectively. An important advantage of the new variables is that they can be related directly to the microscopic parameters of the superfluid:  $X \Leftrightarrow 2/\pi K$  and  $Y \Leftrightarrow 8\pi y$ . In terms of these parameters, the diffusion length is

$$r_d(l) = \lambda e^{-l} \frac{X^{1/2}(l)}{\eta^{1/2}} \quad (7.50)$$

where

$$\lambda = \sqrt{\frac{\pi k_B T \Lambda_0^2}{2b^2 \omega}}. \quad (7.51)$$

In order to carry out a calculation of the dielectric function the initial values of various parameters need to be specified. The values of  $X$  and  $Y$  require no special tuning, they are chosen as follows:  $Y$  must be much less than  $4\pi$  and  $X$  is varied to sweep through the transition. The initial value of  $\eta$  is not determined by the theory at present and is essentially free, as is that of the parameter  $\lambda$ . Finally the value of  $l_c$  is not well defined, as is usual when an approximate cross-over technique like this is employed.

### 7.3.2 Preliminary Results

The results from a simple calculation of the dielectric function using the dynamic renormalization group method and the cross-over technique outlined above is shown in figure (7.2). Following Giorgini and Bowley, the value of  $X(0)$  was varied from 0.71 to 0.91, sweeping through the transition and the value of  $Y(0)$  is defined by the relation

$$Y(0) = \frac{.58 \times X(0)}{.6301} \quad (7.52)$$

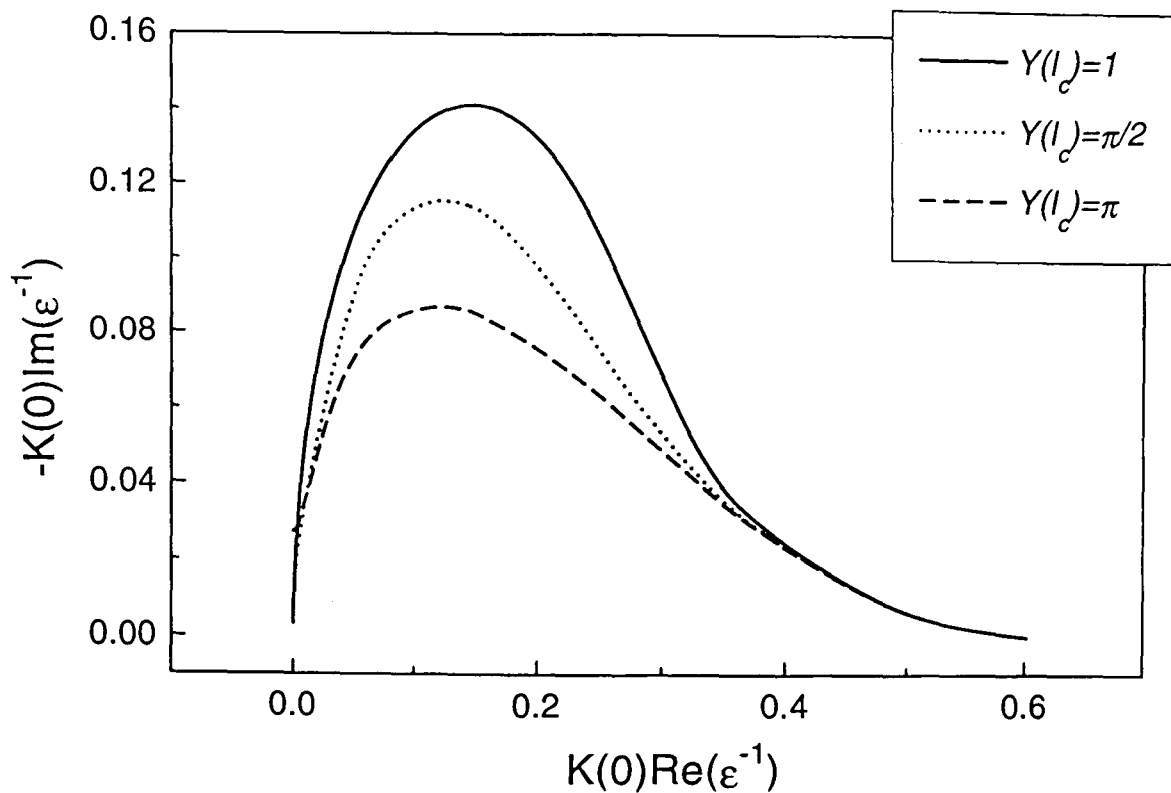


Figure 7.2 Parametric plot of the dynamic dielectric function for superfluid films for different values of the cut-off parameter  $l_c$

The values of the three adjustable parameters were also assigned using the values suggested by Giorgini and Bowley. The assumption is that the results should be essentially insensitive to the values used:  $\eta(0) = X(0)\lambda^2/(4 \times 10^6)$  with  $\lambda = 1.76 \times 10^5$ . The value of  $l_c$  is defined by the value of  $Y$  at which renormalization is stopped. Since it is known that variation in this cut-off leads to considerable differences in the results obtained, the calculation was repeated for a series of different values from  $Y(l_c) = 1$  to  $Y(l_c) = 4\pi$ . From figure (7.2) it is obvious that there is considerable variation in the dielectric function for different values of  $l_c$ . This is probably a result of imprecision in the crossover procedure rather than of any physical significance.

The numerical routines used to integrate the recursion relations are not yet efficient enough to make the calculation routine. The values of the parameters were kept the same as those of Giorgini and Bowley to allow the numerical methods to be checked, rather than for any physical reasons. In the future the numerical methods will be refined so that the dielectric function can be calculated for a whole range of initial conditions.

It was found that except for values of  $l_c$  such that  $Y(l_c) \geq \pi$ , the dominant contribution to  $\text{Im}(\epsilon(\omega)^{-1})$  comes from the region in which the renormalization group approach breaks down. At present the calculation in this regime is the simplest possible and so it is likely that a more sophisticated approach will alter the results significantly.

Despite the lack of available data, it is clear that the results from this method leads to parametric curves of the dielectric function with a shape very similar to those measured by McQueeney in torsional oscillator experiments. Figure (7.3) shows a comparison of the theoretical curve for  $Y(l_c) = 1$  with a subset

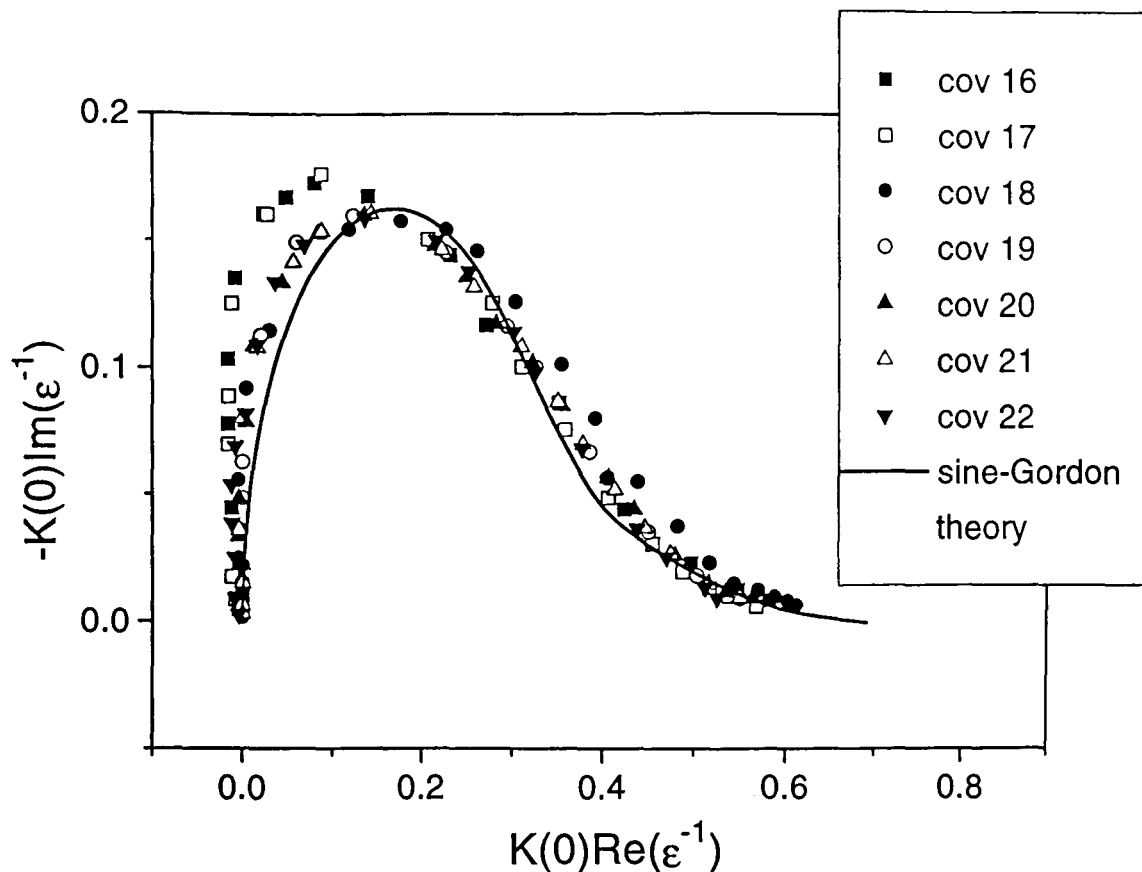


Figure 7.3 Comparison of the sine-Gordon theory for  $Y(l_c) = 1$  with some of the data from McQueeney's thesis. In order to obtain the fit the theoretical curve has been scaled up by 15%.

of the data from McQueeney's thesis. Unfortunately the theoretical curve had to be scaled up by 15% in order to obtain the fit: a procedure which is certainly unsatisfactory. However, the shape of the theoretical curve is much closer to that of experiment than the refined theory, particularly at the left hand side. The naïve comparison made at this stage is in effect a two parameter fit, but the agreement is as good, if not better, than any of the other dynamic theories of superfluid films. Indeed it seems likely that the fit will improve if the theory can be extended to include disorder and non-linear effects.

## 7.4 Variations on the Theme

The dynamic sine-Gordon theory presented here has the advantage that it is readily extended to include other physical effects which may be relevant. This section outlines the way in which the theory might be adapted to include either the effects of disorder in the substrate or atomic layering in the film. This work is in a preliminary stage and the approaches described here are not the only ones available: they are presented here simply as examples of how the theory can be generalized.

### 7.4.1 Inclusion of Disorder

One way in which the dynamic sine-Gordon theory can be extended to include effects of disorder was described in chapter 6. In the context of the roughening transition disorder is modelled by an additional phase in the harmonic term. However, it is not obvious what this extra phase would

correspond to in the superfluid film picture. A more physically appealing approach would be to start from the two-dimensional Coulomb gas model and introduce a spatial variation in the fugacity of the charges. The variation in the fugacity could be used to model the pinning of vortices on inhomogeneities in the substrate.

Consider a chemical potential for a vortex which is generalised to contain an additional spatially dependent term,  $\mu_s(\mathbf{r}) = \mu + h(\mathbf{r})$ , so that the fugacity is now

$$y(\mathbf{r}) = \exp(-\mu_s(\mathbf{r})/k_B T) \quad (7.53)$$

$$= \exp(-\mu/k_B T) \exp(-h(\mathbf{r})/k_B T). \quad (7.54)$$

When the Hubbard-Stratonovich transformation is applied this leads to a partition function in the sine-Gordon picture of the form

$$\mathcal{Z} = C \int \mathcal{D}\phi(\mathbf{r}) \exp\left(-\int d^2\mathbf{r} \left(\frac{1}{8\pi^2 K} (\nabla\phi(\mathbf{r}))^2 - \frac{2y(\mathbf{r})}{a^2} \cos\phi(\mathbf{r})\right)\right). \quad (7.55)$$

The spatial dependence of the fugacity is transferred to the pinning potential of the sine-Gordon model.

The disorder in this model is then characterized by a correlation function for the function  $h(\mathbf{r})$ , leading to a new length scale in the problem. The exact form that the correlation function should take has not been considered in any detail yet, but should certainly be strongly dependent on the details of substrate morphology.

#### 7.4.2 Coupled Layers

The results of torsional oscillator experiments have shown that the number of atomic layers in a film affect its dynamics in a systematic way. It has been suggested that when a superfluid film consists of more than one fluid layer the coupling between the layers is imperfect and depends in some way on the degree of completion of the uppermost layer [65]. In principle, this can be tested using the methods of the sine-Gordon theory described above. The first step is to postulate a Hamiltonian for a set of weakly interacting layers; the Hubbard-Stratonovich transformation is then applied to give a set of coupled sine-Gordon equations which can then be renormalized and so the dynamic response obtained.

The simplest possible Hamiltonian for a system of two weakly coupled layers consists of a two-dimensional Coulomb gas model generalized to include two species of charged particles which interact with both themselves and each other logarithmically, but with different strengths in each case. The idea is that each species should represent the vortices in one or other of the layers: vortices in the same layer interact with each more strongly than vortices in different layers. The most convenient way of doing this is to generalize the Kosterlitz parameter,  $K = \rho_S \hbar^2 / m^2 k_B T$ , so that it describes both the coupling within each layer and between the layers. This is done by writing it as a matrix,

$$\underline{K} = \begin{pmatrix} K_1 & X\sqrt{K_1 K_2} \\ X\sqrt{K_1 K_2} & K_2 \end{pmatrix} \quad (7.56)$$

where  $K_1$  and  $K_2$  are proportional to the superfluid densities in the first and second layers respectively and the strength of the interlayer coupling is given by the new parameter  $X$ . The Hamiltonian for the layered system is then

$$\frac{\mathcal{H}}{k_B T} = - \sum_{ij} \frac{\pi K_{ij}}{A} \int \int_{|\mathbf{r}-\mathbf{r}'|>a} d^2\mathbf{r} d^2\mathbf{r}' n_v^i(\mathbf{r}) \ln \left( \frac{|\mathbf{r}-\mathbf{r}'|}{a} \right) n_v^j(\mathbf{r}'), \quad (7.57)$$

where  $A$  is a constant and the summation runs over all the vortices in both layers (labelled by  $i$  and  $j$  respectively).

The algebra is considerably more complicated than in the single layer model and so the details of the calculation are not given here, but in appendix D. The final result is a pair of coupled sine-Gordon equations which may then be renormalized. The new feature is that the coupling between layers,  $X$ , will also be renormalized: when it scales to infinity the equations will collapse to those of a single layer, but when  $X$  remains finite, or goes to zero, the behaviour of the system will be substantially altered.

Although the model of coupled layers outlined here is very simple, it is by no means the only possible model of the system. In particular, it is possible to formulate a model in which the strength of the interaction between the layers is given by an harmonic Josephson coupling term. Further work will be required to determine whether there is a difference in the physics predicted by different models of layering and which of them provides the best picture of the effects observed in experiment.

## 7.5 Conclusions and Discussion

The theory presented in this chapter is a synthesis of the two principal areas of work in this thesis: the dynamic behaviour of superfluid films and the roughening transition of crystal surfaces. The dynamic renormalization group theory of the sine-Gordon model developed by Nozières and Gallet provides the basis of a more natural theory of superfluid film dynamics than the phenomenological models of AHNS and Minnhagen. Furthermore, it is possible to expand the sine-Gordon model to include the effects of disorder in the substrate or the behaviour of two weakly coupled atomic layers of superfluid. Preliminary results suggest that this new theoretical approach is likely to lead to improved agreement with experiment. However, before any conclusions can be drawn with certainty a good deal of further work will need to be done.

The work described in this chapter is simply an outline. In fact a well defined programme of work remains. The first step will be to provide a more rigorous derivation of the equation of motion that was assumed here. Improved numerical methods would also be very helpful as they would allow the dependence of the dielectric function on the various parameters to be determined. Next a more sophisticated approximation for the strong coupling regime needs to be developed. The most natural way of doing this would be to renormalize the equation of motion in the strong coupling regime. Linearising in the displacement leads to a linear equation which can be renormalized without further approximation. However, an expansion in some parameter

related to  $1/V_0$  would be more generally valid, though the renormalization calculation would now be non-trivial. An alternative scheme could be based on an extension of the Nozières-Gallet renormalization scheme to higher order, in the spirit of Timm. It is to be hoped that such a method would allow a well defined calculational scheme to be developed (like that described in chapter 4) which avoided the need for an arbitrary crossover parameter  $l_c$ .

The work on the inclusion of disorder via a variable fugacity and on the layered sine-Gordon model is still at a very early stage. Indeed it is not yet clear whether the models proposed here will provide the correct description of the corresponding physical effects in real superfluid films. The recursion relations need to be calculated before their worth can be evaluated. However, these models are intrinsically interesting as they are examples of a broad group of possible extensions to the sine-Gordon method. Even if they fail to capture the physics of superfluid films it is quite possible that they may prove applicable to another system which undergoes a Kosterlitz-Thouless transition.

Another possible extension to the work described here would be to calculate the response of a superfluid film in the non-linear regime. Although this has been done before [52, 98, 99], using an extension of the AHNS theory, the idea that the response should be anisotropic is new. A detailed calculation would be of particular interest as it may lead to new predictions which would be open to experimental test.

Hopefully the new theoretical approach presented here will lead to a clearer understanding of the physics of superfluid films. Even though the work is still at an early stage it seems that the method detailed here will provide a more complete theoretical picture of the dynamic behaviour of superfluid films than the alternative phenomenological theories that have been developed in the past. Future work will be directed towards describing the results of the torsional oscillator experiments which are still only poorly understood after twenty years.

---

## Appendix A Vortex-Vortex Interaction

---

The expression for the energy of a single vortex and the interaction energy of a pair of vortices are derived in this appendix. The starting point is the definition of the configuration of the vortex part of the order parameter phase which gives rise to a vortex of winding number  $n$ ,

$$\oint_C \nabla\varphi \cdot d\mathbf{l} = 2\pi n. \quad (\text{A.1})$$

and the associated expression for the vortex contribution to the energy,

$$\frac{\mathcal{H}_v}{k_B T} = \frac{K}{2} \int d^2\mathbf{r} (\nabla\varphi)^2. \quad (\text{A.2})$$

The range of integration in this case includes the whole plane except the core region and so leads to an expression for the energy of a vortex to which the core energy must be added in separately.

When the phase of the order parameter was split into two parts (see section 3.2) the vortex contribution was defined as being a local minima of the energy. For a single vortex configuration, as described by eqn (A.1), this is just  $\varphi = n\phi$ , where  $\phi$  is the angle in plane polar coordinates. Hence,  $|\nabla\varphi| = n/r$ , and so it follows that the energy of an isolated vortex with core radius  $a$ , in a circular box of radius  $L$ , is

$$\frac{\mathcal{H}_v}{k_B T} = \frac{K}{2} n^2 \int_a^L dr 2\pi r \frac{1}{r^2} = \pi K n^2 \ln \frac{L}{a}. \quad (\text{A.3})$$

The total energy of a single vortex is given by this expression, plus the core energy,

$$\frac{U}{k_B T} = \pi K n^2 \ln \frac{L}{a} + \frac{E_c}{k_B T} \quad (\text{A.4})$$

The energy of a pair of vortices of equal but opposite winding number, a distance  $r$  apart, is obtained in the following way. The expression for the energy in eqn (A.2) is integrated by parts,

$$\frac{K}{2} \int d^2\mathbf{r} (\nabla\varphi)^2 = \frac{K}{2} \int d^2\mathbf{r} [\nabla \cdot (\varphi \nabla\varphi) - \varphi \nabla^2\varphi]. \quad (\text{A.5})$$

However, since the region of integration excludes all the vortex cores,  $\nabla^2\varphi = 0$ . Hence on applying the divergence theorem in two-dimensions, a line integral is obtained,

$$\frac{\mathcal{H}_v}{k_B T} = \frac{K}{2} \oint_R dl \varphi (\nabla\varphi \cdot \mathbf{m}), \quad (\text{A.6})$$

where  $\mathbf{m}$  is a unit vector which points normally (outwards) to the contour. The path of integration,  $R$ , is a single continuous contour which bounds the entire region of integration.

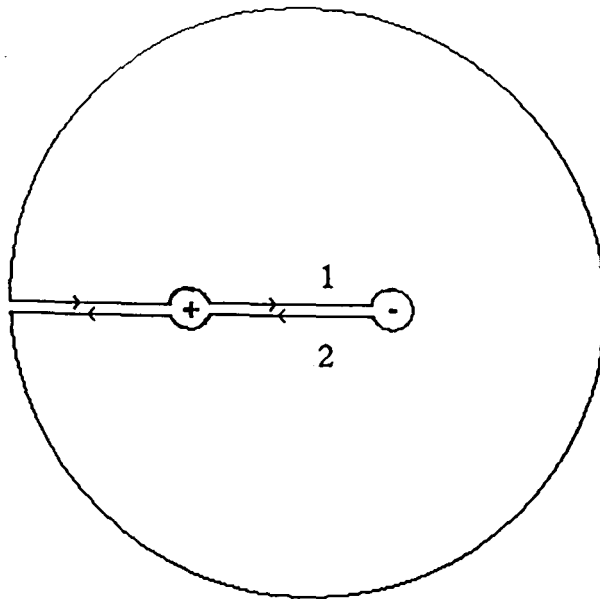


Figure A.1 Schematic representation of the path of integration for a system containing two vortices

For a system with two vortices the contour takes the form shown in figure (A.1). The only important contribution comes from the sections of the path between the two vortices, labelled 1 and 2 in the figure. For a large enough system  $\nabla\varphi \simeq 0$  along the outer edge of the contour, also along the region from the edge to the positive vortex  $\varphi\nabla\varphi$  has the same value on both sides of the contour and so the contributions cancel. The integrations around each of the vortices are finite, but lead to constant values which do not depend on their positions and so are absorbed into the values of the core energies.

The integral is readily evaluated along the parts of the path between the two vortices, by changing variables from the phase to plane polar coordinates defined by the relations  $\varphi = n\phi$  and  $\nabla\varphi = n\hat{\phi}/r$ , so that

$$\frac{K}{2} \oint_{r,a} dl \varphi \nabla\varphi = n(\phi_1 - \phi_2) \frac{K}{2} \int_a^r dr' \frac{n}{r'} \quad (\text{A.7})$$

$$= \pi K n^2 \ln \frac{r}{a}, \quad (\text{A.8})$$

since the value of  $\phi$  differs by  $2\pi$  across the two sides of the line of integration. Therefore the total energy of the pair of vortices is given by the expression:

$$\frac{U}{k_B T} = \pi K n^2 \ln \frac{r}{a} + \frac{2E_c}{k_B T}. \quad (\text{A.9})$$

This reduces to the form of the interaction energy introduced in chapter 3 when the vortices are of unit strength.

---

## Appendix B Calculation of $\Gamma(\mathbf{r}, t)$

---

In chapter 4, it was stated that the solution of the Fokker-Planck equation,

$$\frac{\partial \Gamma(\mathbf{r}, t)}{\partial t} = \frac{2D}{k_B T} \nabla \cdot (\Gamma(\mathbf{r}, t) \nabla U(\mathbf{r}, t) + k_B T \nabla \Gamma(\mathbf{r}, t)), \quad (\text{B.1})$$

for a potential of the form

$$U(\mathbf{r}, t) = U_0(\mathbf{r}) - q\mathbf{E}(t) \cdot \mathbf{r}, \quad (\text{B.2})$$

where  $U_0(\mathbf{r})$  is the static potential, could be written as

$$\Gamma(\mathbf{r}, t) = \Gamma_0(r) \left( 1 + \frac{qrE}{k_B T} g(r) \cos \theta e^{-i\omega t} + \dots \right), \quad (\text{B.3})$$

with the function  $g(r)$  given by the differential equation

$$\frac{i\omega r^2}{2D} g + r^2 \frac{d^2 g}{dr^2} + (3 - rV') r \frac{dg}{dr} - rV' g = -rV'. \quad (\text{B.4})$$

This result is most readily obtained using a double expansion method [52]. If the dynamic pair distribution function is written in terms of its static counterpart,

$$\Gamma_0(\mathbf{r}) = \frac{e^{-U_0(\mathbf{r})/k_B T}}{a^4} = \frac{y_0^2}{a^4} e^{-2\pi \int_0^l dl' K(l')}, \quad (\text{B.5})$$

and some function  $h$ , in the form

$$\Gamma(\mathbf{r}, t) = \frac{e^{-U(\mathbf{r}, t)/k_B T} e^h}{a^4} = \Gamma_0(\mathbf{r}) e^{q\mathbf{E} \cdot \mathbf{r}/k_B T} e^h, \quad (\text{B.6})$$

then substitution into the Fokker-Planck equation leads the relation

$$\frac{1}{2D} \frac{\partial h}{\partial t} = (\nabla h)^2 + \nabla^2 h + \frac{1}{2D} \frac{\partial V}{\partial t} - \nabla V \nabla h, \quad (\text{B.7})$$

where  $V = U/k_B T$ . If the time dependent part of the potential (that is the part related to the oscillating electric field) is explicitly separated from the part which depends on the position alone, i.e. if it is rewritten as

$$V = V_0 - \frac{q\mathbf{E} \cdot \mathbf{r}}{k_B T}, \quad (\text{B.8})$$

then eqn (B.7) becomes

$$\frac{1}{2D} \frac{\partial h}{\partial t} = (\nabla h)^2 + \nabla^2 h - \frac{q}{2D k_B T} \frac{\partial (\mathbf{E} \cdot \mathbf{r})}{\partial t} - \nabla V_0 \nabla h + \frac{q}{k_B T} \nabla h \nabla (\mathbf{E} \cdot \mathbf{r}). \quad (\text{B.9})$$

This equation is exact, but not readily solved and so approximations become necessary. Firstly, it is the linear response which is of primary interest and so

the term  $(\nabla h)^2$  is neglected. Secondly the local electric field will, in general, have the form

$$\mathbf{E}(\mathbf{r}, t) = \mathbf{E}_0 e^{-i\omega t} + \mathbf{E}_1 e^{-i3\omega t} + \dots, \quad (\text{B.10})$$

and so if the external drive varies solely at the fundamental frequency  $\omega$  then terms in  $\mathbf{E}_1$  and all higher harmonics will be much smaller and so, following Bowley and Giorgini [52], they are neglected.

The function  $h$  can be written in the general form

$$h = \sum_n \sum_l H_{l,n}(r) e^{-in\omega t} e^{il\theta}, \quad (\text{B.11})$$

and substitution of this expression into eqn (B.9) leads to the equation for the coefficients,

$$\begin{aligned} \frac{-in\omega}{2D} H_{l,n} &= H''_{l,n} + \frac{H'_{l,n}}{r} - \frac{H_{l,n} l^2}{r} + \frac{i\omega q E_0 r}{2D k_B T} \{ \delta_{l,1} + \delta_{l,-1} \} \delta_{n,1} \\ &\quad - H'_{l,n} V'_0 + \frac{q E_0}{2k_B T} [H'_{l-1,n+1} + H'_{l+1,n+1}] \\ &\quad - \frac{q E_0}{2k_B T} \left[ \frac{l}{r} (H_{l-1,n-1} - H_{l+1,n+1}) \right]. \end{aligned} \quad (\text{B.12})$$

If each coefficient  $H$  is represented as power series expansion in a new parameter,  $X = E_0 q r / 2k_B T$ , so that

$$H(r)_{l,n} = X G_{l,n}^{(1)} + X^2 G_{l,n}^{(2)} + \dots, \quad (\text{B.13})$$

then to first order in  $X$ ,

$$\begin{aligned} \frac{-i\omega}{2D} G_{l,n}^{(1)} r &= [r G_{l,n}^{(1)}]'' + \frac{1}{r} [r G_{l,n}^{(1)}]' - \frac{1}{r^2} G_{l,n}^{(1)} l^2 \\ &\quad - [r G_{l,n}^{(1)}]' V'_0 + \frac{i\omega r}{2D} [\delta_{l,1} + \delta_{l,-1}] \delta_{n,1}. \end{aligned} \quad (\text{B.14})$$

Hence it is clear that the inhomogeneous term is only non-zero for  $n = 1$  and  $l = \pm 1$ . Furthermore, the same equation is obtained for both  $l = \pm 1$ : this means that  $G_{l,n}^{(1)} = 0$  is a valid solution for all other values of  $n$  and  $l$ . Thus if  $G_{\pm 1,1}^{(1)}$  is written simply as  $G$ , then

$$\frac{-i\omega r}{2D} = r G'' + (3 - r V'_0) G' - G' V'_0 + \frac{i\omega r G}{2D}. \quad (\text{B.15})$$

Including both the first order terms in  $X$ , the pair distribution function is

$$\Gamma(\mathbf{r}, t) = \Gamma_0(\mathbf{r}) e^{q E r \cos \theta e^{-i\omega t} (1+G)/k_B T} \quad (\text{B.16})$$

so that on expanding the exponential to first order the expression used in chapter 4 is obtained, with  $g = 1 + G$ . The equation in  $g$  quoted above (eqn B.4) follows immediately from the equation for  $G$ .

---

## Appendix C Duality Transformation

---

The two-dimensional Coulomb gas model has been known to be dual to the sine-Gordon model for some time [9, 97]. However, a detailed knowledge of the mechanics of the transformation is necessary if the extensions of the theory to include the effect of a time varying field is to be understood, therefore this appendix contains a demonstration of the duality.

The interaction between charges is described using a logarithmic interaction potential of the form,

$$\frac{\mathcal{H}_{CG}}{k_B T} = -\pi K \int \int_{|\mathbf{r}-\mathbf{r}'|>a} d^2\mathbf{r} d^2\mathbf{r}' n_v(\mathbf{r}) \ln\left(\frac{|\mathbf{r}-\mathbf{r}'|}{a}\right) n_v(\mathbf{r}'), \quad (\text{C.1})$$

where  $n_v$  is the density of unit charges. The grand partition function is then given by the expression

$$\mathcal{Z} = \sum_{N^+} \frac{1}{N^+!} \sum_{N^-} \frac{1}{N^-!} \prod_{\alpha=1}^{N^+} \int \frac{d^2\mathbf{r}_\alpha}{a^2} \prod_{\beta=1}^{N^-} \int \frac{d^2\mathbf{r}_\beta}{a^2} y^{N^+} y^{N^-} \exp\left(\frac{-\mathcal{H}_{CG}}{k_B T}\right), \quad (\text{C.2})$$

where  $N^+$  and  $N^-$  are the number of positive and negative charges respectively, and  $y$  is their fugacity.

In order to demonstrate the duality of this model with the sine-Gordon model, the starting point is the interaction potential between the charges. This is transformed into reciprocal space, after which the transformation due to Hubbard and Stratonovich is applied to obtain a path integral. Finally, the grand partition function obtained in this procedure is simplified, leading to the sine-Gordon form.

The interaction potential for two charges a distance  $r$  apart in the two-dimensional Coulomb gas may be represented by the Green function

$$G(r) = -\frac{\ln(r/a)}{2\pi} \quad (\text{C.3})$$

where  $a$  is the core size of the charge.  $G(\mathbf{r})$  satisfies Poisson's equation so that

$$\nabla^2 G(\mathbf{r}) = -\delta(\mathbf{r}). \quad (\text{C.4})$$

The Fourier transforms of the Green function are defined by the relations

$$G(\mathbf{q}) = \int d^2\mathbf{r} e^{i\mathbf{q}\cdot\mathbf{r}} G(\mathbf{r}) \quad (\text{C.5})$$

$$G(\mathbf{r}) = \frac{1}{A} \sum_{\mathbf{q}} e^{-i\mathbf{q}\cdot\mathbf{r}} G(\mathbf{q}), \quad (\text{C.6})$$

where  $A$  is a numerical factor. The Fourier transform of  $G(\mathbf{r})$  takes the simple form

$$G(\mathbf{q}) = 1/q^2. \quad (\text{C.7})$$

The density of unit strength charges,  $n_v$ , is defined using the positions of all the positive and negative charges:

$$n_v(\mathbf{r}) = \sum_{\alpha} \delta(\mathbf{r} - \mathbf{r}_{\alpha}) - \sum_{\beta} \delta(\mathbf{r} - \mathbf{r}_{\beta}) \quad (\text{C.8})$$

where the sets  $\{\mathbf{r}_{\alpha}\}$  and  $\{\mathbf{r}_{\beta}\}$  define the positions of the positive and negative charges respectively. Therefore the interaction of the charges is written as

$$\frac{\mathcal{H}_{CG}}{k_B T} = 2\pi^2 K \int \int d^2\mathbf{r} d^2\mathbf{r}' n_v(\mathbf{r}) G(\mathbf{r} - \mathbf{r}') n_v(\mathbf{r}'), \quad (\text{C.9})$$

excluding the core energies (these are included later when the grand partition function is formulated). When the Green function is replaced by its Fourier transform, this leads to a new expression of the form

$$\frac{\mathcal{H}_{CG}}{k_B T} = \frac{2\pi^2 K}{A} \sum_{\mathbf{q}} G(\mathbf{q}) n_v(\mathbf{q}) n_v(-\mathbf{q}) \quad (\text{C.10})$$

$$= \frac{2\pi^2 K}{A} \sum_{\mathbf{q}} q^{-2} |n_v(\mathbf{q})|^2, \quad (\text{C.11})$$

where  $n_v(\mathbf{q})$  is simply the Fourier transform of  $n_v(\mathbf{r})$ .

The Hubbard-Stratonovich transformation is now used to change this expression into a path integral over the auxiliary field  $\phi$ . Essentially this involves the use of the identity (see for example p 399 of ref. [43])

$$(4\pi)^{n/2} (\det \underline{C})^{1/2} e^{\lambda_i C_{ij} \lambda_j} = \int \left( \prod_{i=1}^n dy_i \right) e^{-y_i C_{ij}^{-1} y_j / 4 + \lambda_i y_j} \quad (\text{C.12})$$

where  $\underline{C}$  is an  $n \times n$  matrix with inverse  $\underline{C}^{-1}$  and  $y_i$  and  $\lambda_i$  are  $n$  component vectors.

Using this transformation the Boltzmann factor for a particular arrangement of the charges can be written as

$$e^{-\mathcal{H}_{CG}/k_B T} = C \int \mathcal{D}\phi(\mathbf{r}) \exp \left( \frac{-1}{8\pi^2 K} \int d^2\mathbf{r} (\nabla\phi(\mathbf{r}))^2 \right) \quad (\text{C.13})$$

$$\times \exp \left( i \int d^2\mathbf{r} n_v(\mathbf{r}) \phi(\mathbf{r}) \right). \quad (\text{C.14})$$

where  $C$  is an unimportant constant.

Further simplification is achieved by substituting for the particle density,

$$n_v(\mathbf{r}) = \sum_{\alpha} \delta(\mathbf{r}_{\alpha} - \mathbf{r}) - \sum_{\beta} \delta(\mathbf{r}_{\beta} - \mathbf{r}).$$

On making this substitution eqn (C.13) takes the modified form

$$e^{-\mathcal{H}_{CG}/k_B T} = C \int \mathcal{D}\phi(\mathbf{r}) \exp\left(\frac{-1}{8\pi^2 K} \int d^2\mathbf{r} (\nabla\phi(\mathbf{r}))^2\right) \exp\left(i \sum_{\alpha} \phi(\mathbf{r}_{\alpha})\right) \times \exp\left(-i \sum_{\beta} \phi(\mathbf{r}_{\beta})\right). \quad (\text{C.15})$$

Thus the grand partition function is now written as

$$\mathcal{Z} = C \int \mathcal{D}\phi(\mathbf{r}) \sum_{N^+} \frac{1}{N^+!} \sum_{N^-} \frac{1}{N^-!} \prod_{\alpha=1}^{N^+} \int \frac{d^2\mathbf{r}_{\alpha}}{a^2} \prod_{\beta=1}^{N^-} \int \frac{d^2\mathbf{r}_{\beta}}{a^2} y^{N^+} y^{N^-} \times \exp(i(\phi(\mathbf{r}_{\alpha}) - \phi(\mathbf{r}_{\beta}))) \exp\left(-\frac{1}{8\pi^2 K} \int d^2\mathbf{r} (\nabla\phi(\mathbf{r}))^2\right). \quad (\text{C.16})$$

This expression is greatly simplified by the use of the identity

$$1 + \sum_{N=1}^{\infty} \frac{1}{N!} \prod_{i=1}^N y^N \int d^2\mathbf{r}_i f(\mathbf{r}_i) \equiv e^{y \int d^2\mathbf{r} f(\mathbf{r})}, \quad (\text{C.17})$$

and so the grand partition function is then,

$$\mathcal{Z} = C \int \mathcal{D}\phi(\mathbf{r}) \exp\left(-\left(\frac{1}{8\pi^2 K} \int d^2\mathbf{r} (\nabla\phi(\mathbf{r}))^2 - \frac{2y}{a^2} \int d^2\mathbf{r} \cos \phi(\mathbf{r})\right)\right), \quad (\text{C.18})$$

which is of course the partition function for the sine-Gordon model.

---

## Appendix D Layered Sine-Gordon Model

---

Here the derivation of two coupled sine-Gordon equations from the model of layered superfluid films postulated in chapter 7 is outlined. The Hamiltonian for the layered system is

$$\frac{\mathcal{H}}{k_{\text{B}}T} = \sum_{ij} \frac{-\pi K_{ij}}{A} \int \int_{|\mathbf{r}-\mathbf{r}'|>a} d^2\mathbf{r} d^2\mathbf{r}' n_v^i(\mathbf{r}) \ln\left(\frac{|\mathbf{r}-\mathbf{r}'|}{a}\right) n_v^j(\mathbf{r}'), \quad (\text{D.1})$$

where the Kosterlitz parameter has been generalized to a matrix,

$$\underline{K} = \begin{pmatrix} K_1 & X\sqrt{K_1K_2} \\ X\sqrt{K_1K_2} & K_2 \end{pmatrix} \quad (\text{D.2})$$

with the strength of the interlayer coupling given by the new parameter  $X$ .

Progress is made by diagonalising the matrix  $\underline{K}$  using an orthogonal transformation of the form

$$U = \begin{pmatrix} \cos\theta & \sin\theta \\ -\sin\theta & \cos\theta \end{pmatrix} \quad (\text{D.3})$$

so that,

$$U^{-1}\underline{K}U = \begin{pmatrix} K_a & 0 \\ 0 & K_b \end{pmatrix}, \quad (\text{D.4})$$

where the new parameters are defined by:

$$K_a = K_1 \cos^2\theta + K_2 \sin^2\theta - 2X\sqrt{K_1K_2} \sin\theta \cos\theta \quad (\text{D.5})$$

$$K_b = K_1 \sin^2\theta + K_2 \cos^2\theta + 2X\sqrt{K_1K_2} \sin\theta \cos\theta, \quad (\text{D.6})$$

and

$$\tan 2\theta = \frac{2X\sqrt{K_1K_2}}{K_2 - K_1}.$$

The terms in the interaction energy (eqn D.1) may then be written as:

$$\begin{aligned} n_v^i(\mathbf{q})K_{ij}n_v^j(\mathbf{q}) &= \begin{pmatrix} n_v^{(1)}(\mathbf{q}) & n_v^{(2)}(\mathbf{q}) \end{pmatrix} U U^{-1} \underline{K} U U^{-1} \begin{pmatrix} n_v^{(1)}(-\mathbf{q}) \\ n_v^{(2)}(-\mathbf{q}) \end{pmatrix} \\ &= K_a \xi_v^{(1)}(\mathbf{q}) \xi_v^{(1)}(-\mathbf{q}) + K_b \xi_v^{(2)}(\mathbf{q}) \xi_v^{(2)}(-\mathbf{q}), \end{aligned} \quad (\text{D.7})$$

where the following definitions have been used,

$$\xi_v^{(1)}(\mathbf{q}) = \cos\theta n_v^{(1)}(\mathbf{q}) - \sin\theta n_v^{(2)}(\mathbf{q}) \quad (\text{D.8})$$

$$\xi_v^{(2)}(\mathbf{q}) = \cos\theta n_v^{(2)}(\mathbf{q}) + \sin\theta n_v^{(1)}(\mathbf{q}). \quad (\text{D.9})$$

Substituting eqn (D.7) into the Hamiltonian, eqn (D.1), and carrying out a Fourier transform leads to a grand partition function of the form

$$\begin{aligned} \mathcal{Z} = & \sum_{N_1^+} \frac{1}{N_1^+!} \sum_{N_1^-} \frac{1}{N_1^-!} \sum_{N_2^+} \frac{1}{N_2^+!} \sum_{N_2^-} \frac{1}{N_2^-!} \prod_{\alpha_1=1}^{N_1^+} \int \frac{d^2\mathbf{r}_{\alpha_1}}{a^2} \\ & \prod_{\beta_1=1}^{N_1^-} \int \frac{d^2\mathbf{r}_{\beta_1}}{a^2} y^{N_1^+} y^{N_1^-} \prod_{\alpha_2=1}^{N_2^+} \int \frac{d^2\mathbf{r}_{\alpha_2}}{a^2} \prod_{\beta_2=1}^{N_2^-} \int \frac{d^2\mathbf{r}_{\beta_2}}{a^2} y^{N_2^+} y^{N_2^-} \\ & \exp \left( \frac{-1}{k_B T} \left\{ \frac{2\pi^2}{A} \sum_{\mathbf{q}} \left( K_a \frac{\xi_v^{(1)}(\mathbf{q}) \xi_v^{(1)}(-\mathbf{q})}{q^2} + K_b \frac{\xi_v^{(2)}(\mathbf{q}) \xi_v^{(2)}(-\mathbf{q})}{q^2} \right) \right\} \right), \end{aligned} \quad (\text{D.10})$$

where the subscripts 1 and 2 refer to the two different layers, so that for instance  $N_1^+$  is the number of positive vortices in the first layer. The Hubbard-Stratonovich transformation may now be applied to eqn (D.10), this time two auxiliary fields are required,  $\phi_a$  and  $\phi_b$ , so that the partition function becomes

$$\mathcal{Z} = C \int \mathcal{D}\phi_a(\mathbf{r}) \int \mathcal{D}\phi_b(\mathbf{r}) \exp \left( \frac{-\mathcal{H}}{k_B T} \right), \quad (\text{D.11})$$

with

$$\begin{aligned} \frac{-\mathcal{H}}{k_B T} = & \frac{-1}{8\pi^2 K_a} \int d^2\mathbf{r} (\nabla\phi_a(\mathbf{r}))^2 - \frac{1}{8\pi^2 K_b} \int d^2\mathbf{r} (\nabla\phi_b(\mathbf{r}))^2 \\ & + \frac{2y_1}{a^2} \int d^2\mathbf{r} (\cos(\phi_a(\mathbf{r}) \cos\theta + \phi_b(\mathbf{r}) \sin\theta)) \\ & + \frac{2y_2}{a^2} \int d^2\mathbf{r} (\cos(\phi_b(\mathbf{r}) \cos\theta - \phi_a(\mathbf{r}) \sin\theta)), \end{aligned} \quad (\text{D.12})$$

and  $C$  a constant.

The system is assumed to be described by model A dynamics, of the form

$$\eta_i \frac{\partial\phi_i}{\partial t} = -\frac{\delta\mathcal{H}[\phi_a, \phi_b]}{\delta\phi_i} + R_i(t), \quad (\text{D.13})$$

where the noise term,  $R_i$ , may differ in magnitude from layer to layer. Thus the partition function given by eqn (D.11) leads to a pair of coupled Langevin equations,

$$\begin{aligned} \eta_a \frac{\partial\phi_a}{\partial t} = & \frac{k_B T}{4\pi^2 K_a} \nabla^2 \phi_a - \frac{2y_1 k_B T}{a^2} \cos\theta \sin(\phi_a(\mathbf{r}) \cos\theta + \phi_b(\mathbf{r}) \sin\theta) \\ & + \frac{2y_2 k_B T}{a^2} \sin\theta \sin(\phi_b(\mathbf{r}) \cos\theta - \phi_a(\mathbf{r}) \sin\theta) + R_a(t) \end{aligned} \quad (\text{D.14})$$

$$\begin{aligned} \eta_b \frac{\partial\phi_b}{\partial t} = & \frac{k_B T}{4\pi^2 K_b} \nabla^2 \phi_b - \frac{2y_2 k_B T}{a^2} \cos\theta \sin(\phi_b(\mathbf{r}) \cos\theta - \phi_a(\mathbf{r}) \sin\theta) \\ & - \frac{2y_1 k_B T}{a^2} \sin\theta \sin(\phi_a(\mathbf{r}) \cos\theta + \phi_b(\mathbf{r}) \sin\theta) + R_b(t). \end{aligned} \quad (\text{D.15})$$

---

## References

---

- [1] Kosterlitz J.M. and Thouless D.J., *J. Phys. C*, **6**, 1181 (1973)
- [2] Kosterlitz J.M. and Thouless D.J., *Progress in Low Temperature Physics*, **7**, 371 (1978)
- [3] Kosterlitz J.M., *J. Phys. C*, **7**, 1046 (1974)
- [4] Hohenberg P.C., *Phys. Rev.*, **158**, 383 (1967)
- [5] Mermin N.D. and Wagner H., *Phys. Rev. Lett.*, **17**, 1133 (1966)
- [6] Berezinskii V.L., *JETP*, **34**, 610 (1972)
- [7] Ambegaokar V., Halperin B.I., Nelson D.R. and Siggia E.D., *Phys. Rev. Lett*, **40**, 783 (1978)
- [8] Ambegaokar V., Halperin B.I., Nelson D.R. and Siggia E.D., *Phys. Rev. B*, **21**, 1806 (1980)
- [9] Chaikin P.M. and Lubensky T.C., 'Principles of Condensed Matter Physics', (Cambridge University Press, Cambridge, UK, 1995)
- [10] Tilley D.R. and Tilley J., 'Superfluidity and Superconductivity', (third edition, IOP Publishing, Bristol, UK, 1990)
- [11] Thouless D.J., 'Condensed matter physics in less than three dimensions', in 'The New Physics', edited by Davies P., (Cambridge University Press, Cambridge, UK, 1989)
- [12] Donnelly R.J., 'Quantized Vortices in Helium II', (Cambridge University Press, Cambridge, UK, 1991)
- [13] Timm C., *Physica C*, **265**, 31 (1996)
- [14] Minnhagen P., *Rev. Mod. Phys.*, **59**, 1001 (1987)
- [15] Amit D.J., Goldschmidt Y.Y. and Grinstein G.J., *J. Phys. A*, **13**, 585 (1980)
- [16] Bowley R.M., Armour A.D. and Benedict K., *J. Low Temp. Phys.*, **113**, 71 (1998)
- [17] Burton W.K. and Cabrera N., *Disc. Faraday Soc.* **5**, 33 (1949)
- [18] Knops H.J.F. and Den Ouden L.W.J., *Physica*, **103A**, 597-608 (1980)
- [19] Nozières P. and Gallet F. , *J. de Physique*, **48**, 353 (1987)
- [20] Nozières, 'Shape and Growth of Crystals', in 'Solids far from Equilibrium', edited by Godrèche C., (Cambridge University Press, Cambridge, UK, 1991)

- [21] Rost M. and Spohn H., *Phys. Rev. E*, **49**, 3709 (1994)
- [22] Gallet F., Balibar S. and Rolley E., *J. de Physique*, **48**, 369 (1987)
- [23] Toner J. and Di Vincenzo D.P., *Phys. Rev. B*, **41**, 632 (1990)
- [24] Tsai Y.-C and Shapir Y, *Phys. Rev. Lett.*, **69**, 1773 (1992); *Phys. Rev. E*, **50**, 3546 (1994)
- [25] Scheidl S., *Phys. Rev. Lett*, **75**, 4760 (1995)
- [26] Bowley R.M. and Armour A.D., *J. Low Temp. Phys.*, **107**, 225 (1997)
- [27] Jeanneret B., Flückiger Ph., Gavilano J.L., Leeman Ch. and Martinoli P., *Phys. Rev. B*, **40**, 11374 (1989)
- [28] Halperin B.I. and Nelson D.R., *J. Low Temp. Phys.*, **36**, 599 (1979)
- [29] Rogers C.T., Myers K.E., Eckstein J.N. and Bozovic I., *Phys. Rev. Lett.*, **69**, 160 (1992)
- [30] Chui S.T. and Weeks J.D., *Phys. Rev. B*, **14**, 4978 (1976)
- [31] De Gennes P.G. and Prost J., 'The Physics of Liquid Crystals', (Oxford University Press, Oxford, UK, 1993)
- [32] Halperin B.I., in 'Proceedings of Kyoto Summer Institute 1979 – Physics of Low-Dimensional Systems', edited by Y. Nagaoka and S. Hikami (Publication Office, Prog. Theor. Phys., Kyoto)
- [33] Nelson D.R., 'Defect Mediated Phase Transitions', in 'Phase Transitions and Critical Phenomena', vol. 7, edited by C. Domb and J.L. Lebowtiz (Academic Press, New York 1983)
- [34] Grinstein G. and Lee D-H., *Phys. Rev. Lett.*, **66**, 177 (1991)
- [35] Andreev A.F., *Pis'ma Zh. Eksp. Teor. Fiz* **53**, 1204 (1990) [ *JETP Lett* **52**, 619 (1990)].
- [36] Andreev A.F., in 'Excitations in two dimensional and Three dimensional Quantum Fluids', edited by Wyatt A.F.G. and Lauter H.J., p397 (Plenum Press, New York, USA, 1991).
- [37] Armour A.D., Bowley R.M. and Nozières P., *J. Low Temp. Phys.*, **110**, 127 (1998)
- [38] Onsager L., *Phys. Rev.*, **65**, 1232 (1949)
- [39] Stanley H.E., 'Introduction to Phase Transitions and Critical Phenomena', (Oxford University Press, Oxford, UK, 1971)
- [40] Kadanoff L.P., *Physics*, **2**, 263 (1966)
- [41] Wilson K.G., *Rev. Mod. Phys.*, **47**, 773 (1975)
- [42] Fisher M.E., 'Scaling, Universality and the Renormalization Group', in 'Critical Phenomena', edited by Hahne J.W., (Lecture Notes in Physics, vol. 186, Springer-Verlag, Berlin, Germany, 1983)

- [43] Binney J.J., Dowrick N.J., Fisher A.J. and Newman M.E.J., 'The Theory of Critical Phenomena', (Oxford University Press, Oxford, UK, 1992)
- [44] Le Bellac M., 'Quantum and Statistical Field Theory', (Oxford University Press, Oxford, UK, 1991)
- [45] Cardy J., 'Scaling and Renormalization in Statistical Physics', (Cambridge University Press, Cambridge, UK, 1996)
- [46] Goldenfeld N., 'Lectures on Phase Transitions and the Renormalization Group', (Frontiers in Physics Series, no. 85, Addison-Wesley, Reading, Massachusetts, USA, 1992)
- [47] Sethna J.P., 'Broken Symmetry and Topology', in 'Lectures in the Sciences of Complexity', edited by Nadel L. and Stein D.S., (Addison-Wesley, Reading, Massachusetts, USA, 1992)
- [48] Amit D.J., 'Field Theory, the Renormalization Group, and Critical Phenomena', (Mc Graw-Hill, New York, USA, 1978)
- [49] Hohenberg P.C. and Halperin B.I., *Rev. Mod. Phys.*, **49**, 435 (1977)
- [50] Anderson P.W., 'Basic Notions of Condensed Matter Physics', (Frontiers in Physics Series, no. 55, Addison-Wesley, Reading, Massachusetts, USA, 1984)
- [51] Bishop D.J. and Reppy J.D., *Phys Rev. Lett*, **40**, 1727 (1978); Bishop D.J. and Reppy J.D., *Phys Rev. B*, **22**, 5171 (1980)
- [52] Bowley R.M. and Giorgini S., *J. Low Temp. Phys.*, **92**, 263 (1993)
- [53] Long E. and Meyer L., *Phys. Rev.*, **79**, 1031 (1950)
- [54] Gulácsi Z. and Gulácsi M., *Advances in Physics*, **47**, 1 (1998)
- [55] Young A.P., *J. Phys. C*, **11**, L453 (1978)
- [56] Chorin A.J. and Hald O.H., *Physica D*, **99**, 442 (1997)
- [57] Nelson D.R. and Kosterlitz J.M., *Phys. Rev. Lett.*, **39**, 1202 (1977)
- [58] Ambegaokar V. and Teitel S., *Phys. Rev. B*, **19**, 1667 (1979)
- [59] Rudinick I., *Phys. Rev. Lett.*, **40**, 1454 (1978)
- [60] Agnolet G., McQueeney D.F. and Reppy J.D., *Phys. Rev. B*, **39**, 8934 (1989)
- [61] McQueeney D.F., PhD Thesis (Cornell University, New York, USA, 1988)
- [62] Wallin M., *Phys. Rev. B*, **41**, 6575 (1990)
- [63] Crowell P.A. and Reppy J.D., *Phys. Rev. Lett.*, **70**, 3291 (1993); Crowell and Reppy J.D., *Phys. Rev. B*, **53**, 2701 (1996)

- [64] Press W.H., Teukolsky S.A., Vetterling W.T. and Flannery B.P., 'Numerical Recipes in Fortran', (Cambridge University Press, Cambridge, UK, 2nd ed. 1992)
- [65] Saunders J., private communication
- [66] Nyéki J., Ray R., Sheshin G., Maidanov V., V. Mikheev, Cowan B. and Saunders J., *Low Temp. Phys.*, **23**, 379 (1997)
- [67] Bowley R.M., Armour A.D., Nyéki J., Cowan B. and Saunders J., *J. Low Temp. Phys.*, **113**, 399 (1998)
- [68] Ohta T. and Jasnow D., *Phys. Rev. B*, **20**, 139 (1979)
- [69] Nozières P., 'La Transition Rugeuse par la Joie', lecture notes (unpublished)
- [70] Houghton A., Kenway R.D. and Ying S.C., *Phys. Rev. B*, **23**, 298 (1981)
- [71] Goldschmidt Y.Y. and Schaub B., *Nucl. Phys.*, **B251** 77 (1985)
- [72] Rieger H. and Blasum U., *Phys. Rev. B*, **55**, R7394 (1997)
- [73] Marianari E., Monasson R. and Ruiz-Lorenzo J.J., *J. Phys. A*, **28**, 3975 (1995)
- [74] Andreev A.F. and Parsin A.Y., *Zh. Eksp. Teor. Fiz.*, **75**, 1511 (1978) [*JETP* **48**, 763]
- [75] Giorgini S. and Bowley R.M., *J. Phys. I (France)*, **5**, 815 (1995)
- [76] Conrad E.H. and Engel T., *Surface Science*, **299/300**, 391 (1994)
- [77] Jackson K.A. and Miller C.E., *J. Crystal Growth*, **40**, 169 (1977); Pavlovska A. and Nenow D., *J. Crystal Growth*, **39**, 340, (1977)
- [78] Wolf P.E., Gallet F., Balibar S., Rolley E. and Nozières P., *J. de Physique*, **46**, 1987 (1985)
- [79] Rolley E., Chevalier E., Guthmann C. and Balibar S., *Phys. Rev. Lett.*, **72**, 872 (1994); Rolley E., Guthmann C., Chevalier E. and Balibar S., *J. Low Temp. Phys.*, **99**, 851 (1995)
- [80] Balibar S., in proceedings of the workshop on liquid/solid interfaces in helium (Otaniemi, Finland, 1996), unpublished
- [81] Balibar S. and Nozières P., *Solid State Comm.*, **92**, 19 (1994)
- [82] Balibar S., Guthmann C. and Rolley E., *J. Phys. I (France)*, **3**, 1475 (1993)
- [83] Weeks J.D., 'The Roughening Transition', in 'Ordering in Strongly Fluctuating Condensed Matter Systems' edited by Riste, (Plenum Press, New York, USA, 1980)
- [84] Weeks J.D., Gilmer G.H. and Leamy H.J., *Phys. Rev. Lett.*, **31**, 549 (1973)

- 
- [85] Leamy H.J. and Gilmer G.H., *J. Crystal Growth*, **24**, 499 (1974)
  - [86] Martin P.C., Siggia E.D. and Rose H.A., *Phys. Rev. A*, **8**, 423 (1973)
  - [87] Cule D. and Shapir Y., *Phys. Rev. Lett.*, **74**, 114 (1995)
  - [88] Rieger H., *Phys. Rev. Lett.*, **74**, 4964 (1995)
  - [89] Nabarro F.R.N., 'Theory of crystal dislocations', (Oxford University Press, Oxford, UK, 1967)
  - [90] Nozières P., private communication
  - [91] Uwaha M. and Nozières P., *J. de Physique*, **48**, 407 (1987)
  - [92] Barabási A.-L. and Stanley H.E., 'Fractal Concepts in Surface Growth', (Cambridge University Press, Cambridge, UK, 1994), ch. 10
  - [93] Mott N., 'Metal-Insulator Transitions', (Taylor and Francis, London, U.K. 2nd ed. 1990)
  - [94] Nozières P., *Annales de Physique*, **20** (3 S2), 417 (1995)
  - [95] Bowley R.M. and Sanchez, 'Introductory Statistical Mechanics', (Oxford University Press, Oxford, UK, 1996)
  - [96] Park J.-M. and Lubensky T.C., *Phys. Rev. E*, **53**, 2665 (1996)
  - [97] Samuel S., *Phys. Rev. D*, **18**, 1916 (1978)
  - [98] Bowley R.M. and Giorgini S., *J. Low Temp. Phys.*, **93**, 987 (1993)
  - [99] Giorgini S. and Bowley R.M., *J. Low Temp. Phys.*, **95**, 729 (1994)